



THE HONG KONG
POLYTECHNIC UNIVERSITY

香港理工大學

Pao Yue-kong Library

包玉剛圖書館

Copyright Undertaking

This thesis is protected by copyright, with all rights reserved.

By reading and using the thesis, the reader understands and agrees to the following terms:

1. The reader will abide by the rules and legal ordinances governing copyright regarding the use of the thesis.
2. The reader will use the thesis for the purpose of research or private study only and not for distribution or further reproduction or any other purpose.
3. The reader agrees to indemnify and hold the University harmless from and against any loss, damage, cost, liability or expenses arising from copyright infringement or unauthorized usage.

IMPORTANT

If you have reasons to believe that any materials in this thesis are deemed not suitable to be distributed in this form, or a copyright owner having difficulty with the material being included in our database, please contact lbsys@polyu.edu.hk providing details. The Library will look into your claim and consider taking remedial action upon receipt of the written requests.

**THE ADOPTION OF
LASER MICRO-CUTTING AND HEATING
IN ULTRA-PRECISION MACHINING
PROCESS**

HAN JIDE

M.Phil

The Hong Kong Polytechnic University

2018

The Hong Kong Polytechnic University
Department of Industrial and Systems Engineering

**The Adoption of Laser Micro-cutting
and Heating in Ultra-precision
Machining Process**

HAN Jide

**A thesis submitted in partial fulfillment of the
requirements for the degree of Master of Philosophy**

June 2017

Certificate of originality

I hereby declare that this thesis is my own work and that, to the best of my knowledge and belief, it reproduces no material previously published or written, nor material that has been accepted for the award of any other degree or diploma, except where due acknowledgement has been made in the text.

_____ (Signed)

HAN Jide (Name of student)

Abstract

Diamond machining is an important method for the manufacturing of high precision components with excellent surface finish and high form accuracy. There are limitations in this method for machining such as single crystal silicon and oxygen-free high conductivity (OFHC) copper which are often used in many cases. In this research, two aspects of using laser to assist machining were investigated. Firstly, a hybrid machining method combining laser grooving and diamond shaping was proposed which aimed at machining silicon lenticular lens mold inserts. An exploratory study on the use of a diamond tool to perform the final shaping of a silicon groove roughly cut by laser was performed. Secondly, the formation of surface defects of OFHC copper in the diamond cutting process was investigated and laser heating was introduced in the cutting process to investigate its influence on the cutting performance of OFHC copper.

In machining silicon, cracks are easily formed on the machined workpiece surface when the cutting depth is larger than the critical depth of cut which is far less than 1 μm , so machining microstructures with large feature sizes such as lenticular lens mold inserts is time consuming as well as costly. In this research, a hybrid machining method to fabricate silicon lenticular lens mold inserts by combining laser grooving with diamond shaping was proposed. Firstly, laser micro-machining equipment was developed and used to perform laser grooving experiments on silicon workpiece. The influence of the laser parameters, including laser power, laser scan speed and defocus depth on the laser

grooving depth was investigated. Grooves were then generated on the silicon workpiece surface with a designed profile shape. Secondly, diamond cutting of laser generated grooves was conducted to investigate the influence of finish cutting depth on the surface quality of grooves produced by this hybrid method. The experimental results indicated that by reducing the finish cutting depth, the surface quality of the machined grooves could be improved. When the finish cutting depth was 4 μm , the surface roughness was 644 nm, and was reduced to 126 nm when the finish cutting depth was 0.2 μm . This preliminary result shows that it is possible to use this method to fabricate silicon lenticular lens mold inserts, however the surface quality still needs to be further improved to fulfill the requirements of a commercial product.

Due to the high thermal conductivity and high purity of OFHC copper, it is an ideal material to use for making high power laser mirrors, which require high quality defect-free surfaces to make sure a high laser damage threshold could be achieved. While the cutting performance of OFHC copper in ultra-precision machining is sensitive to the machining parameters. The machined surface quality of OFHC copper deteriorates rapidly with increasing cutting depth. In this research, the second part of our work was to investigate the influence of laser heating on the cutting performance of OFHC copper in the diamond cutting process. Firstly, the formation of surface delamination, which caused the machined surface roughness of OFHC copper to increase, was investigated by using taper cutting experiments and the finite element method (FEM). It was

suspected that the formation of surface defects in OFHC copper was influenced by the stress and strain conditions of the workpiece material in the cutting region during the diamond cutting process. Diamond cutting experiments assisted with laser heating were undertaken to investigate the influence of laser power on the cutting performance of OFHC copper. It was found that the use of laser heating was beneficial for the suppression of the surface delamination of OFHC copper at large depth of cut in the diamond cutting process, and led to an improvement in the quality of the machined surface. This research is helpful in enhancing our understanding on the formation of surface defects of OFHC copper in the diamond cutting process and is also useful in designing suitable experimental parameters in the manufacturing practice in order to achieve good surface quality in the diamond cutting of OFHC copper.

Publications arising from this study

Journal paper:

1. **J.D. Han**, L.H. Li, C.Y. Chan, W.B. Lee. Investigation on the formation of surface defects of OFHC copper in diamond micro-grooving process. *The International Journal of Advanced Manufacturing Technology*. 93.9-12 (2017): 4133-4141.
2. **J.D. Han**, L.H. Li, W.B. Lee. Investigation on the effects of laser heating on surface quality of OFHC copper in diamond cutting process. *Precision Engineering*. (Minor revision).
3. **J.D. Han**, L.H. Li, W.B. Lee. A hybrid machining process combining laser ablation and diamond cutting for machining lenticular lens silicon mold. *Journal of Manufacturing Processes*. (Under review)

Conference:

1. **J.D. Han**, W.B. Lee, C.Y. Chan. Establishment of a laser assisted ultra-precision machining system. euspen's 16th international conference & exhibition, Nottingham, UK, May 2016, P4.36. (Conference)
2. **J.D. Han**, W.B. Lee, C.Y. Chan, L.H. Li. Diamond micro-grooving of Ti6Al4V assisted with laser ablation. ASPEN/ASPE Spring Topical Meeting, Hong Kong, 14-17 March 2017, P03.0072. (Conference)

Acknowledgements

Foremost, I would like to express my sincere gratitude to my chief supervisor, Prof. W.B. Lee, Chair Professor of the Department of Industrial and Systems Engineering and Director of the Partner State Key Laboratory of Ultra-precision Machining Technology of The Hong Kong Polytechnic University, for his continuous support to my research. His encouragement, patience and valuable advice are of great help in enabling me finish my M.Phil study.

I would like to thank Dr. L.H. Li, Dr. C.Y. Chan and Prof. C.F. Cheung for their valuable suggestions and kind help on my research work. Many thanks to the technicians in the Partner State Key Laboratory of Ultra-precision Machining Technology of The Hong Kong Polytechnic University for their support. Many thanks to my friends Dr. P. Huang, Mr. N.H. Yu, Mr. W. Yuan, Dr. Z.W. Zhu, Dr. X.D. Zhang, Mr. H.C. Wong, Dr. G.B. Xiao, Dr. H.T. Wang, for their valuable advices. My sincere thanks also to Prof. C.Y. Tang and Mr. L. Wei for their kind recommendation. Special thanks to Ms. W.L. Shi for her encouragement.

Finally, I would like to express my utmost thanks to my parents and all my family members for their support, understanding and encouragement during my study.

Contents

Certificate of originality	i
Abstract	ii
Publications arising from this study	v
Acknowledgements	vi
List of figures	x
List of tables.....	xvi
Chapter 1 Introduction	1
1.1 Background and motivation of the research	1
1.2 Research objectives.....	5
1.3 Organization of the thesis	6
Chapter 2 Literature review	8
2.1 Ultra-precision diamond cutting	8
2.1.1 Introduction.....	8
2.1.2 Diamond tools	11
2.1.3 Material removal	12
2.1.4 Surface finish	13
2.1.5 Tool wear.....	15
2.2 Laser assisted machining (LAM).....	16
2.2.1 Introduction.....	16

2.2.2 LAM at the macroscale	17
2.2.3 LAM at the microscale.....	20
2.3 Machinability	23
2.3.1 Introduction.....	23
2.3.2 Machinability criteria.....	25
2.3.3 Machinability of single crystal silicon.....	28
2.3.4 Machinability of OFHC copper	32
Chapter 3 Design of experimental facilities	35
3.1 Design and test of laser micro-machining equipment	35
3.1.1 Design of the machine	35
3.1.2 Test of the machine	36
3.2 Installation of laser assisted diamond cutting machine	41
3.2.1 Design of the machine	41
3.2.2 Alignment of laser and diamond tool axis	42
Chapter 4 A hybrid machining process combining laser grooving and diamond shaping	46
4.1 Introduction.....	46
4.2 Laser grooving of silicon	49
4.2.1 Influence of laser parameters on groove depth.....	49
4.2.2 Laser grooving experiment and result	53
4.3 Diamond shaping of grooves produced by laser grooving	57

4.3.1	Diamond tool alignment method	57
4.3.2	Diamond shaping with varying depth of cut.....	60
4.4	Summary	63
Chapter 5 Laser assisted diamond cutting of OFHC copper.....		64
5.1	Introduction.....	64
5.2	Surface defects of OFHC copper in diamond cutting.....	65
5.2.1	Experimentation.....	65
5.2.2	Results and discussion	67
5.3	Diamond cutting of OFHC copper assisted with laser heating .	80
5.3.1	Experimentation.....	80
5.3.2	Simulation of temperature distribution	83
5.3.3	Results and discussion	87
5.4	Summary	95
Chapter 6 Overall conclusions and suggestions for future studies.....		97
6.1	Overall conclusions.....	97
6.2	Suggestions for further studies	100
References..		102

List of figures

Figure 1.1 Schematic diagram of lenticular lens array	2
Figure 1.2 Schematic diagram of a conventional laser assisted turning system	4
Figure 2.1 The magnification of core component of diamond cutting machine	8
Figure 2.2 Mold insert and the injection-molded camera lenses for mobile phones (Zhang, et al., 2014)	10
Figure 2.3 Diamond turned aspheric lenses	10
(http://www.knightoptical.com/stock/optical-components/uvvisnir-optics/lenses/aspheric-lenses/diamond-turned-aspheric-lenses/).....	10
Figure 2.4 Types of diamond tools with different tool geometries (http://cloud.taipeitradeshows.com.tw/2013/timos/E-letter8/cont_p_6_4_1_taiwan.html)	11
Figure 2.5 Schematic of the micro and nano-cutting process	13
Figure 2.6 Comparison of the tool wear condition after machining Al6061 (left) and St1215 (right) (Lane et al., 2010)	16
Figure 2.7 Schematic diagram of laser assisted turning setup	18
Figure 2.8 An alternative configuration of LAM setup: (a) End view; (b) Side view	19
Figure 2.9 Illustration of laser assisted milling configuration	19
Figure 2.10 Schematic diagram of μ -LAM setup	20
Figure 2.11 Laser assisted micro-grooving setup.....	21

Figure 2.12 Laser assisted micro-milling setup	22
Figure 2.13 Factors affecting machinability (Stephenson et al., 2016)	24
Figure 2.14 The schematic diagram of crystal structure of single crystal silicon (http://course.bnu.edu.cn/course/ssphysics/html/5netketang/5netketang.htm)	29
Figure 2.15 Ductile-regime machining model (Blake and Scattergood, 1991) ...	29
Figure 2.16 Schematic diagram of damage fraction propagation during ductile- regime machining process (Blackley et al., 1991)	30
Figure 2.17 The influence of grain orientation on chip formation and surface quality of OFHC copper in diamond cutting process (Ding et al. 2012)	33
Figure 2.18 Schematic diagram of the Young's modulus along different direction of some cubic structured metals (Prohászka et al., 2006)	34
Figure 3.1 The schematic diagram of laser micro-machining setup	35
Figure 3.2 The actual picture of 2 μm pulsed laser controller and generator	36
Figure 3.3 The real picture of XY motion platform and Z motion platform.....	37
Figure 3.4 Three-axis CNC machine controller and stepping motor controller ..	38
Figure 3.5 The user interface of CNC controller software.....	38
Figure 3.6 The actual setup of visualization module	39
Figure 3.7 Actual picture of laser surface modification setup	40
Figure 3.8 Laser ablation marks on silicon workpiece surface	40
Figure 3.9 Design sketch of the laser assisted diamond cutting machine	41

Figure 3.10 Optoform30 ultra-precision CNC machine	43
Figure 3.11 The actual setup of the laser assisted diamond cutting machine	43
Figure 3.12 The schematic diagram of laser tool alignment method	44
Figure 3.13 The optical microscopic image of the laser heated spot and the tool mark.....	45
Figure 4.1 Schematic diagram of lenticular lens and mold insert.....	46
Figure 4.2 Illustration of the hybrid machining method	47
Figure 4.3 Flow chart of the hybrid machining process	48
Figure 4.4 Cross-section view of laser machined grooves on silicon workpiece surface	50
Figure 4.5 The influence of laser power on groove depth	51
Figure 4.6 The influence of scan speed on groove depth.....	51
Figure 4.7 Illustration of definition of defocus depth	52
Figure 4.8 The influence of defocus depth on groove depth.....	53
Figure 4.9 The procedure to determine defocus depth profile	54
Figure 4.10 Defocus depth profile for a lenticular lens groove depth of 50 μm ..	55
Figure 4.11 Defocus depth profile for a lenticular lens groove depth of 80 μm ..	55
Figure 4.12 Cross-section profile of laser machined groove (designed depth 50 μm)	56
Figure 4.13 Cross-section profile of laser machined groove (designed depth 80 μm)	56

Figure 4.14 Diamond cutting experimental setup	58
Figure 4.15 CCD camera captured image shows the tool alignment process	59
Figure 4.16 Schematic diagram of the alignment method between diamond tool and laser generated groove	59
Figure 4.17 Groove surface profiles after finish cutting with different cutting depth	61
Figure 4.18 Relationship between depth of cut and groove surface roughness ...	62
Figure 5.1 (a) Experimental setup; (b) Copper and brass workpiece; (c) Schematic of taper cutting; (d) and (e) Metallographic microstructure of copper and brass	66
Figure 5.2 The procedure of calculating surface roughness from a curved surface	68
Figure 5.3 Surface roughness at the bottom of the grooves at different depth of cut of copper and brass.....	69
Figure 5.4 Surface profile of micro-groove at different depth of cut measured by 3D optical surface profiler (OFHC copper)	70
Figure 5.5 Surface profile of micro-groove at different depth of cut measured by 3D optical surface profiler (C37700 brass).....	70
Figure 5.6 SEM image of surface defects: (a) and (b) ripple-like defects at depth of cut around 5 μm ; (c) and (d) delamination at depth of cut around 20 μm	71

Figure 5.7 Detail of the delamination in Figure 5.6(d) with enlarged scale	72
Figure 5.8 Other delamination defects found in this experiment.....	72
Figure 5.9 Superposition of the cross-section profiles of micro-groove at the depth of cut from 0 to 20 μm	74
Figure 5.10 Cutting chips at 20 μm depth of cut (a) OFHC copper; (b) C37700 brass	74
Figure 5.11 Optical microscopic image of machined groove surface of copper after chemical etching (a) depth of cut 3.7 μm ; (b) depth of cut 12.2 μm	75
Figure 5.12 Optical microscopic image of machined groove surface of brass after chemical etching (a) depth of cut 1.4 μm ; (b) depth of cut 16.2 μm	75
Figure 5.13 SEM image of machined groove surface of copper after chemical etching (a) and (b) depth of cut 3.7 μm ; (c) and (d) depth of cut 12.2 μm ..	76
Figure 5.14 Simulated effective strain of (a) OFHC copper and (b) C37700 brass	78
Figure 5.15 Stress contour along X direction (a) OFHC copper; (b) C37700 brass	79
Figure 5.16 The metallographic structure and hardness of copper	81
Figure 5.17 Laser assisted diamond cutting experimental setup.....	82
Figure 5.18 Schematic diagram of laser assisted diamond cutting experiment ...	83
Figure 5.19 Cross-section view of simulated temperature field distribution to a laser power of 4W	86

Figure 5.20 Cross-section view of simulated temperature field distribution to a laser power of 12W	86
Figure 5.21 Transient temperature distribution along line MN	87
Figure 5.22 Surface roughness of machined grooves with and without laser assistance.....	88
Figure 5.23 Surface quality of the grooves measured by Zygo at depth of cut around 19-20 μm : (a) no laser; (b) laser power: 4 W; (c) laser power: 12 W	88
Figure 5.24 Surface quality of the grooves measured by SEM at depth of cut around 19-20 μm : (a) no laser; (b) laser power: 4 W; (c) laser power: 12 W	89
Figure 5.25 Superposition of the cross-section profiles of micro-grooves at the depth of cut from 0 to 20 μm	90
Figure 5.26 Main force in cutting grooves with varying depth of cut	90
Figure 5.27 Schematic diagram of engineering stress strain curve of OFHC copper	91
Figure 5.28 Influence of temperature on true stress strain curve and strain hardening rate of OFHC copper (Shi and Zhu, 2006).....	94
Figure 5.29 Engineering stress strain curve of OFHC copper at different temperatures (https://www.copper.org/resources/properties/144_8/)	94

List of tables

Table 3.1 The specifications of laser device	37
Table 4.1 The influence of laser scan speed and laser power on groove depth ...	50
Table 4.2 The influence of defocus depth on groove depth	52
Table 5.1 The values of the simulation parameters	85

Chapter 1 Introduction

1.1 Background and motivation of the research

Diamond machining is an important method in manufacturing high precision components used in many areas, such as optical components and injection mold inserts. However, there are technical or economic restrictions on the use of single point diamond cutting tools such as in machining brittle materials or when a larger depth of cut is required. In this study, laser is used to assist machining in the single point diamond machining process. There are two parts of this study. Part 1 is an exploratory study on the use of diamond tools to perform the final shaping of a silicon groove roughly cut by a laser. The groove is first formed by laser machining and then followed by fine shaping with a diamond tool. In Part 2, the focus is on investigating the relationship between the depth of cut and the generation of defects of oxygen-free high conductivity (OFHC) copper at large depth of cut. The work concerns on the performance of laser heating on the reduction in surface defects in the diamond cutting of OFHC copper.

The lenticular lens is the key component of a commonly used autostereoscopic 3D-LCD display. A schematic diagram of a lenticular lens is shown in Figure 1.1. Conventionally, the lenticular lens is made of plastic using the injection molding method. However, the reliability and image quality of this kind of 3D-LCD display is

low, because the thermal expansion between lenticular lens and the LCD panel is different and causes location shift between them (Hiroshi et al., 2011). Lenticular lenses made of glass are therefore needed for high quality large 3D-LCD panels. Precision glass molding is a very promising method in the large-scale industrial production of lenticular lenses. The economic fabrication of the mold is crucial to lower the production cost.

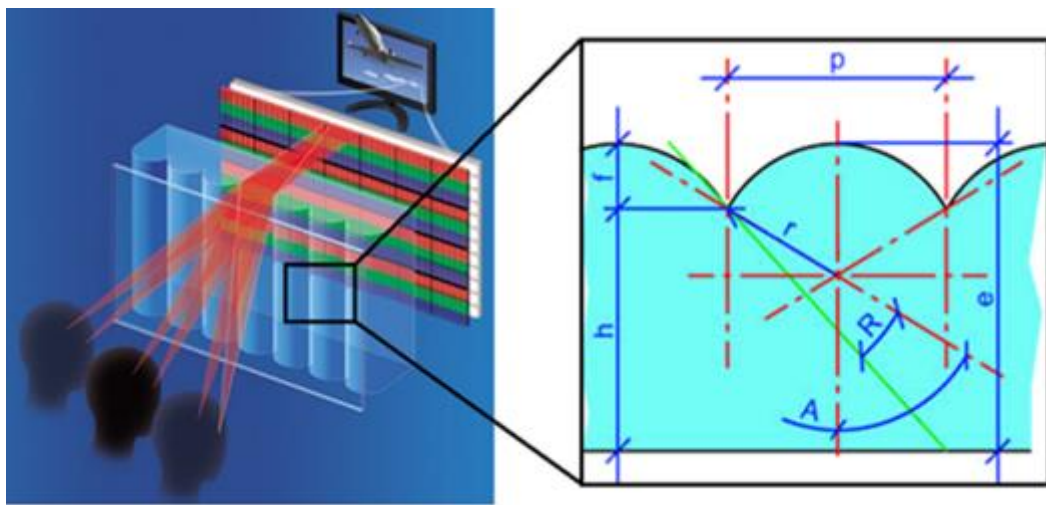


Figure 1.1 Schematic diagram of lenticular lens array

In the precision glass molding process, silicon is often used as the mold material due to the available processing methods and high thermal stability which brings about fast heating and cooling (Franssila, 2010). However, it is difficult to machine silicon due to its brittle nature. Cracks are easily formed on the machined surface in the diamond cutting of single crystal silicon. In order to suppress the formation of cracks, the depth of cut should be confined to a very small value. This value, which known as the critical depth of cut, is normally far less than $1\mu\text{m}$ for single crystal silicon (Fang et al., 2011).

This limits the efficiency of the diamond machining process. For the lenticular lenses that are used in commercial products, the value of f (shown in Figure 1.1) is normally in the range of tens of micrometers (Yeh et al., 2012). That means machining silicon mold inserts using the conventional method is very time consuming. In this research, we proposed a hybrid machining method to fabricate silicon lenticular lens mold inserts by combining laser grooving with diamond shaping. A feasibility study was conducted, and the experimental results show that it is possible to use this method to fabricate silicon lenticular lens mold inserts.

The second part of our research was to investigate the influence of laser heating on the cutting performance of OFHC copper in the diamond cutting process. Laser assisted machining (LAM) as a machining method uses a laser beam with high power density to heat the material in front of the cutting tool, and then remove the heated area using a conventional cutting tool when the temperature of this heated area reaches a desirable range. The cutting force and tool wear can be reduced while machining difficult-to-machine materials using the LAM method (Masood et al., 2011). Figure 1.2 shows the schematic diagram of a conventional laser assisted turning system (Abdulghani et al., 2013). In this system, the cylindrical workpiece is mounted on a rotational spindle, the laser beam is focused on the side surface of the workpiece, and the heated material is subsequently removed by a conventional cutting tool.

In recent years, a lot of work has been done in this area, but most studies focused on the conventional machining process resulting in low machining accuracy. Little research has been conducted in the ultra-precision machining process. This research was one of the pilot studies to investigate the laser heating effect on cutting performance in the diamond cutting process.

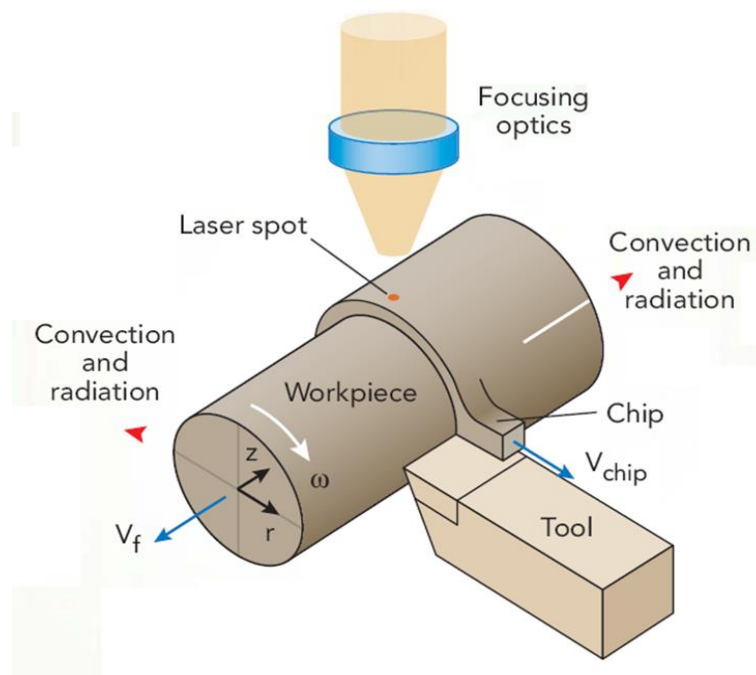


Figure 1.2 Schematic diagram of a conventional laser assisted turning system

OFHC copper is widely used in high power laser reflectors because of its superior electric and thermal conductivity which leads to a high laser damage threshold (Zhang and Zhang, 1997). Normally, OFHC copper is considered as a diamond machinable material. However, in the diamond cutting of OFHC copper process, the surface quality deteriorated rapidly with increasing depth of cut due to the formation of surface defects (Brinksmeier and Schmütz, 1997). This research investigated the reasons for the

formation of surface defects on OFHC copper in the diamond cutting process. To further understand the formation of these surface defects, laser heating was adopted during the diamond cutting process to investigate its influence on the improvement of the surface quality of OFHC copper at large depth of cut.

1.2 Research objectives

In this research, two aspects of using laser to assist machining were undertaken. Firstly, a hybrid machining process combining laser grooving and diamond shaping was proposed to fabricate lenticular lens mold inserts in order to improve machining efficiency as well as reduce tool wear. Secondly, laser heating was adopted in the diamond cutting of OFHC copper to investigate its influence of the cutting performance in the ultra-precision machining process. The main research objectives are:

- 1) To design and set up experimental facilities for laser micro-machining and laser assisted machining on a diamond turning machine.
- 2) To develop a hybrid machining process to machine lenticular lens mold inserts made of single crystal silicon. Firstly, laser grooving experiments were conducted to investigate the relationship between the laser parameters and the grooving depth. Secondly, diamond shaping was conducted on laser grooved silicon surfaces to investigate the influence of machining parameters on the surface quality of the grooves generated by this hybrid method.

3) To investigate the influence of laser heating on the cutting performance of OFHC copper in the diamond cutting process. Firstly, the formation of surface defects of OFHC copper in the diamond cutting process at different depth of cut, without laser heating, was investigated. Secondly, laser heating was adopted in the diamond cutting of OFHC copper to investigate its influence on the improvement of surface quality.

1.3 Organization of the thesis

This thesis consists of six chapters. The main content of each chapter is described below.

Chapter 1 is the introduction part. The background and motivation of this research are described and, research objectives are also proposed.

Chapter 2 is the literature review. A brief review of related knowledge and the state of the art in ultra-precision machining, and the laser assisted machining area are presented in this chapter.

Chapter 3 describes the process of establishing the experimental facilities, including designing and testing of the equipment.

Chapter 4 describes the hybrid machining process in machining lenticular lens mold inserts that combines laser grooving and diamond shaping. Laser grooving experiments and the subsequent diamond shaping process are presented in this chapter.

Chapter 5 presents the experimental work on laser assisted diamond cutting of OFHC copper. The reasons for the formation of surface defects and the effect of laser heating in the diamond cutting of OFHC copper are discussed in this chapter.

Chapter 6 is the conclusion part. The conclusions derived from this research are summarized, and suggestions for future work are given.

Chapter 2 Literature review

2.1 Ultra-precision diamond cutting

2.1.1 Introduction

Diamond cutting is an ultra-precision machining method for the fabrication of surfaces and microstructures with excellent quality and performance (Zhang et al., 2015). The diamond cutting process can produce mirror like surfaces with surface roughness less than ten nanometers and form accuracy in the order of $0.1\ \mu\text{m}$ (Davies et al., 2003). In the diamond cutting process, the cutting tool is fixed to a motion platform with several axes. The removal of material is realized by the relative motion between the rotated workpiece and the fixed diamond tool. (Brinksmeier et al., 2012).



Figure 2.1 The magnification of core component of diamond cutting machine

Figure 2.1 shows an actual picture of the core component of an ultra-precision diamond cutting machine. With the development of machining technology and machine tools, diamond cutting is now a highly reliable material processing method and can achieve extremely fine surface finish and high form accuracy on various of materials, such as some kinds of copper alloys, aluminum alloys, PMMA and precious metals (Brinksmeier et al., 2012). Diamond cutting is mainly used to fabricate components for advanced applications that require excellent surface finish and minimized form error. These applications can be found in such industries as aerospace, electronics, semiconductor and biomedical etc. (Zhang et al., 2014). There are a variety of precision components that can be fabricated by diamond cutting. Major product components include optical components like reflectors and lenses, which are mostly machined directly from the stock material.

Diamond cutting has now been applied to the manufacture of mold inserts for the mass production of high-quality plastic lenses using injection molding method. Figure 2.2 shows a photograph of an injection mold insert and the injection-molded camera lenses for mobile phones (Zhang et al., 2014). Figure 2.3 shows the diamond turned aspheric lenses that are typically used in certain optical systems, such as night vision goggles and missile guidance systems (Knight Optical Website).



Figure 2.2 Mold insert and the injection-molded camera lenses for mobile phones

(Zhang, et al., 2014)



Figure 2.3 Diamond turned aspheric lenses

(<http://www.knightoptical.com/stock/optical-components/uvvisnir-optics/lenses/aspheric-lenses/diamond-turned-aspheric-lenses/>)

2.1.2 Diamond tools

Normally, the diamond tools that being used in ultra-precision machining are made of single crystal diamond. As diamond is anisotropic, its mechanical properties vary dramatically along different crystallographic planes and orientations, in particular the corresponding wear resistance is significantly different (Zong et al., 2010). So it is important to choose the right plane and orientation in order to get a better performance of the diamond tools when used to cut materials. According to the research work of Pramanik (2009), the rake face of a diamond tool with a $\langle 110 \rangle$ crystal orientation performs better than that of $\langle 100 \rangle$ crystal orientation in terms of wear resistance, surface finishing, and cutting force.



Figure 2.4 Types of diamond tools with different tool geometries

(http://cloud.taipeitradeshows.com.tw/2013/timos/E-letter8/cont_p_6_4_1_taiwan.html)

Due to the exceptional hardness of diamond, there is no way to fabricate diamond tools using the cutting method. Typically, for a normal shaped diamond tool it is made by mechanical polishing. For a complex shape or a micrometer and nanometer scale diamond tool, using a focused ion beam is an effective way to fabricate it (Orloff et al., 2003). Figure 2.4 shows different types of diamond tools, with different tool geometries, that are used in ultra-precision diamond cutting machines.

2.1.3 Material removal

As schematically illustrated in Figure 2.5, in the micro and nano cutting process, the uncut chip thickness a is comparable to the cutter radius r , which is typically the situation in ultra-precision diamond cutting, the undeformed chip thickness a is no longer distinguished from the tool edge radius r , compared with conventional machining. The shear plane model (Ernst et al., 1941) that was established for conventional machining may not be applicable in diamond cutting process any more, as this model assumed that the tool has perfect edge sharpness.

In the ultra-precision diamond cutting process, because the undeformed chip thickness is typically in the order of several micrometers, the size effect cannot be neglected (Zorev 1966). Size effect is claimed to be attributed to many factors, including subsurface plastic flow (Nakayama et al., 1968), strain inhomogeneity (Shaw 1980),

extensive plastic deformation (Moriwaki et al., 1989), material plowing and elastic recovery (Lucca et al., 1991), and strain gradients (Liu et al., 2006). The tool edge radius in return has an influence on the cutting force (Masuko 1956), cutting energy (Bitans et al., 1965), and minimum uncut chip thickness (Ikawa et al., 1991).

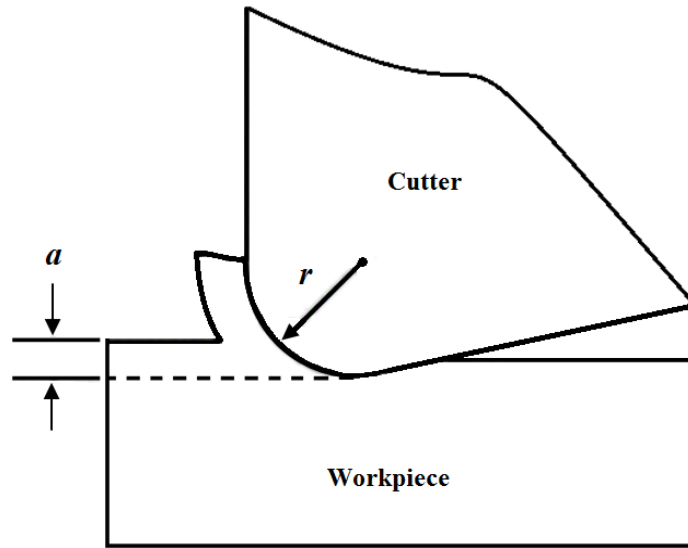


Figure 2.5 Schematic of the micro and nano-cutting process

2.1.4 Surface finish

Form accuracy and surface roughness are two main factors that govern the functionality and performance of many optical components. With the diamond cutting method, extremely high form accuracy within the sub-micrometer range and low surface roughness within a few nanometers can now be achieved on many engineering materials, such as copper and aluminum alloys. In diamond cutting, form accuracy is affected by many factors, such as machine accuracy, programming accuracy, setup accuracy,

cutting-edge quality, tool wear, operating temperature, humidity and stability conditions.

On the other hand, the surface roughness is largely dependent on the tool nose radius and the feed rate, however it is still largely affected by other machining parameters, such as tool rake angle, tool wear condition, depth of cut, machine dynamics, and material properties (Zhang et al., 2015). The theoretical surface roughness due to feed marks is expressed as follows (Vyas et al., 1999):

$$R_{th} = \frac{f_r^2}{8r_n}$$

Here, f_r denotes the feed rate, and r_n denotes the nose radius of the diamond tool.

From this equation, it can be predicted that the surface roughness will be reduced by increasing the nose radius, but the experimental surface roughness values are usually several times larger than the theoretical ones. Hence, there are clearly other factors that affect the surface roughness which are not accounted for in this formula. Taking into account all those factors might work to some extent, but considering the complexity in real industrial situations, it is impractical in terms of the time and calculation effort needed.

The ultra-precision diamond cutting process always induces residual stress onto the surface and into the subsurface region of the workpiece through surface plastic deformation. It is governed by factors such as depth of cut, tool geometry, and tool wear condition. Residual stress is detrimental to the parts produced in terms of fatigue

strength, corrosion resistance, and form accuracy (Brinksmeier et al., 1982). During ultra-precision diamond cutting process, the machined surface is deformed plastically and elastically when the workpiece is subjected to material removal. Due to the tool edge radius effect, when the chip is formed continuously through plastic deformation, the machined surface is unavoidably subjected to elastic deformation. After the tool moves on, the machined surface will recover elastically to the original position. Elastic recovery is detrimental, as it will cause the formation of burrs and deterioration of the surface finish (Liu et al., 2007).

2.1.5 Tool wear

The wear conditions of diamond tools have a direct influence on machining performance during diamond cutting. If the diamond tool is worn, the surface quality and form accuracy are likely to be worsened, while the cutting force and vibration during cutting are likely to be higher. For some soft and non-ferrous metals, such as copper and aluminum, the diamond tool wear develops very slowly and steadily. High-quality surface finish can be achieved even after the continuous cutting of several hundred kilometers (Zhang et al., 2014). For some hard materials, such as hard alloys and ferrous metals such as steel, the diamond tool wear rate is very high. Even after a very short distance of cutting, the diamond tool might wear out.

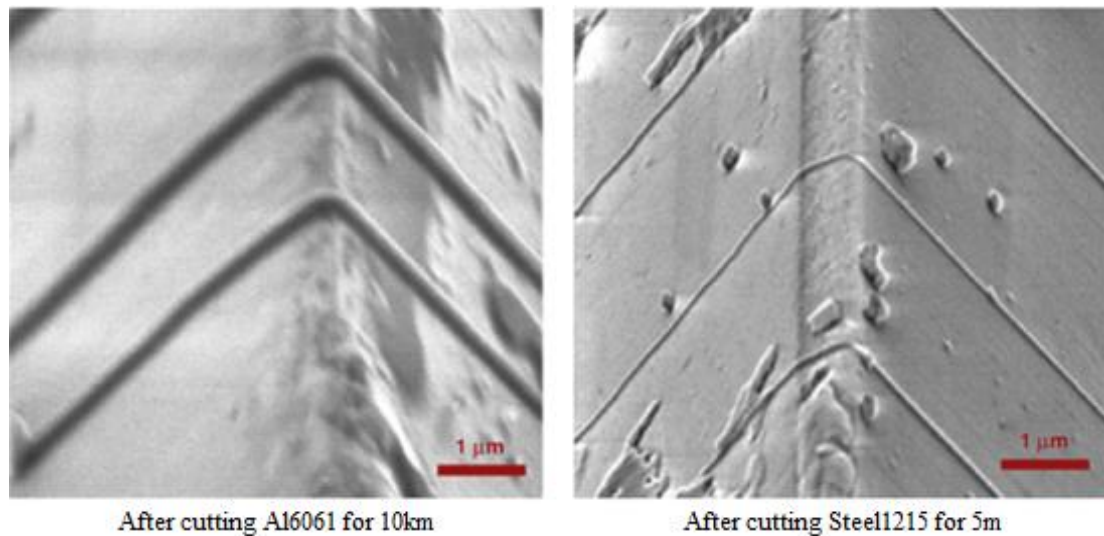


Figure 2.6 Comparison of the tool wear condition after machining Al6061 (left) and St1215 (right) (Lane et al., 2010)

Figure 2.6 shows the tool wear status after a certain length of cut of aluminum 6061 and steel 1215 (Lane et al., 2010). From this picture, it can be clearly seen that even when the cutting length of steel was only 5 m, its tool wear was much more serious than the tool used to cut aluminum for a distance of 10 km. It is believed that when cutting ferrous metals, the tribochemical aspect plays a dominant role, and can be subdivided into three types: diffusion wear, oxidation, and catalyzed graphitization (Evans et al., 1991).

2.2 Laser assisted machining (LAM)

2.2.1 Introduction

LAM has emerged as an alternative machining method that can provide improved machining performance while machining difficult-to-cut materials, such as hard alloys and ceramics. LAM uses a high power laser beam to heat the material ahead of the cutting tool during the cutting process. Most of the hard materials become softer when they are heated up. Therefore, the cutting force and tool wear during the cutting process can be reduced. According to the size of the laser spot and the heat affected zone, LAM can be categorized as macroscale LAM and microscale LAM. For the macroscale LAM, the laser spot diameter is in the order of several millimeters, while for the microscale LAM, it is of the order of tens of micrometers.

2.2.2 LAM at the macroscale

LAM at the macroscale has been investigated extensively, and the workpiece materials were usually hard alloys and ceramics. The most typical application of laser beam heating in the machining process is laser assisted turning. Figure 2.7 shows the schematic diagram of a laser assisted turning setup (Amin and Ginta, 2014). In this diagram, the laser beam is designed to normal to the workpiece surface. The parameters that can affect the machining process are the laser power density, laser spot diameter, incident angle, and the distance between the laser beam and cutting tool.

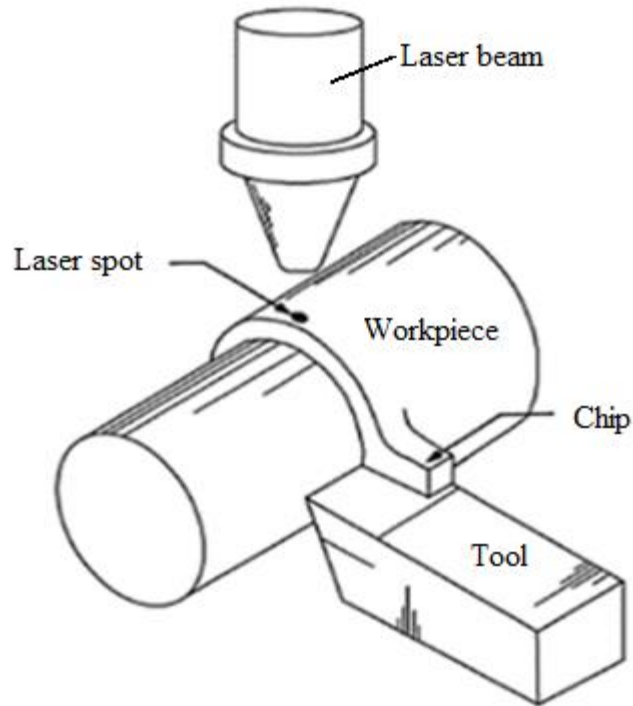


Figure 2.7 Schematic diagram of laser assisted turning setup

This setup is relatively easy to realize because both the laser equipment and cutting tool are fixed. However, there are also disadvantages for this configuration, for example, the heating efficiency is relatively low, therefore, a large power laser is required to achieve a desirable temperature in the cutting area. Another alternative configuration is to let the laser beam perpendicular to the cutting plane as illustrated in Figure 2.8 (Sun et al., 2008). For this setup, the heating efficiency of laser beam is higher than in the previous one since the heating area of this setup is more confined to the cutting area, and will be immediately removed by the cutting tool.

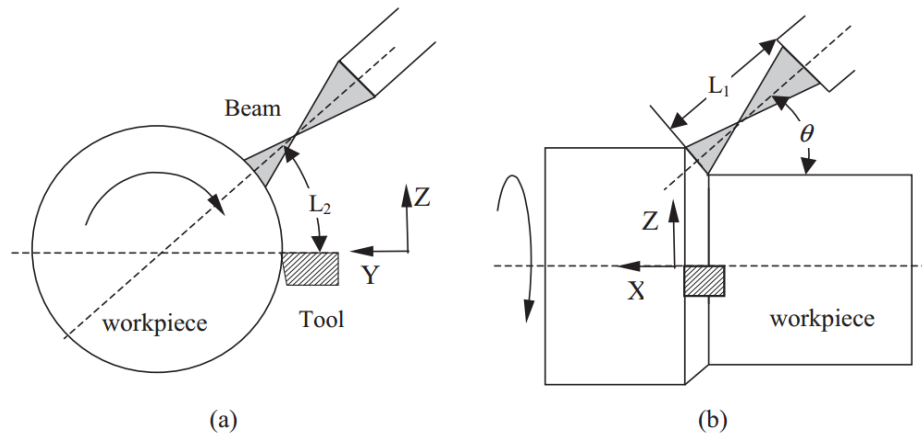


Figure 2.8 An alternative configuration of LAM setup: (a) End view; (b) Side view

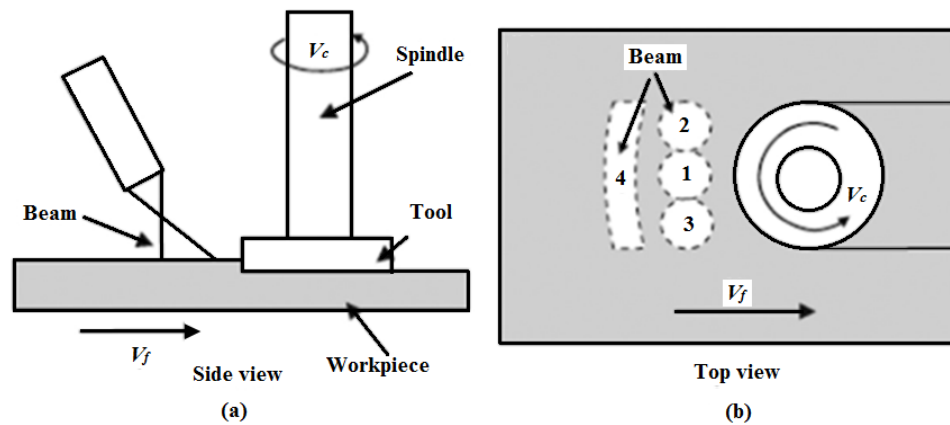


Figure 2.9 Illustration of laser assisted milling configuration

Laser assisted milling is a more complex process because the tool is rotating during the milling process. Generally, for surface milling, the laser beam is located in front of the milling tool along the feed direction. For laser assisted milling at the macroscale, the spot size of the laser heated area is normally smaller than the milling tool, which makes it impossible to have the heated area cover the whole milling area as shown in Figure 2.9 (Sun et al., 2008). Another configuration is just using a line beam with high power that can cover the milling width (position 4) (Thomas & Vigneau, 1999).

2.2.3 LAM at the microscale

LAM at the microscale has been used for machining both brittle materials and hard alloys. Ravindra et al. (2012) used an infrared laser to assist the cutting of brittle materials at the microscale. They reported that for similar applied loads, the LAM method could generate greater depth of cut compared with conventional cutting processes, and the schematic diagram of the equipment used is shown in Figure 2.10. In this setup, the diameter of the laser beam was around $10\ \mu\text{m}$, the laser beam transmitted through an optical fiber and passed through the diamond tool which enabled the laser beam to irradiate the workpiece material at the tool workpiece interface.

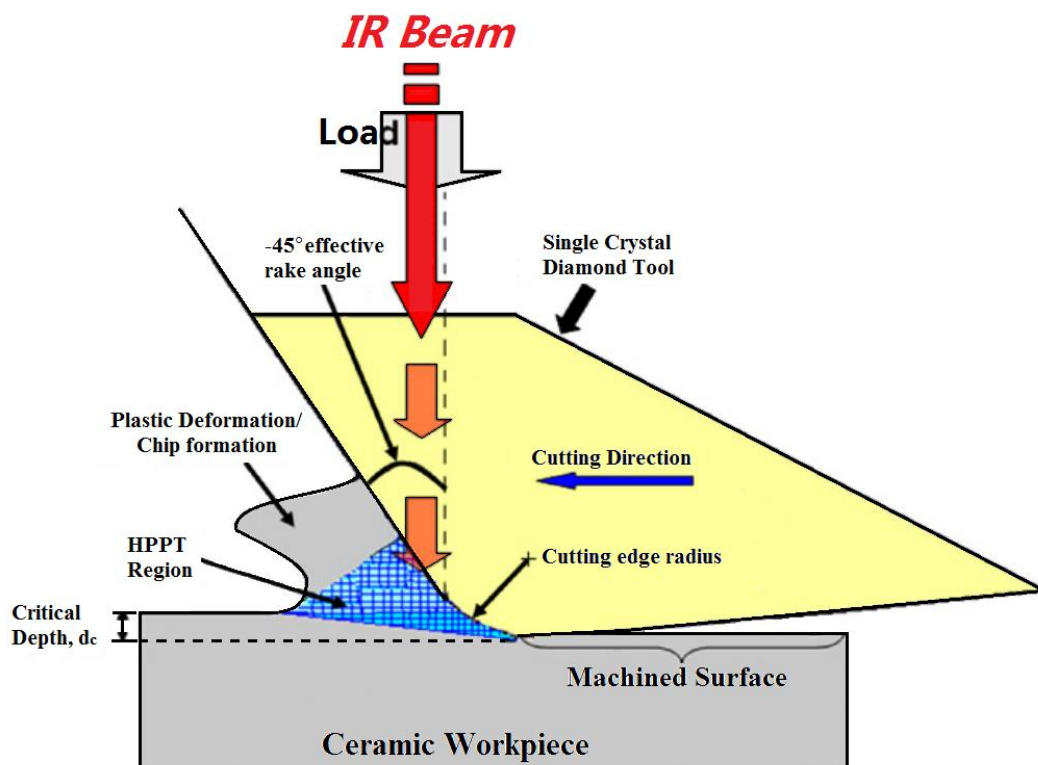


Figure 2.10 Schematic diagram of μ -LAM setup

Singh et al. (2007) conducted a research to take advantage of the thermal softening effect induced by laser heating in a micro-grooving process, and developed a two-axis laser assisted micro-grooving device, as shown in Figure 2.11. They reported that the reduction of the cutting force could reach 56% when using this setup to cut H13 tool steel with the assistance of a 35 W fiber laser. Kumar et al. (2011) developed a laser assisted micro-milling device, as shown in Figure 2.12. They used this setup to perform a series of micro LAM experiments on A2 tool steel. A maximum of 69% reduction of cutting force when using a laser to assist milling when compared with conventional milling processes was reported. They also reported that the amount and rate of tool wear, as measured by the rounding of the tool corners, were significantly lower with laser assistance than without laser assistance.

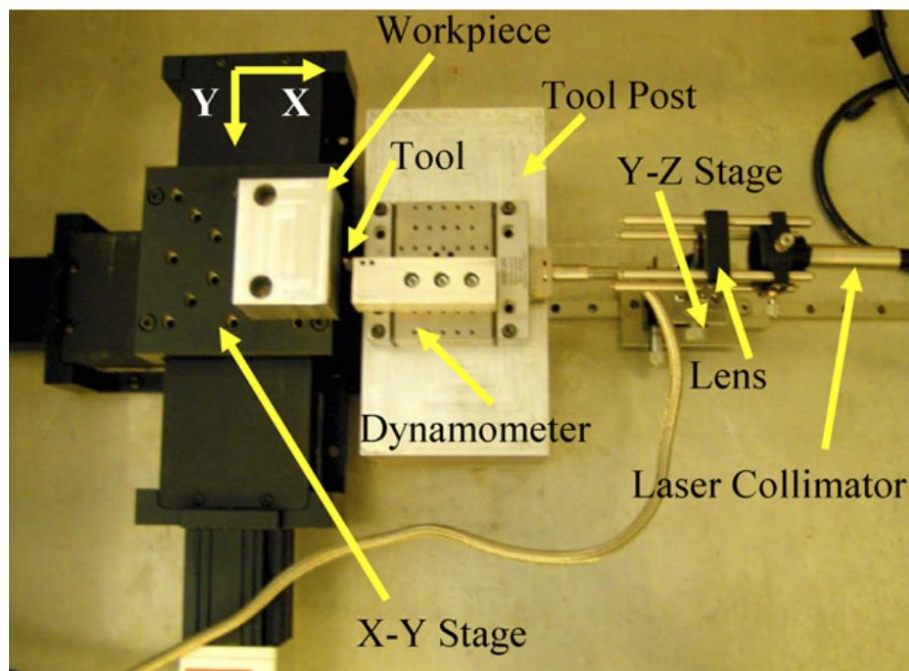


Figure 2.11 Laser assisted micro-grooving setup

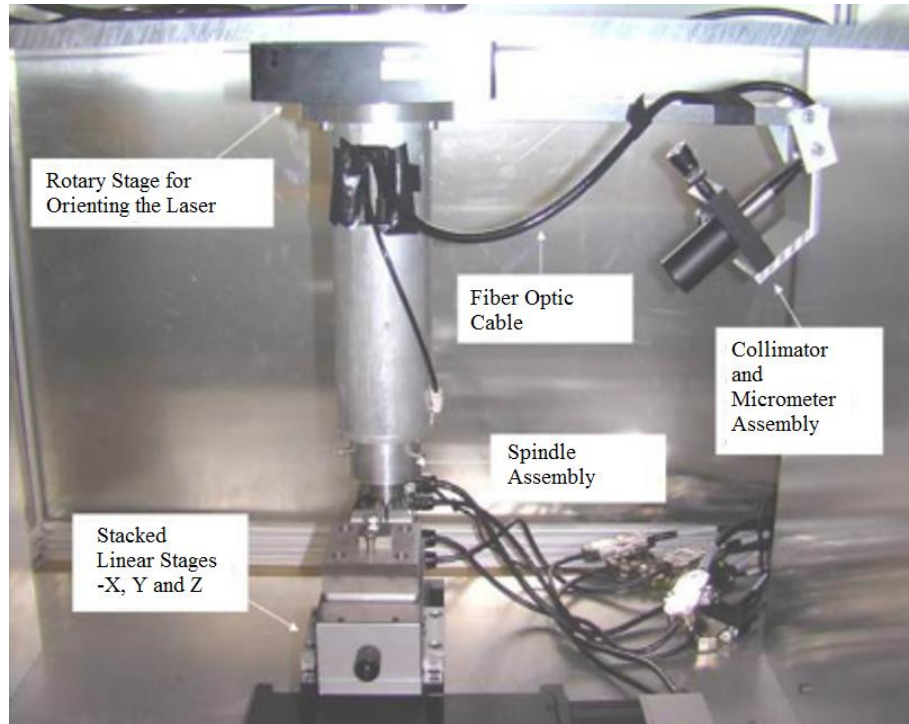


Figure 2.12 Laser assisted micro-milling setup

Despite there being extensive research on the use of lasers to assist in machining difficult-to-machine materials both in the macroscale and microscale, most of these research studies took advantage of the thermal softening effect of difficult-to-machine materials and aimed at reducing the cutting force and tool wear. Few research has taken the machined surface quality into consideration, which is a key parameter in precision machining. Further, most previous research focused on hard and brittle materials, and attention has been rarely paid on the influence of the laser heating effect on some soft but still unsatisfactory machinability materials such as OFHC copper on the diamond machining process. OFHC copper is generally considered as a diamond machinable material with extremely low tool wear rate. However, the machined surface quality of

OFHC copper is unsatisfactory at some cutting conditions, especially when the depth of cut is a little bit high (Brinksmeier et al., 1997). In this research, the influence of laser heating on the diamond machining of OFHC copper was investigated, to enhance our understanding of the influence of thermal effects on the machinability change in soft materials. It can also provide an alternative method for designing suitable experiment parameters in manufacturing practice in order to enhance both machining efficiency and machined surface quality in ultra-precision machining.

2.3 Machinability

2.3.1 Introduction

In the area of metal machining, the term “machinability” means the ease or difficulty with which a material can be machined (Armarego et al., 1969). However, machinability is not purely an intrinsic property of a material. It is influenced by both the material properties and machining conditions, and the important factors include chemical composition, microstructure, mechanical and physical properties of the work material, machine tool condition, cutting fluid and cutting conditions. All these factors influence the performance of a machining process as well as the surface roughness of machined components. Figure 2.13 shows some of the factors that can affect machinability.

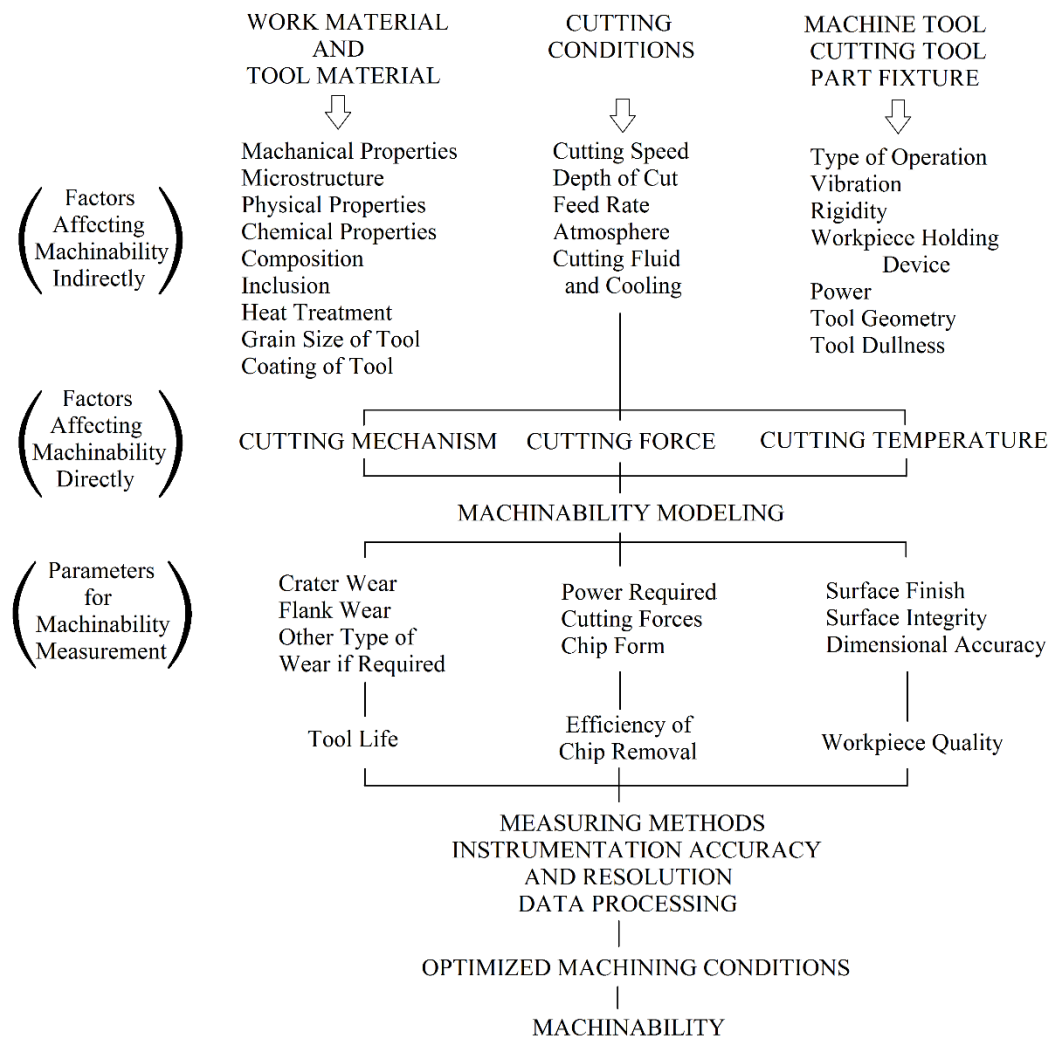


Figure 2.13 Factors affecting machinability (Stephenson et al., 2016)

Since the machinability of a material is concerned with both the material properties and cutting conditions, the machinability rating should depend on the test conditions and parameters chosen to quantify the results. Because there are so many criteria that could be used to assess the machinability of work material, from different aspects, each criteria may give different results in assessing the machinability of a work material at the same cutting condition. For example, work material from same material family may require similar specific cutting energy to remove the material but may result in different

tool wear rate due to the different distribution pattern of the abrasive particles in the matrix. Thus, when using machining power consumption criteria, the materials are assessed to have similar machinability, while when using tool wear rate criteria, there would be remarkable differences in machinability. Also, when the cutting condition is changed, the machinability of the work material assessed by a certain criteria can also change.

Despite the complex situation in assessing the machinability of work material, there is always a primary factor that we care about most in industrial machining practice, which can be used as the main consideration in rating the machinability of work materials. In many cases, the overall machining cost, which primarily depends on tool wear rate under certain cutting conditions, is the main concern in manufacturing processes. The rating of machinability therefore can be achieved by testing the tool life. Other criteria may also be used in assessing the machinability of work material, and are discussed in the following section.

2.3.2 Machinability criteria

There are many factors that could be used to assess the machinability of a material at a given machining condition, and the most commonly accepted ones are as follows (Trent et al., 2000):

(1) Tool life or tool wear rate.

Tool life is defined as the amount of material being removed by a tool, under certain cutting conditions, before the cutting performance of the tool deteriorates to a predefined level. Tool life is the most commonly used and also most meaningful machinability criterion (Groover and Mikell, 1976). Both the machining cost and machined part surface quality are dramatically influenced by tool wear. When the tool wear rate under a given machining condition is decreasing, the machinability will increase. Since the tool wear rate is always associated with the machining conditions, when the machining condition changes, the tool wear rate will change.

(2) Cutting force or power consumption.

Cutting force is directly related to power consumption or specific cutting energy. There are mainly two reasons for choosing cutting force or power consumption as a criterion to assess the machinability of materials. Firstly, in the metal cutting process, cutting force directly reflects the difficulty of a material to be machined; a low cutting force corresponding to good machinability. Secondly, from the point of view of machining cost, a lower cutting force means less energy is required to remove unit volume of material, which means the overall machining cost should be lower. Though both the main cutting force and the thrust cutting force could be used in the rating of machinability, a more popular way is the use of a combination of two force components.

The advantage of using cutting force or power consumption as an indicator of machinability is that it is not sensitive to the tool material and is mainly determined by the workpiece material properties.

(3) Chip formation or chip shapes.

Machinability can be reflected by the shape of the cutting chips formed during the machining process. Materials that form short chips are more favorable in the machining process than those that produce long, difficult to break chips or powder like chips. Machinability rating based on chip shape is quite qualitative and therefore not widely used.

(4) Machined part surface quality.

The surface quality of a machined part under a given machining condition can also be used as a criterion to rate machinability. Generally, there is a positive correlation between the surface quality of machined parts that can be achieved under a given machining condition and machinability. The most commonly used parameter in describing surface quality is surface roughness (Ra). However, the rating of machinability according to surface quality sometimes leads to difficulties in determining the differences in machinability between different materials under certain machining conditions. For example, in ultra-precision machining process, the surface quality of machined copper and brass parts mainly depends on the quality of the

diamond tool cutting edge and is hardly influenced by the material properties when at a small depth of cut. Thus, the differences in machinability between copper and brass using the surface quality criterion cannot be determined.

2.3.3 Machinability of single crystal silicon

Single crystal silicon, also called monocrystalline silicon, is the most important semiconductor material. The crystal lattice in single crystal silicon is continuous, unbroken to its edges, so there are no grain boundaries inside the single crystal silicon solid (Wikipedia: monocrystalline silicon). The crystal structure of single crystal silicon is shown in Figure 2.14, which is face centered cubic, the same as the structure of a diamond. Silicon is a brittle material which exhibits low fracture toughness, make it prone to fracture rather than plastically deform when being machined (Goel et al., 2015). However, it is still possible to machine single crystal silicon at a fine depth of cut of less than 1 μm using appropriate machining parameters, and the chips are generated through plastic deformation instead of fracture. This kind of machining method is called ductile-regime machining (Goel et al., 2015). There exists a critical value of depth of cut, when the cutting depth is smaller than this value, there will only be plastic deformation, otherwise brittle fracture will occur.

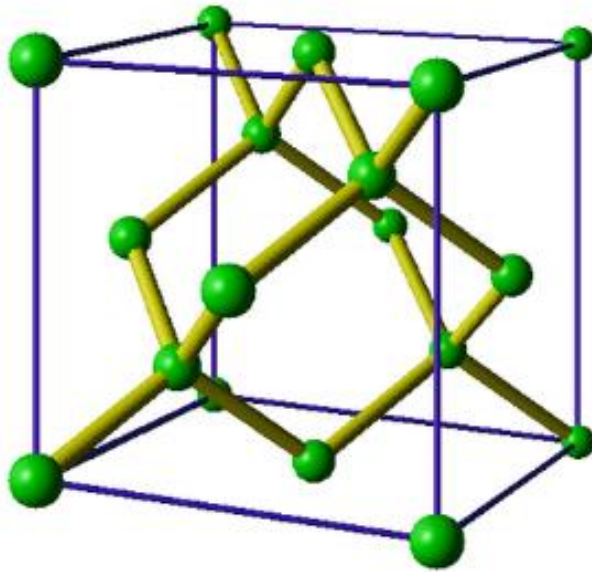


Figure 2.14 The schematic diagram of crystal structure of single crystal silicon
 (<http://course.bnu.edu.cn/course/ssphysics/html/5netketang/5netketang.htm>)

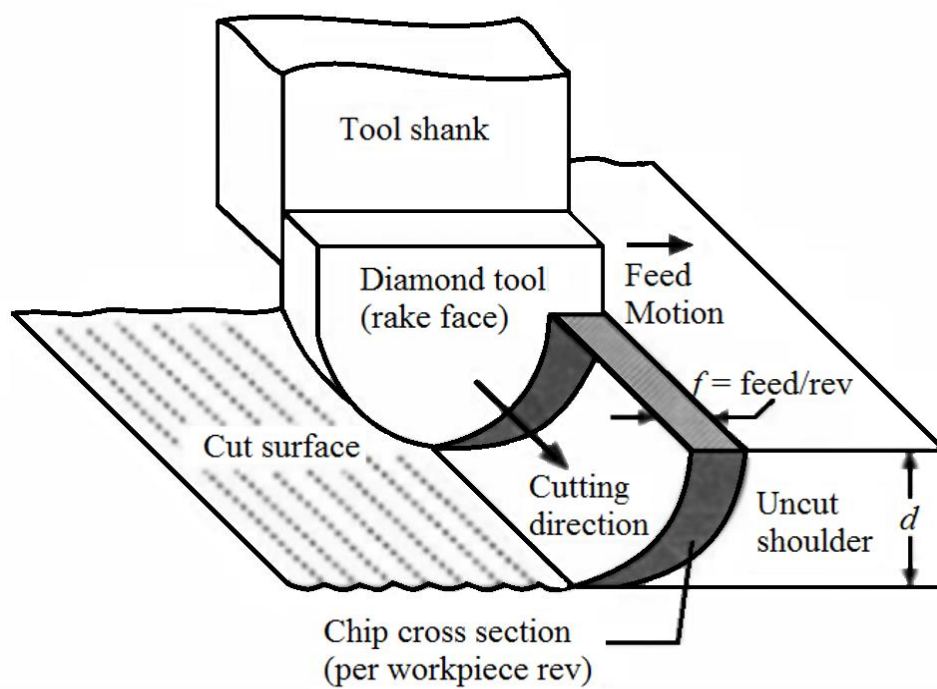


Figure 2.15 Ductile-regime machining model (Blake and Scattergood, 1991)

Figure 2.15 and Figure 2.16 show the schematic diagram of the brittle-ductile transition model when using a round nose diamond tool to cut brittle materials (Blake and Scattergood, 1991). As shown in Figure 2.16, f is feed rate, R is diamond tool nose radius, t_c is critical chip thickness, y_c is crack length, and W_d is the horizontal component of the distance between the tool nose center and the critical chip thickness. In Blake et al.'s model, they suggested that a smooth surface free from fracture damage is achievable even with brittle fractures in the cutting area, as long as the brittle fractures do not reach the final machined surface. The micro cracks in the remaining area of the uncut shoulder is removed by the diamond tool in the following cutting process, so the fractures will not affect the final surface (Goel et al., 2015).

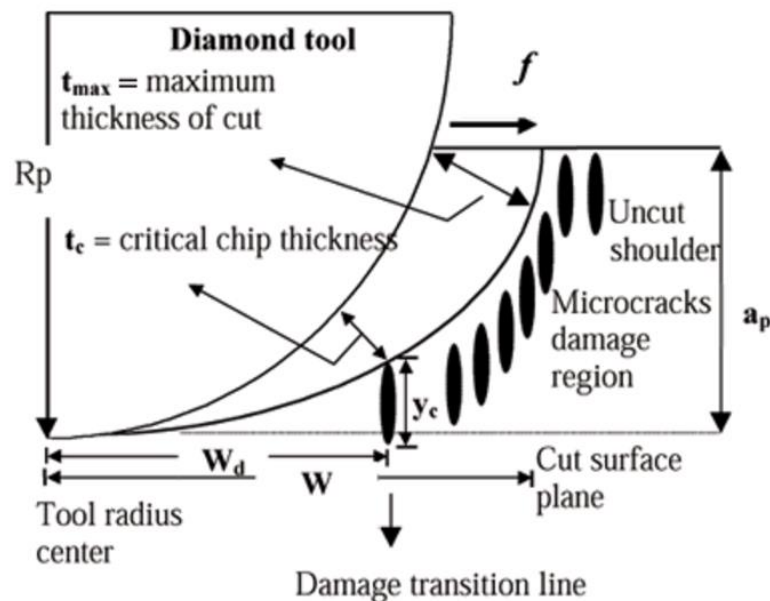


Figure 2.16 Schematic diagram of damage fraction propagation during ductile-regime machining process (Blackley et al., 1991)

The occurrence of the brittle-ductile transition phenomenon in brittle materials during the diamond cutting process provides a promising way of using the diamond cutting method to machine single crystal silicon in a ductile regime which not only improves the machined surface quality but also increases the machining efficiency. Much research work has been done on the ductile-regime machining of single crystal silicon in terms of both experimental study and molecular dynamics simulation. In the diamond cutting of brittle materials, the critical depth of cut is a very important parameter since it directly indicates the maximum potential material removal efficiency. One approach in previous research was in trying to increase the critical depth of cut of single crystal silicon by modifying its surface structure. According to the work of Fang et al. (Fang et al., 2011), they achieved a critical depth of cut of 923.566 nm on a modified silicon surface by fluorine ion implantation compared with that of unmodified silicon of 236 nm. The tool wear during diamond turning of the modified silicon surface was also reduced. A similar experiment from To et al. (To et al., 2013) also confirmed the availability of using the hydrogen ion implantation method to improve the machinability of single crystal silicon. All these experiments revealed that it is possible to improve the machinability of brittle materials, such as single crystal silicon, by modifying their surface structures. Since the ion implantation process is costly, its application is limited. Besides, the effective layer thickness of ion implanted silicon is typically around several micrometers, at maximum. It is of little help in fabricating structures with feature size in the range of tens of micrometers which is typically the

size of lenticular lens. Therefore other methods may need to be developed to fabricate lenticular lens mold inserts.

2.3.4 Machinability of OFHC copper

Unlike single crystal silicon, which is brittle and easy to crack when machining, OFHC copper is a soft material that is easy to deform under an applied load. OFHC copper is generally considered as a diamond machinable material. When machining OFHC copper with a diamond tool, the tool wear rate is extremely low, and a mirror like surface can be achieved under well-controlled cutting conditions. However, the machining performance of OFHC copper is highly sensitive to the cutting parameters and material microstructure. Ding et al. (2012) investigated the influence of crystallographic effects on the cutting performance of polycrystalline OFHC copper using diamond micro-tools. It was found that the machined surface quality, cutting force and chip formation were highly dependent on the crystal orientation and cutting depth, as shown in Figure 2.17. The fact that the cutting performance is highly sensitive to crystal orientation is due to the anisotropic behavior of OFHC copper. Figure 2.18 shows the schematic diagram of the Young's modulus along different direction of some cubic structured metals. It can be seen that Young's modulus of copper is highly anisotropic in different directions. Because the lattice structure of copper is face-centered cubic (FCC), the packing densities of atoms differ in different directions, thus its elastic and

plastic properties are strongly directionally dependent. Brinksmeier and Schmütz (1997) performed a plunge-cut experiment with a gradually increased depth of cut from 0 to 10 μm . It was found that a smooth surface could be obtained at a depth of cut smaller than 2 μm . When the depth of cut was larger than 2 μm , the machined surface quality deteriorated rapidly due to the formation of surface defects in the form of dents and ripples. Since the formation of these defects was always accompanied with big fluctuations of cutting force, it was suspected that a high cutting force would induce the formation of surface defects. With laser assistance, the cutting force can be reduced in machining process, therefore it would be helpful to suppress the formation of surface defects of OFHC copper by using laser heating to assist machining in the diamond cutting process.

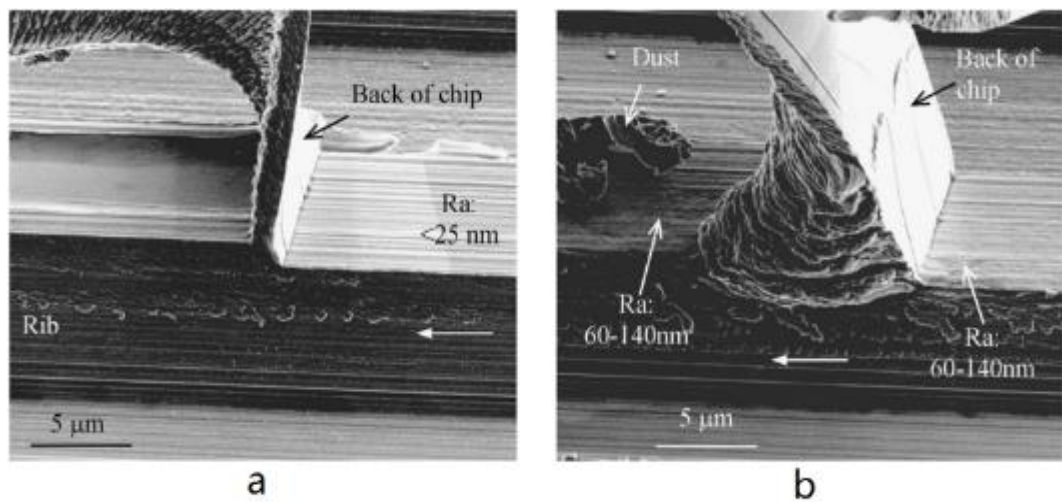


Figure 2.17 The influence of grain orientation on chip formation and surface quality of OFHC copper in diamond cutting process (Ding et al. 2012)

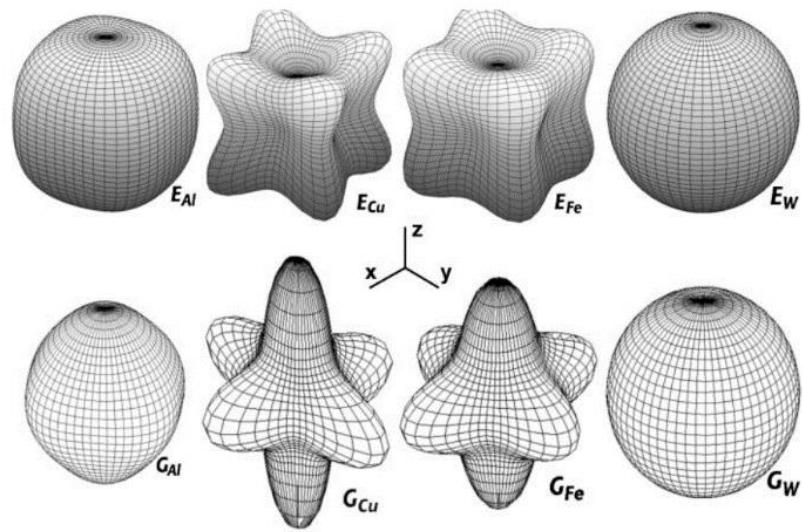


Figure 2.18 Schematic diagram of the Young's modulus along different direction of some cubic structured metals (Prohászka et al., 2006)

Chapter 3 Design of experimental facilities

3.1 Design and test of laser micro-machining equipment

3.1.1 Design of the machine

In this research, in order to investigate the influence of laser parameters on the profile of laser machined grooves on a silicon workpiece, a laser micro-machining setup was established. Figure 3.1 shows the schematic diagram of this laser micro-machining setup, which is mainly composed of three parts: (I) three-dimensional motion platform; (II) laser controller and transmission module; (III) visualization module.

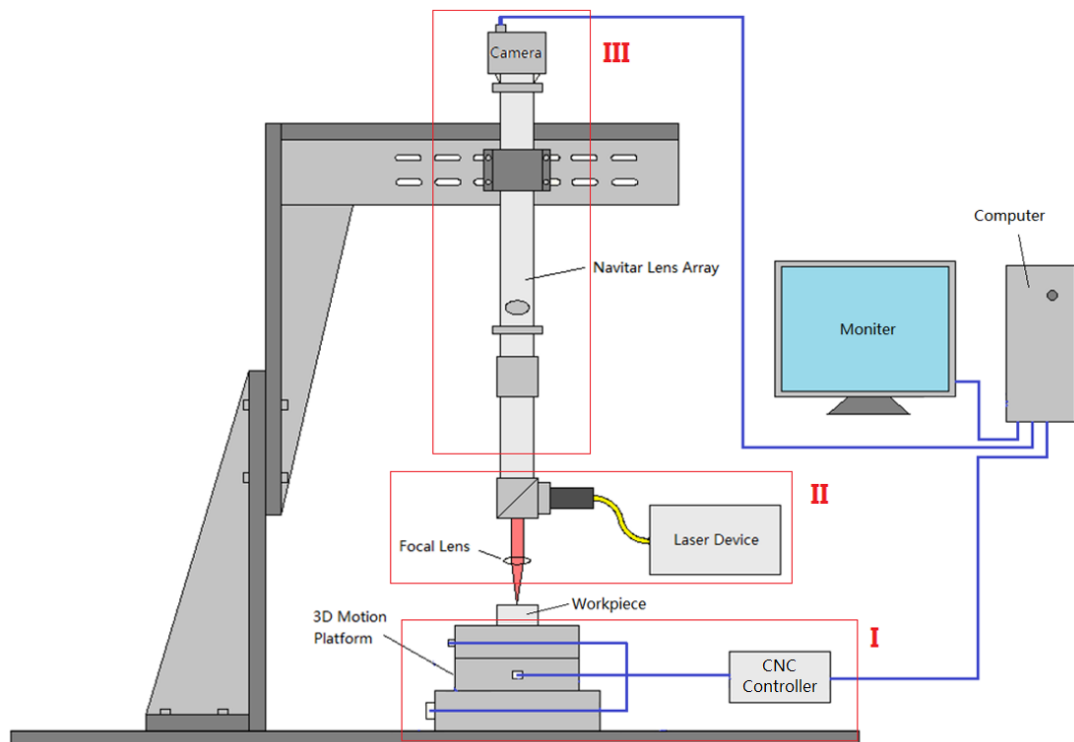


Figure 3.1 The schematic diagram of laser micro-machining setup

During the laser micro-machining process, the workpiece is placed on the three-dimensional motion platform. The laser beam that passes through a fiber optic cable is divided into two beams when it goes through the beam splitter; one is transmitted horizontally while another is transmitted vertically. The vertical beam is then focused by a focal lens. The distance between the workpiece and the focal lens can be adjusted by controlling the movement of the three-dimensional motion platform, therefore the desired laser spot size that irradiates onto the workpiece surface can be obtained.

3.1.2 Test of the machine

The laser used in this laser micro-machining experiment was a nanosecond pulsed fiber laser with a wavelength of 2 μm . Table 3.1 lists the specifications of the laser device.

Figure 3.2 shows the actual picture of the laser device.



Laser controller



Laser generator

Figure 3.2 The actual picture of 2 μm pulsed laser controller and generator

Table 3.1 The specifications of laser device

Parameter	Unit	Value
Operation mode	-	Pulsed
Wavelength	nm	2000
Max. average power	W	10
Max. pulse energy	mJ	0.333
Pulse width	ns	30
Pulse repetition rate	Hz	30000

The three-dimensional motion platform comprises a Z axis motion platform and an XY motion platform. The travel range of the Z platform is 10mm, and for the XY platform, it is 50 mm. The repeatability of these two platforms is 0.5 um. Figure 3.3 shows the actual picture of the two motion platforms.

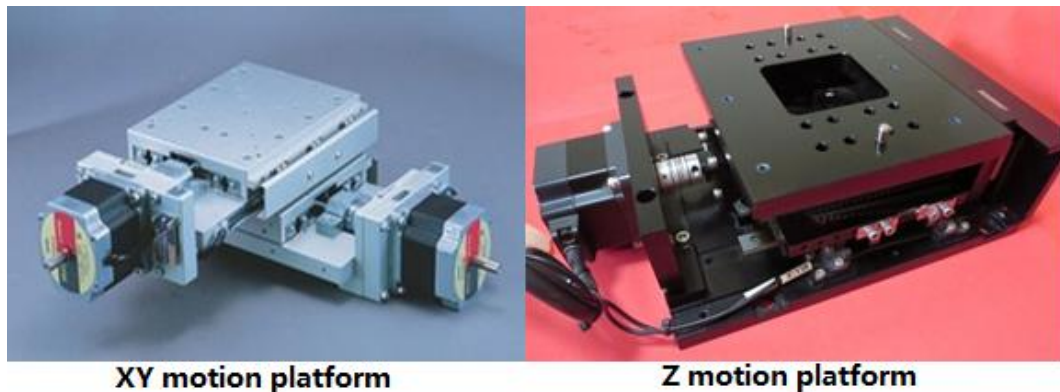


Figure 3.3 The real picture of XY motion platform and Z motion platform

Each axis of these platforms is driven by a 5-phase stepping motor. These three stepping motors are then controlled by a three-axis CNC machine controller and three stepping motor controllers, as shown in Figure 3.4. The standard G-code file is capable of

controlling the movement of the motion platform. Figure 3.5 shows the user interface of the controller software.

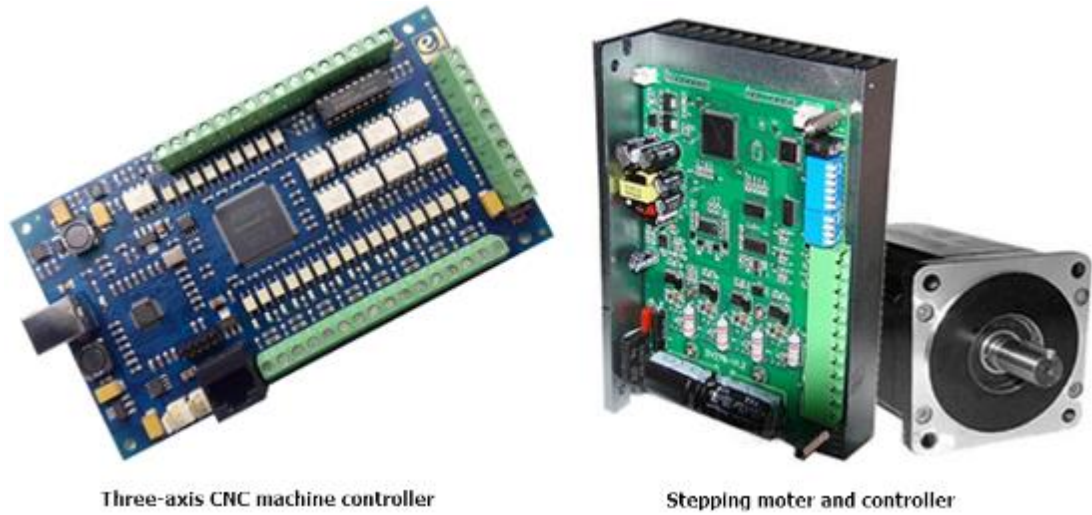


Figure 3.4 Three-axis CNC machine controller and stepping motor controller

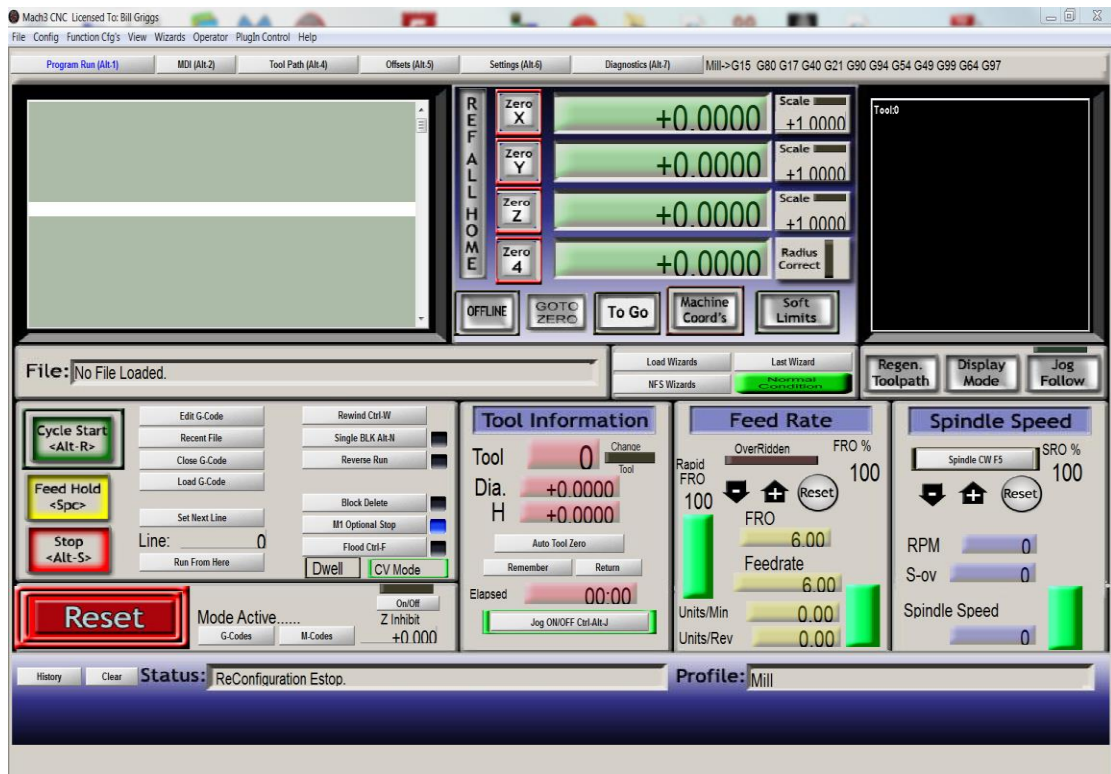


Figure 3.5 The user interface of CNC controller software

A visualization module, mainly composed of a CCD camera and a tele-centric lens, was also integrated into the laser micro-machining setup to assist in adjusting the position of the laser machining area. Figure 3.6 shows the actual setup of the visualization module.

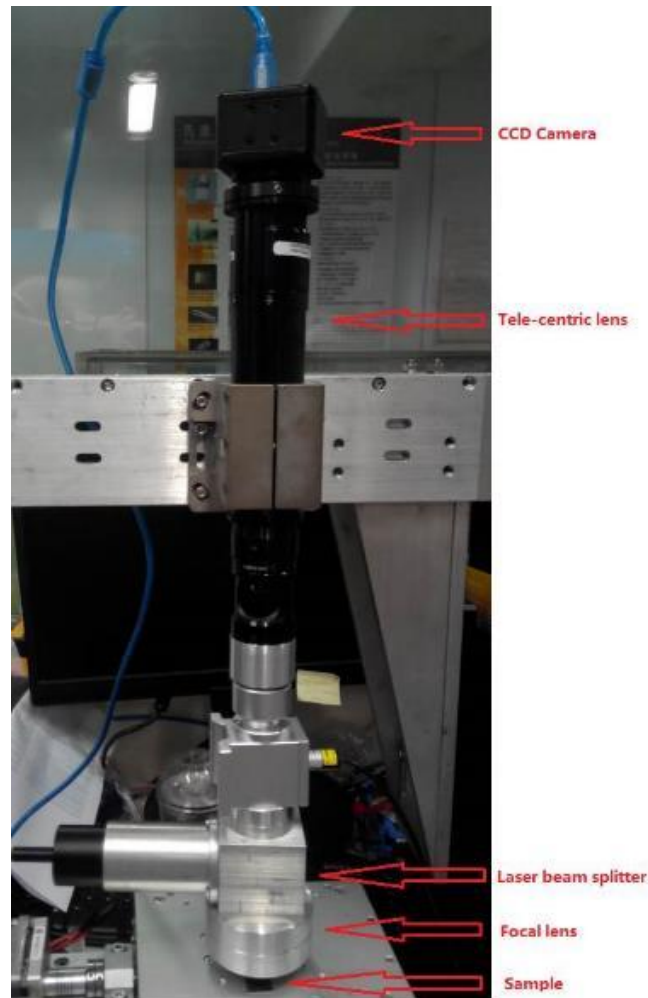


Figure 3.6 The actual setup of visualization module

Figure 3.7 shows the laser micro-machining setup. Figure 3.8 shows the laser groove marks on the silicon workpiece generated by this homemade laser machine. It can be seen from the test results that the position and the size of the laser irradiation spot on the material surface can be controlled with high stability.

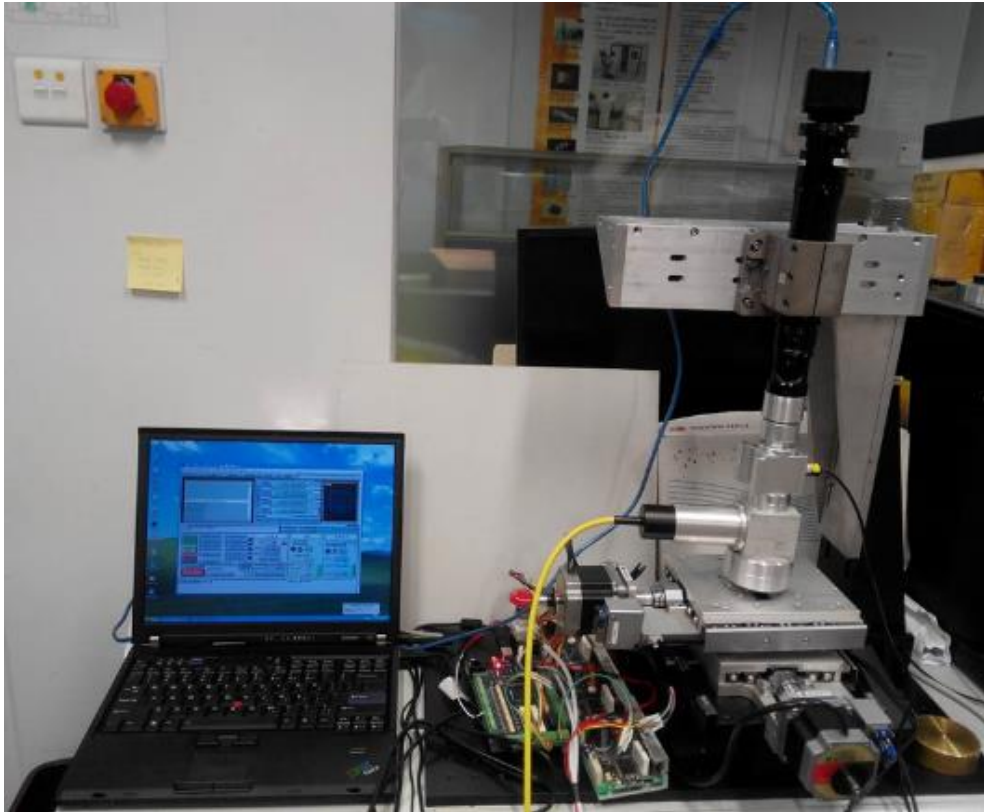


Figure 3.7 Actual picture of laser surface modification setup

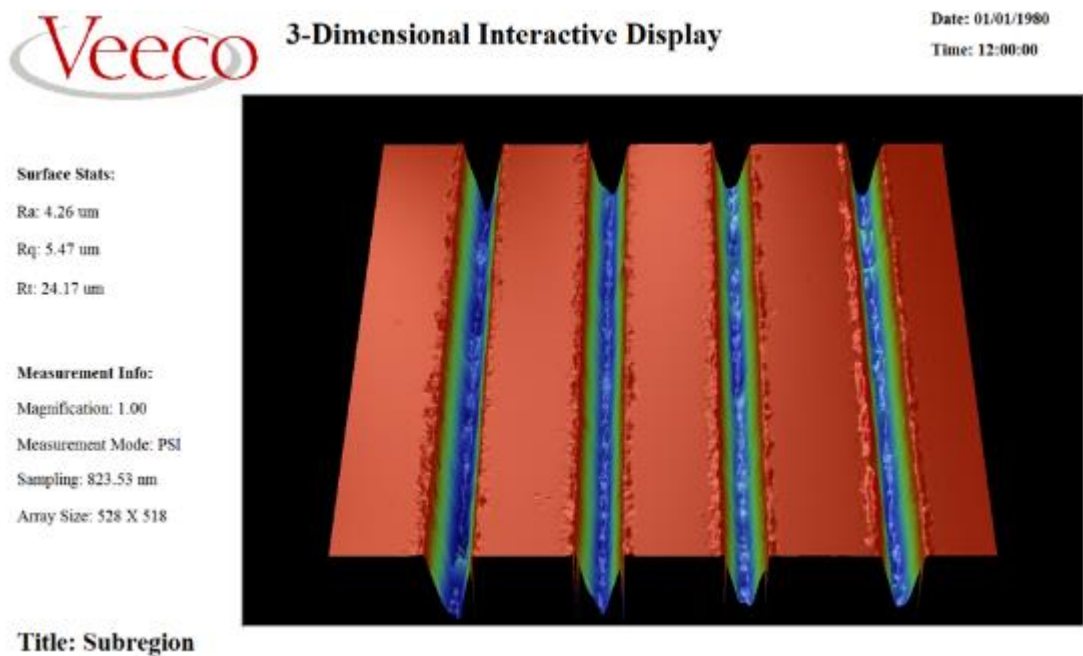


Figure 3.8 Laser ablation marks on silicon workpiece surface

3.2 Installation of laser assisted diamond cutting machine

3.2.1 Design of the machine

In order to investigate the laser heating effect on the cutting performance and machining accuracy of OFHC copper in the diamond cutting process, the establishment of a laser assisted diamond cutting equipment is a prerequisite. In this research, a fiber laser unit was incorporated into the Optoform30 ultra-precision machining system, and a video microscope was adopted to assist in adjusting the relative position between the laser spot and the diamond tool, with high precision.

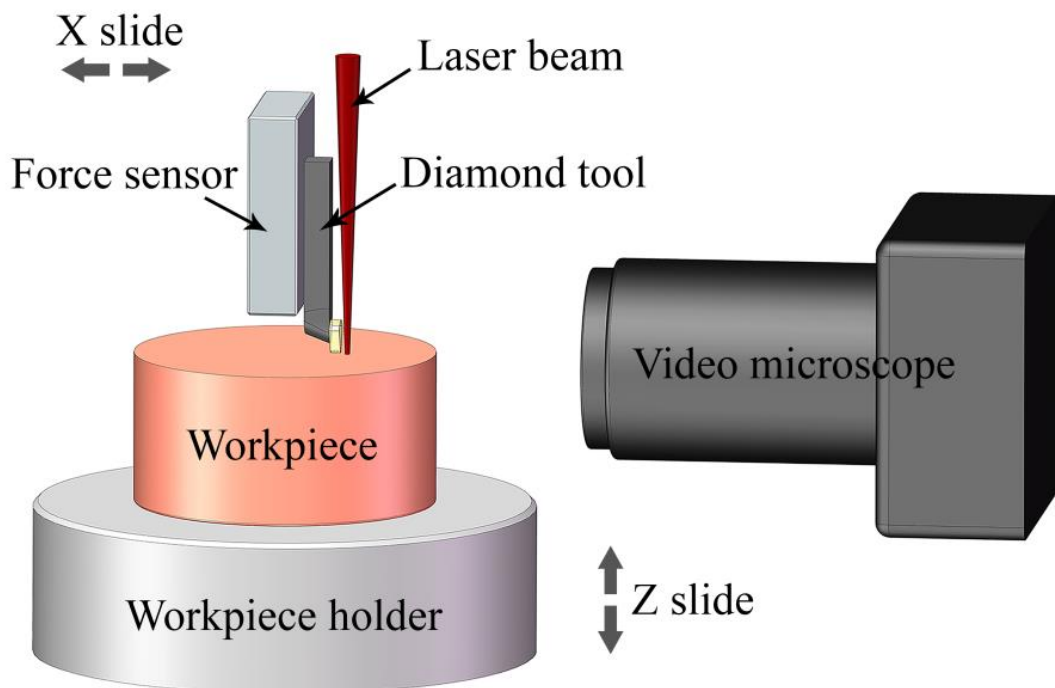


Figure 3.9 Design sketch of the laser assisted diamond cutting machine

Figure 3.9 shows the design sketch of the laser assisted diamond cutting machine. The laser beam is designed to focus to a point on the workpiece surface right in front of the cutting tool. In this way, the temperature of the cutting area can be increased to a desirable range that is high enough to soften the material. The spot size of the laser beam at the focal area is in the order of tens of micrometers. The video microscope is used to assist in adjusting the relative position between the diamond tool and the laser focal area. Fine adjustment of the relative position between the laser spot and the diamond cutting tool can be realized by this method.

3.2.2 Alignment of laser and diamond tool axis

This setup is mainly composed of three parts: an ultra-precision CNC machine, a fiber laser unit, and a video microscope. Figure 3.10 shows the two-axis Optoform30 ultra-precision CNC machine. The travel of the X and Z slides are 150 mm and 100 mm, respectively. The video microscope and the fiber laser unit adopted in this setup are the same as in the laser micro-machining setup, described in section 3.1. The maximum magnification of the video microscope is around 400. The laser source is a Nd:YAG laser that works in a continuous mode with a wavelength of 1064 nm. The maximum power output is 20 W. The output laser beam diameter is 3 mm. Figure 3.11 shows the actual laser assisted diamond cutting machine.



Figure 3.10 Optoform30 ultra-precision CNC machine

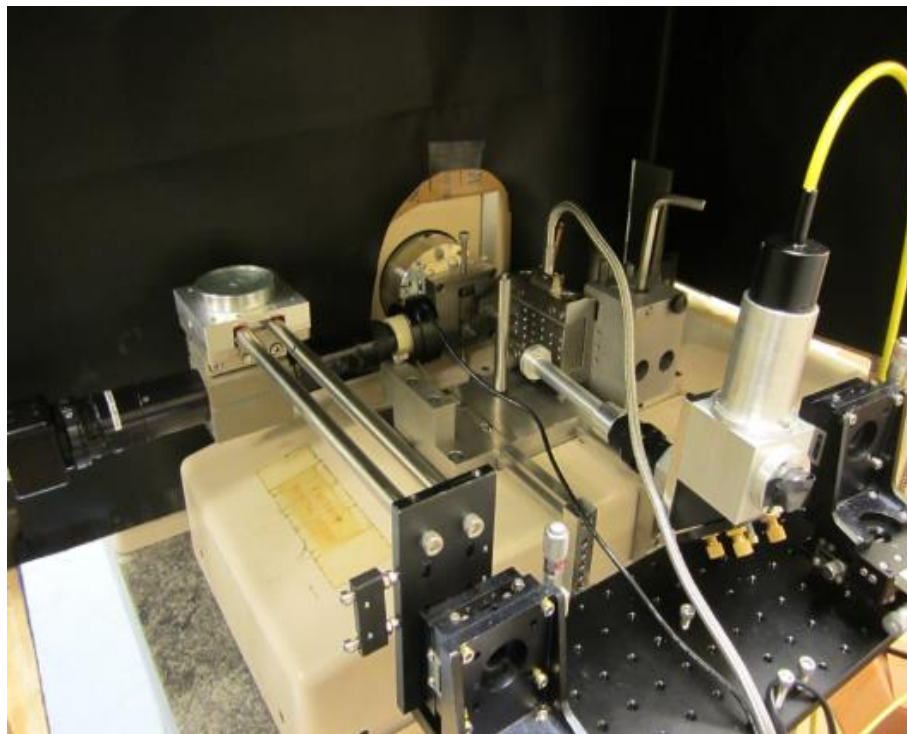


Figure 3.11 The actual setup of the laser assisted diamond cutting machine

For the LAM experiment, the distance between the laser spot and machine tool is an important parameter since it influences the temperature distribution in the cutting area.

In LAM at the macroscale, there is no difficulty in adjusting the laser tool distance, because both the laser spot and the machine tool are visible to the naked eye. However, for the LAM at the microscale, both the machine tool tip and the laser spot are too small to be identified by naked eye, which makes it impossible to do tool laser alignment using conventional methods. With the assistance of a video microscope, this problem was solved easily. Figure 3.12 shows the schematic diagram of the video microscope assisted laser tool alignment method from the side view.

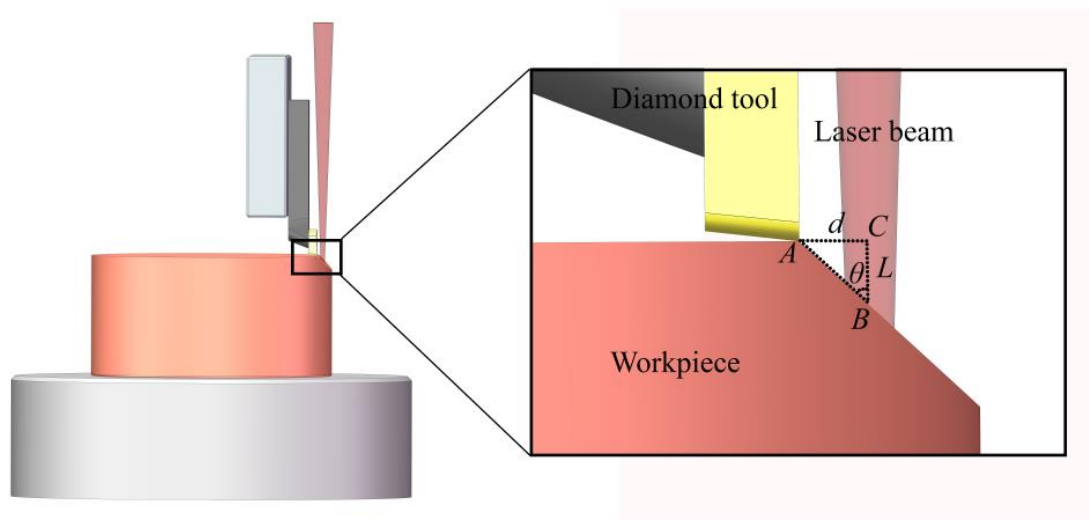


Figure 3.12 The schematic diagram of laser tool alignment method

As shown in this diagram, one of the corners of the rectangular workpiece was intentionally cut off, therefore, a chamfer with an angle of θ was formed. Because both the machine tool tip and the laser spot size were very small, they could be taken as two points, which were marked as A and B , respectively. L and d were the vertical and horizontal components of the distance between point A and point B . From the view of the video microscope, point A and point C were in the same position. The distance

between B and C , which marked as L , can be measured from the video microscope.

Thus the laser tool distance d can be calculated as,

$$d = L * \tan \theta$$

The laser collimator was mounted on a three-axis motion platform which enabled the laser beam position to be adjusted independently from the machine tool. By adjusting the measured length L , a desirable tool laser distance d can be obtained. Figure 3.13 is an optical microscopic image which shows the relative position between the laser heated spot and the tool mark, which indicated that the relative position between the laser spot and diamond tool can be adjusted with a very high precision.

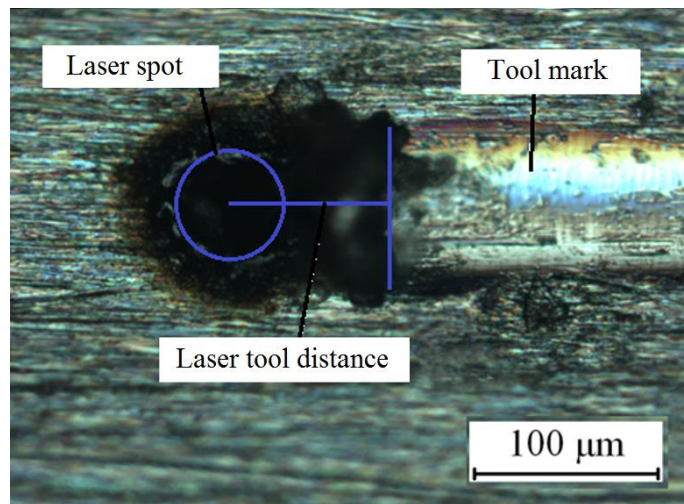


Figure 3.13 The optical microscopic image of the laser heated spot and the tool mark

Chapter 4 A hybrid machining process combining laser grooving and diamond shaping

4.1 Introduction

Single crystal silicon is an important mold material used in the precision glass molding industry due to its high thermal stability and available processing methods. However, silicon is also a brittle material that is relatively difficult to cut using a diamond tool, because cracks are easily formed on the machined surface during the cutting process. Generally speaking, by controlling the depth of cut to less than a critical value, crack-free machining could be achieved. Since the critical depth of cut of single crystal silicon is only a few hundreds of nanometers, it is still a rather time consuming process to fabricate microstructures with feature sizes far larger than the value of critical depth of cut. The lenticular lens is just such kind of microstructure.

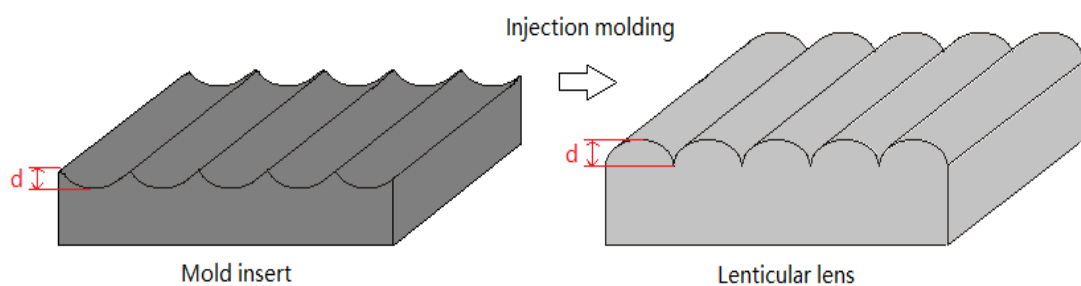


Figure 4.1 Schematic diagram of lenticular lens and mold insert

Figure 4.1 shows the schematic diagram of the shape of a lenticular lens and its mold insert. As shown in this figure, the depth of the lenticular lens d is typically in the order

of tens of micrometers. That means generating this kind of microstructures on a silicon workpiece surface with the ductile region machining method will have extremely low efficiency. Furthermore, the tool wear problem will be very serious.

In order to improve the machining efficiency as well as reduce the tool wear in fabricating lenticular lens mold inserts using silicon material, a new machining method therefore needs to be developed. In this research, we propose a hybrid machining method to fabricate silicon lenticular lens mold inserts that combining laser grooving and diamond shaping.

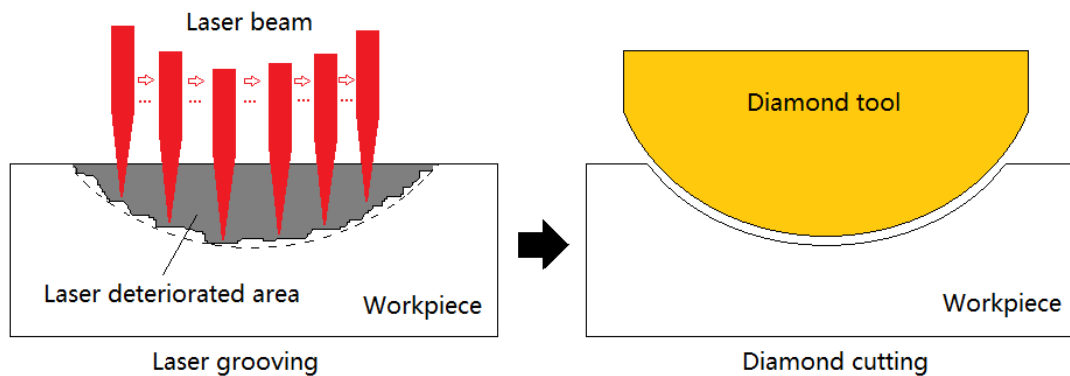


Figure 4.2 Illustration of the hybrid machining method

Figure 4.2 illustrates the process of this hybrid machining method. During this hybrid machining process, firstly, the workpiece material is grooved by a high power nanosecond laser beam. By controlling the laser scan parameters, grooves with pre-designed shapes can be generated on the silicon workpiece surface. Secondly, the diamond tool will be aligned to the same position of the grooves generated by laser to

remove the remaining material and perform finish cutting. Since most of the material is removed in the laser grooving step, which is a relatively fast and low cost process, this machining method is expected to have high efficiency, as well as being cost effective, compared with the conventional diamond machining method.

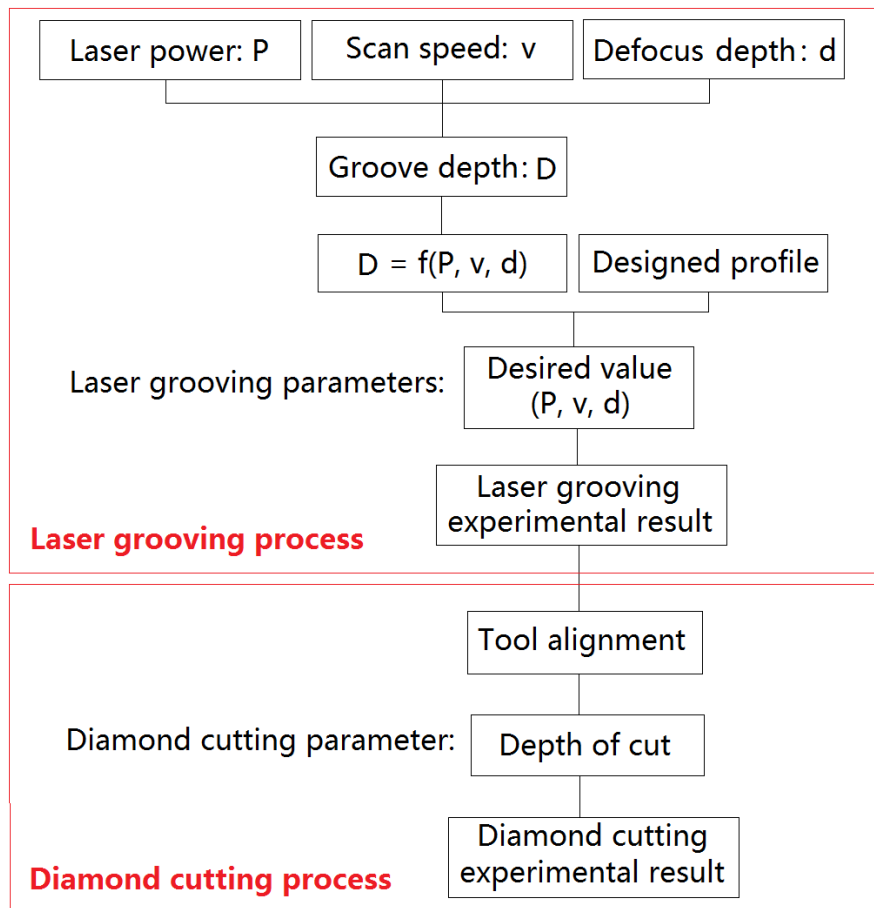


Figure 4.3 Flow chart of the hybrid machining process

In this research, a feasibility study of this hybrid machining method was performed. Figure 4.3 shows the flow chart of the hybrid machining process. Firstly, the influence of the laser machining parameters, such as scan speed, laser power and defocus depth on grooving depth was investigated. Then grooves with pre-designed shapes were

generated by the laser grooving method with the optimized laser machining parameters. Finally, diamond tool alignment and finish cutting experiment with varying cutting depth were realized. The experimental results indicated that it is possible to use this method to machine lenticular lens mold inserts using silicon as the mold material in terms of improving machining efficiency as well as reducing tool wear.

4.2 Laser grooving of silicon

Laser grooving experiments were conducted on the homemade laser micro-machining setup developed by the author, as described in chapter 3. The laser used was a nanosecond pulsed laser of wavelength 2 μm . The pulse duration and repetition rate of this laser were 30 ns and 30 kHz, respectively. The workpiece material was single crystal silicon. In order to find the optimum laser machining parameters for a designed value of groove depth, the influence of laser scan speed, laser power, and defocus depth on grooving depth was investigated.

4.2.1 Influence of laser parameters on groove depth

Figure 4.4 shows a typical optical microscopic image of the cross-section view of laser machined grooves on a silicon workpiece surface. The laser power was 4.3 W and the scan speed was 50 mm/min in this case. The workpiece surface was adjusted to be at the focal point of the laser beam.

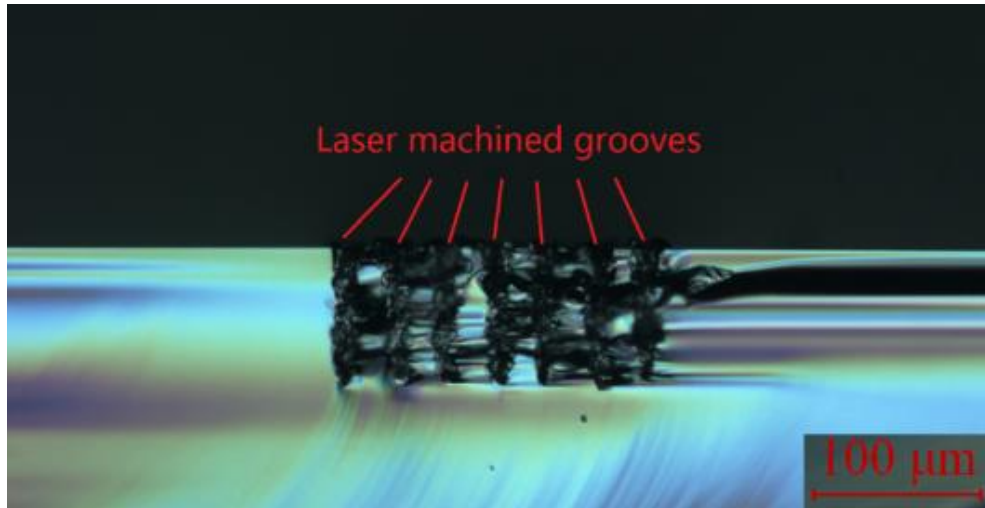


Figure 4.4 Cross-section view of laser machined grooves on silicon workpiece surface

It can be seen from this image that the depths of these laser generated grooves were almost the same, which means the repeatability of the laser grooving process was reliable, and thus acceptable for our purpose. A laser grooving experiment with changed laser power and scan speed was conducted. Table 4.1 lists the experimental results of the depths of laser machined grooves with different laser power and scan speed. The experimental result is plotted in Figure 4.5 and Figure 4.6. It can be seen that the relationship between groove depth and laser power could be well fitted with a linear function, and so was the relationship between groove depth and scan speed.

Table 4.1 The influence of laser scan speed and laser power on groove depth

Speed (mm/min)	Laser power (W)							
	2	2.3	2.7	3.1	3.5	3.9	4.3	5.3
100	15	21	28	35	42	50	59	80
200	13	19	27	32	38	46	53	70
300	12	17	26	30	36	42	48	64
400	8	15	24	28	32	41	44	60

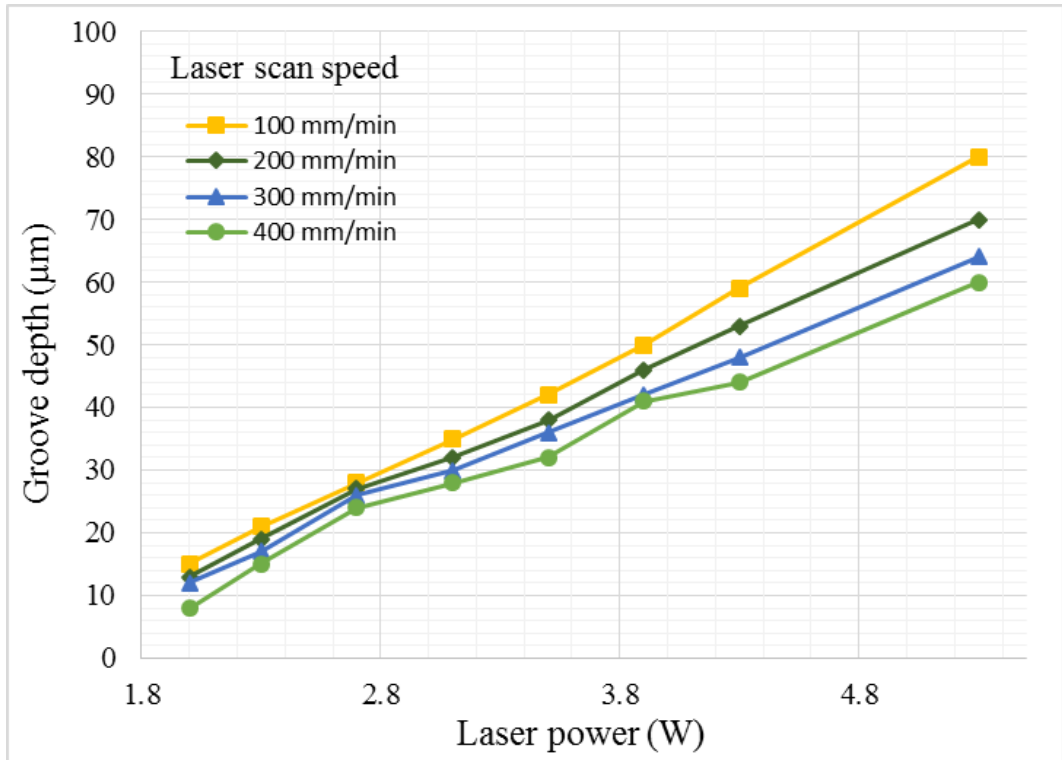


Figure 4.5 The influence of laser power on groove depth

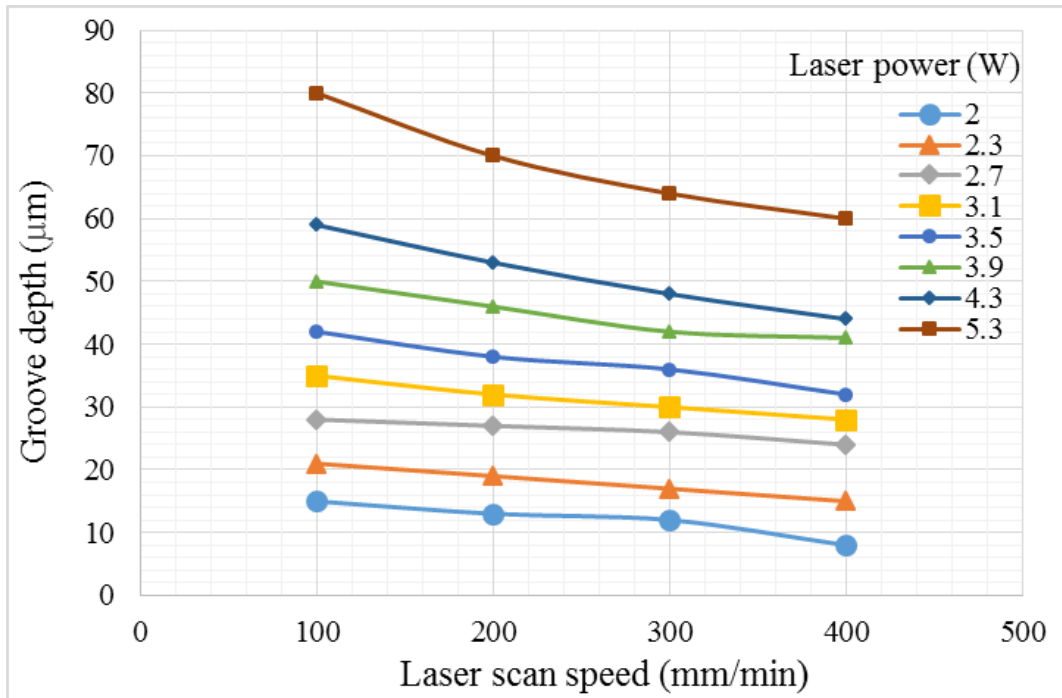


Figure 4.6 The influence of scan speed on groove depth

The influence of the defocus depth on the groove depth was also investigated in the laser grooving process. The definition of the defocus depth is illustrated in Figure 4.7, and refers to the distance between the workpiece surface and laser beam focal point.

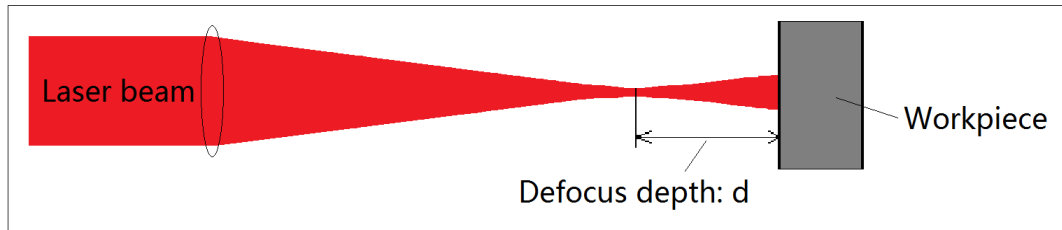


Figure 4.7 Illustration of definition of defocus depth

The experimental result is shown in Table 4.2 and is also plotted in Figure 4.8. The laser scan speed was fixed to 400 mm/min for all the experiments. Unlike the relationship between groove depth and laser power which could be fitted with a linear function, the effect of defocus depth on groove depth was non-linear.

Table 4.2 The influence of defocus depth on groove depth

Defocus depth (mm)	Laser power			
	2.3W	3.3W	4.3W	5.3W
0	28	47	65	83
0.03	26	50	64	83
0.06	26	46	64	82
0.09	23	45	61	75
0.12	18	34	53	69
0.15	8	28	43	62
0.18	0	13	31	52
0.21		5	20	44
0.24		0	4	25
0.27			0	15
0.3				0

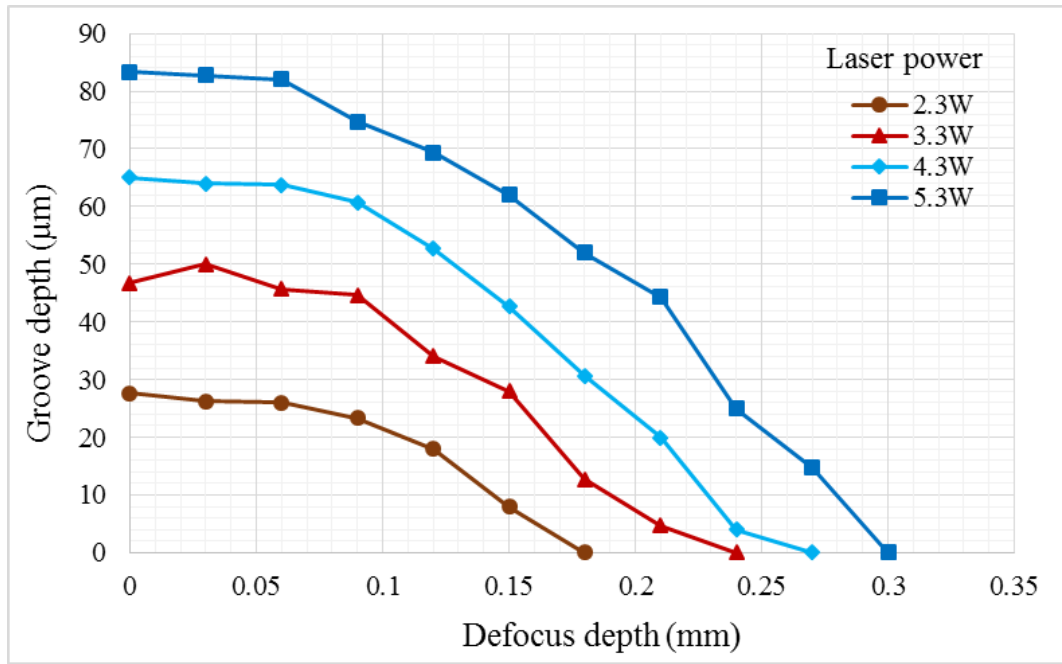


Figure 4.8 The influence of defocus depth on groove depth

4.2.2 Laser grooving experiment and result

The cross-section profile of the lenticular lens groove is an arc. In this design, we chose the arc radius to be 0.5 mm, and the groove depths to be 50 μm and 80 μm. Then the width of the grooves were calculated to be 0.436 mm and 0.543 mm, respectively. The width of a single laser machined groove was around 5 μm, which could be estimated from Figure 4.4. Thus to generate one lenticular lens groove, tens of, or even more than one hundred repetitions of laser scanning was required. For the lenticular lens groove, at different position of the arc, the depth was different. As discussed in section 4.2.1, both the laser power, scan speed and defocus depth could influence the groove depth produced by laser scanning. There are several methods to produce a groove of a given

depth. Since it is relatively easier to adjust the defocus depth by a numerically controlled 3-axis motion platform than adjusting the laser power, therefore in this experiment by changing the defocus depth rather than changing the laser power, grooves with varying depths could be realized.

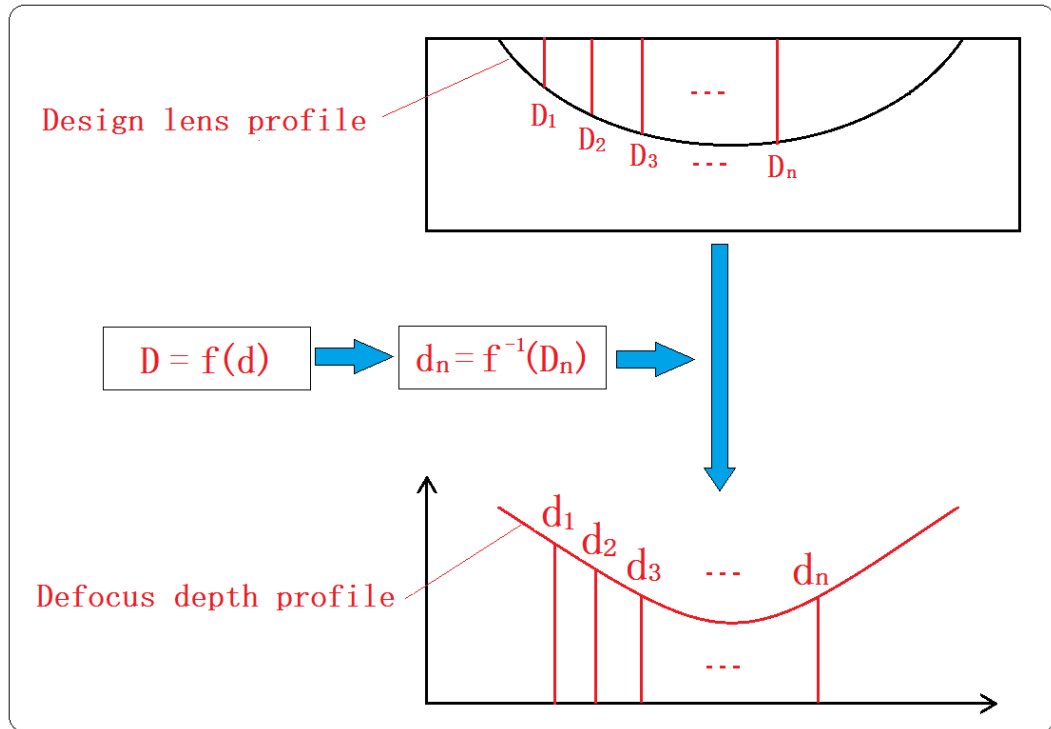


Figure 4.9 The procedure to determine defocus depth profile

Figure 4.9 shows the procedure to determine the defocus depth profile. Firstly, the actual depth of a design lenticular lens at different positions D_n was calculated. Then according to the relationship between the groove depth and defocus depth obtained from the experimental result, the defocus depth d_n could be calculated. The interval between two laser scanning lines was set to be $5 \mu\text{m}$. The defocus depth profiles for a designed

lenticular lens groove depth of 50 μm and 80 μm are shown in Figure 4.10 and Figure 4.11, respectively. The corresponding laser powers were 4.3 W and 5.3 W.

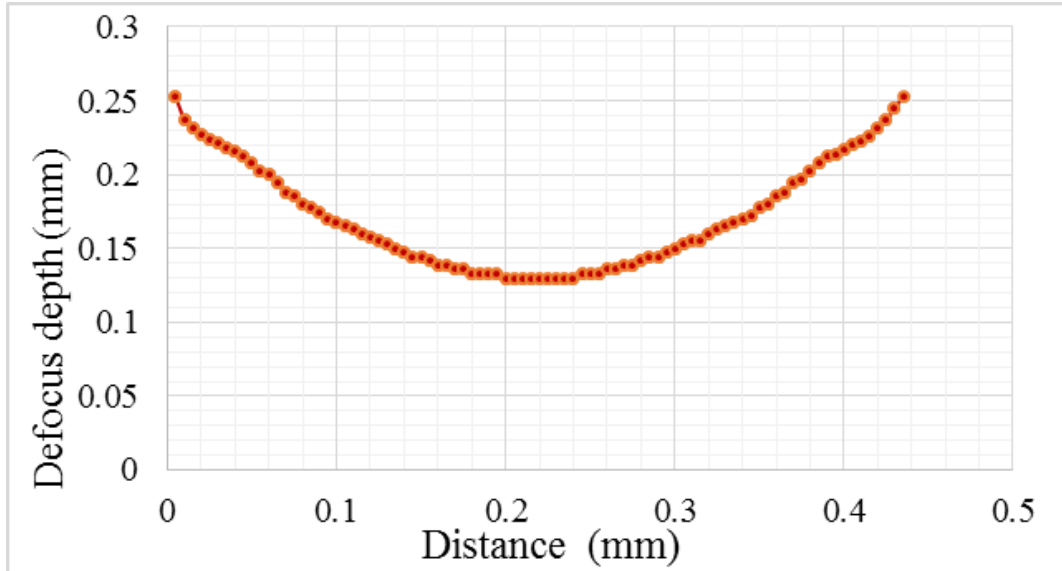


Figure 4.10 Defocus depth profile for a lenticular lens groove depth of 50 μm

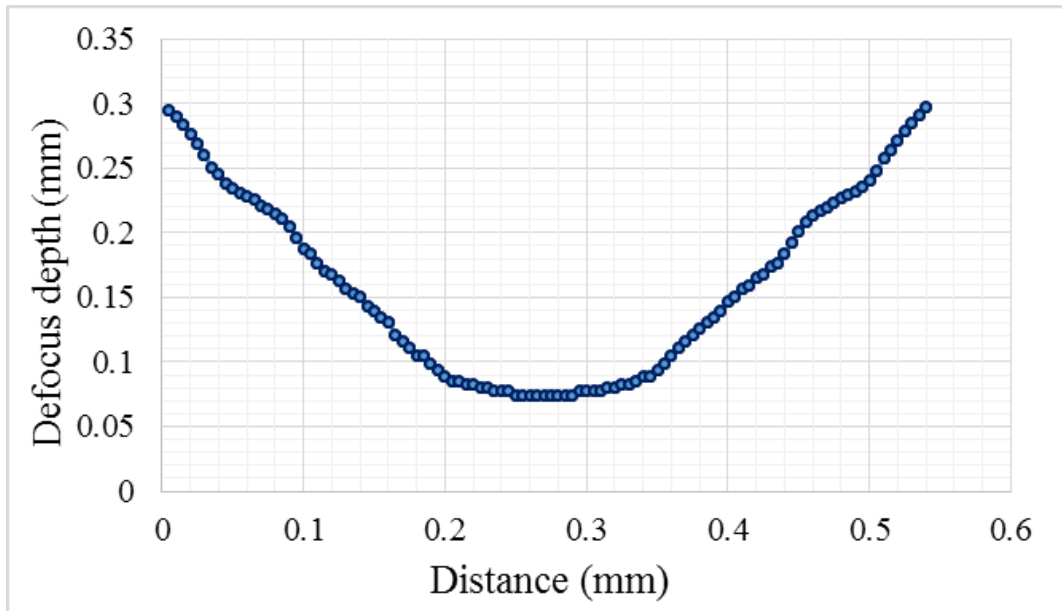


Figure 4.11 Defocus depth profile for a lenticular lens groove depth of 80 μm

The optical microscopic images of the cross-section profiles of the laser machined grooves are shown in Figure 4.12 and Figure 4.13. The red line shows the design lenticular lens profile. The experimental results agreed well with the design profiles.

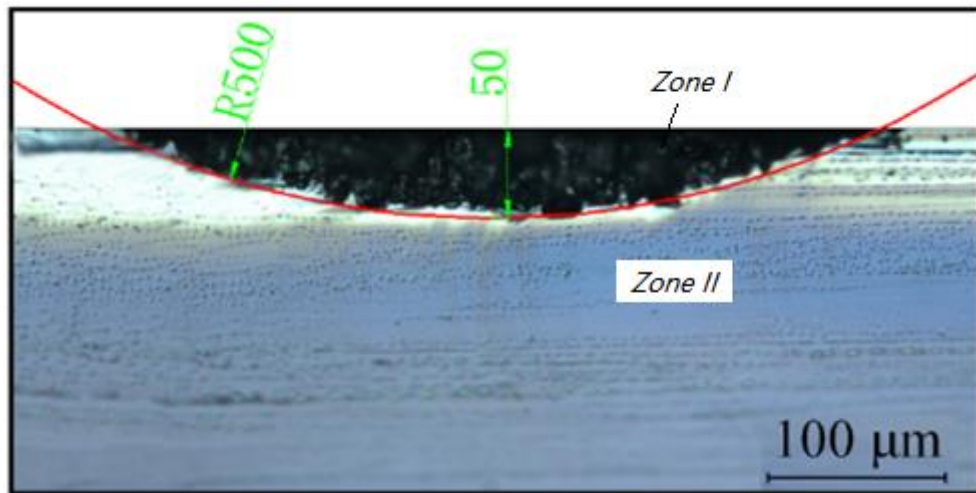


Figure 4.12 Cross-section profile of laser machined groove (designed depth 50 µm)

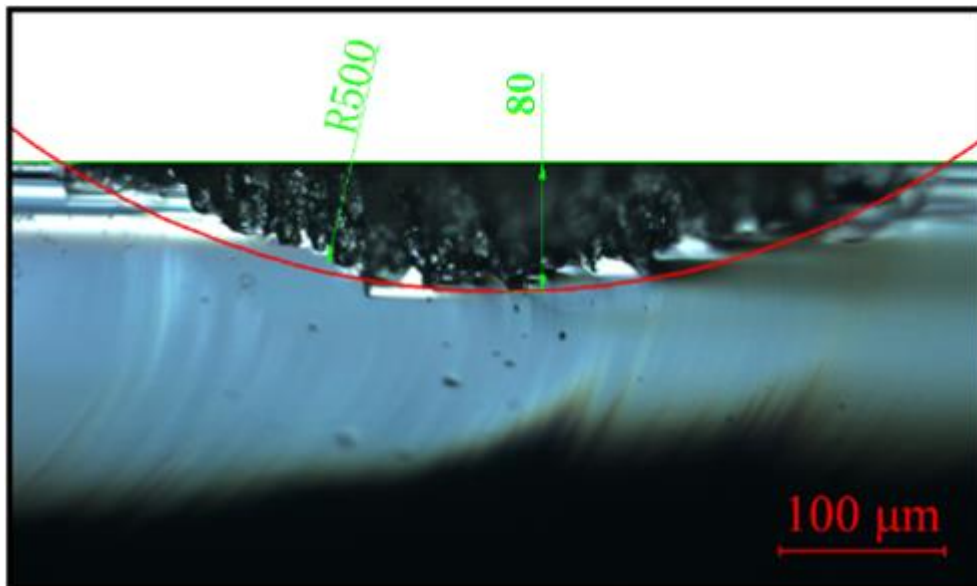


Figure 4.13 Cross-section profile of laser machined groove (designed depth 80 µm)

4.3 Diamond shaping of grooves produced by laser grooving

A rough shape of the groove can be obtained by laser cutting on silicon. However, the shape and surface quality of the laser generated grooves was still not satisfactory. In laser grooving, instead of directly removing from the workpiece surface, the melt-off materials piled up on the workpiece surface and needed to be removed by the subsequently diamond shaping process. Since the laser grooving experiment was performed on the laser micro-machining equipment, when the workpiece was moved to the diamond cutting machine, tool alignment was needed to align the groove axis cut by laser with the axis of the diamond tool travel. Subsequently, diamond cutting with different finish cutting depth was conducted to investigate the influence of depth of cut on the surface quality of machined grooves.

4.3.1 Diamond tool alignment method

The diamond cutting experiment was performed on a Nanoform200 ultra-precision lathe. Figure 4.14 shows the setup of the diamond cutting experiment. A CCD camera was mounted on the lathe to assist in the alignment work. Figure 4.15 shows an image of the tool alignment process captured by the CCD camera, and Figure 4.16 shows the schematic diagram of the alignment method between diamond tool and laser generated groove. The tilt stage as shown in Figure 4.14 could be used to tilt the workpiece to rotate around Y coordinate axis to make sure the cutting process can be performed under

a constant depth of cut. The Y motion stage was used to shift the workpiece along the vertical direction to enable the groove center line to be in the same altitude with tool center line. The silicon workpiece was mounted on a cylindrical workpiece holder which could rotate around X coordinate axis. The reference line was used as a reference in adjusting the workpiece around X coordinate axis to make sure the tool center line and groove center line always in the same altitude throughout the diamond cutting process. In this alignment process, one end of the reference line was adjusted to be at the same altitude with the diamond tool center line. The diamond tool could be moved back and forth along Y coordinate axis. Rotate the workpiece holder around X coordinate axis to minimize the deviation of the distance between the reference line and tool center line. Repeat this process until this deviation reduced to an acceptable level.

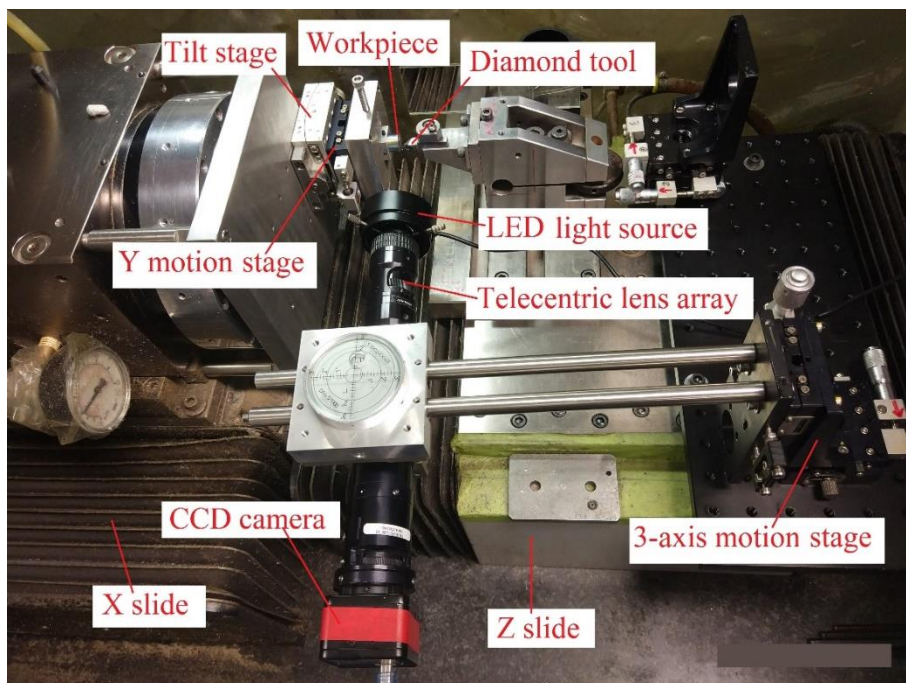


Figure 4.14 Diamond cutting experimental setup

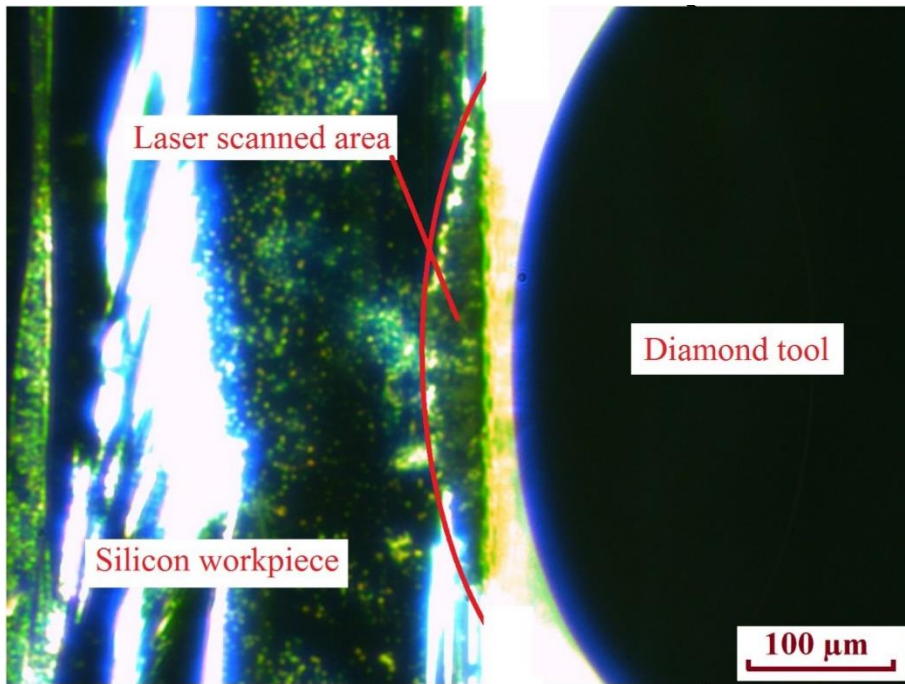


Figure 4.15 CCD camera captured image shows the tool alignment process

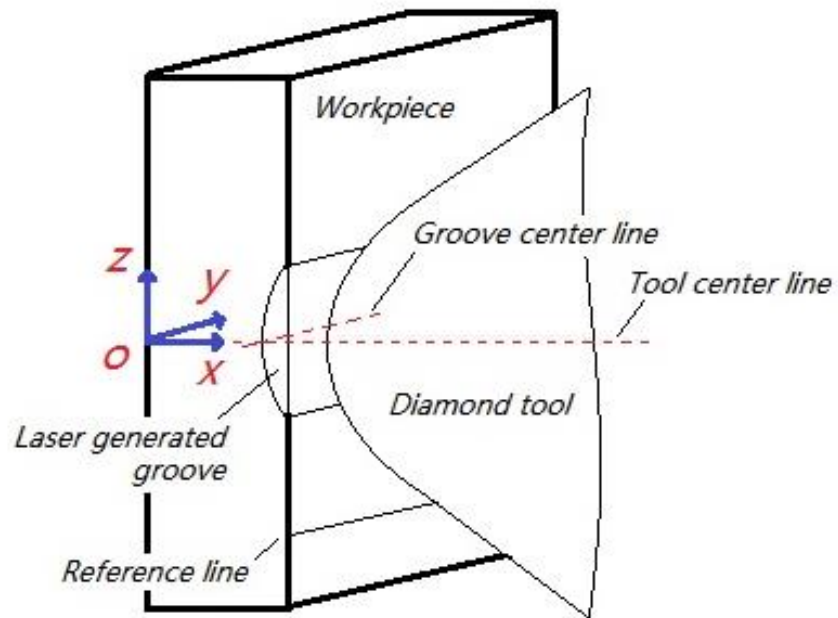


Figure 4.16 Schematic diagram of the alignment method between diamond tool and laser generated groove

4.3.2 Diamond shaping with varying depth of cut

After the tool alignment work was completed, diamond cutting experiments would then be performed. The diamond cutting tool served as the shaper of the prior groove to give it the final shape. Firstly, rough cutting was conducted to remove the laser deteriorated material which was still attached to the workpiece surface. The depth of rough cut was set to be slightly larger than the laser grooved depth. Since the material in the region that had been deteriorated by laser beam and was no longer chemically bonded to the base material, it would be very easy to remove without causing large cracks to form on the machined workpiece surface even when the depth of cut was as large as tens of micrometers. As shown in Figure 4.12, the workpiece could be divided into two regions after laser grooving process, which marked as *Zone I* and *Zone II* in this figure. *In Zone I*, the crystal structure of silicon was totally destructed by laser irradiation and part of the debris piled up on the laser treated area, this part of material would be removed in the subsequent diamond cutting process, thus it would not affect the final surface quality of the lenticular lens. *In Zone II*, the material was totally unaffected by laser irradiation thus remained its original crystal structure. Secondly, finish cutting was performed to determine the relationship between the surface roughness and finish cutting depth. The first pass of finish cutting was to remove the deteriorated material in *Zone I*, and the following passes were performed on the fresh silicon surface generated by the first pass. The final surface quality was affected by both cutting conditions and diamond tool

conditions, since in diamond machining of silicon, there exists a critical value under a given cutting condition and diamond tool condition, beyond which cracks would form on the machined surface. In this research, by fixing the diamond tool condition, we only investigated the influence of finish cutting depth on the surface quality of machined grooves.

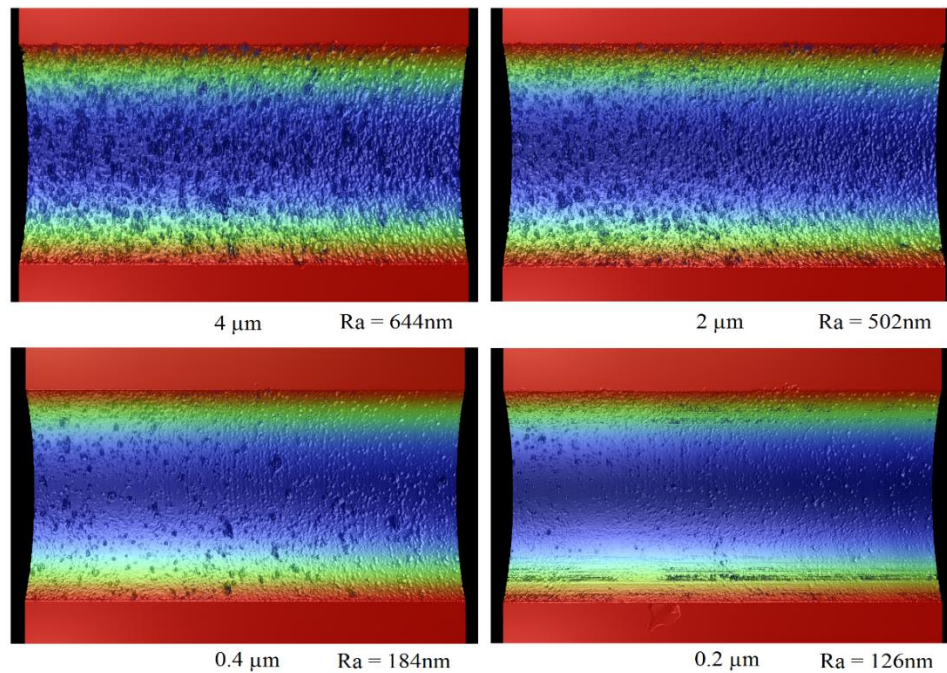


Figure 4.17 Groove surface profiles after finish cutting with different cutting depth

Figure 4.17 shows the groove surface profiles after finish cutting with different depths of cut. For each of the depth of cut values, the total cutting depth was the same. For example, if the total finish cutting depth was 4 μm, it would need one pass for a depth of cut of 4 μm and twenty passes for a depth of cut of 0.2 μm.

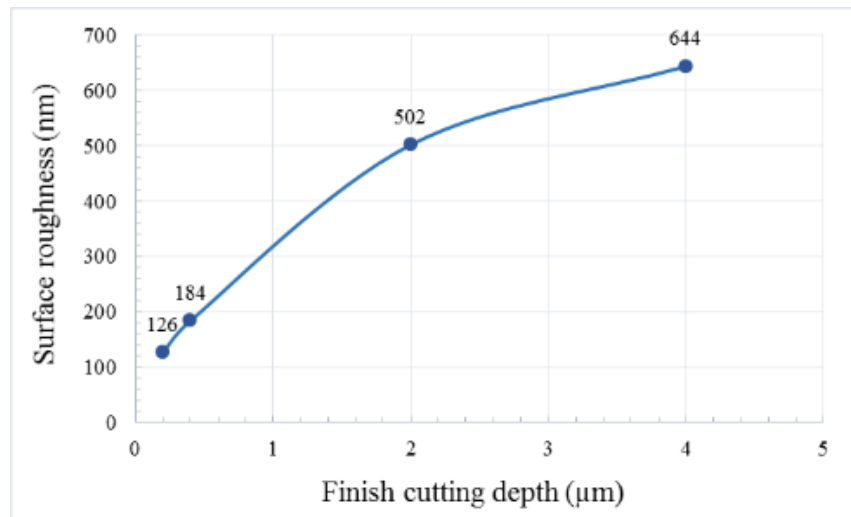


Figure 4.18 Relationship between depth of cut and groove surface roughness

Figure 4.18 shows the relationship between the finish cutting depth and the groove surface roughness. The surface roughness was measured on the bottom of the grooves with a sampling area of $250 \mu\text{m} \times 500 \mu\text{m}$. It can be seen that the surface roughness decreased with decreasing finish cutting depth. When the finish cutting depth was $4 \mu\text{m}$, large cracks frequently formed on the machined groove surface, causing the surface roughness to be very high. When the finish cutting depth was $0.2 \mu\text{m}$, the machined groove surface appeared to be much smoother with fewer and smaller cracks formed. The surface roughness was thus dramatically reduced compared with those with larger finish cutting depths. However, even though the machined surface quality could be improved significantly with a smaller finish cutting depth, the surface roughness, which was in the order of 100 nm , was still too large to fulfill the requirement of a practically useful high quality lenticular lens mold insert. Part of the reason is that the diamond tool being used in this research was not specially designed for machining brittle

materials whose rake angle should be negative. What we used in this research was a conventional diamond tool with zero rake angle. It cannot sufficiently suppress the formation of cracks while machining brittle materials like single crystal silicon, thus led to a poor machined surface. Further work is still required to make this method useful for the fabrication of lenticular lens silicon mold.

4.4 Summary

In this chapter, a hybrid machining method that combining laser ablation and diamond cutting was proposed to machining lenticular lens silicon mold. A feasibility study was performed to investigate the availability of using this method to fabricate lenticular lens mold. The influence of laser power, laser scan speed and defocus depth on the laser ablation depth was investigated. It was found that there was a linear relationship between laser power and laser ablation depth, and so was the relationship between laser scan speed and laser ablation depth. While the influence of defocus depth on laser ablation depth was a non-linear effect. In the diamond cutting process, the machined surface quality could be improved significantly by reducing the finish depth of cut. The experimental results indicated that it could be a possible method in manufacturing lenticular lens silicon mold or other similar microstructures, with improved machining efficiency as well as reduced tool wear. Further work is required to obtain a better surface finish down to the nanometer level.

Chapter 5 Laser assisted diamond cutting of OFHC copper

5.1 Introduction

The surface quality of high precision components plays a vital role in their applications, especially in optical components. Because of the high thermal conductivity and high purity of OFHC copper, it is the most suitable material for high power laser mirrors which require a high laser damage threshold. The cutting performance of OFHC copper in the ultra-precision machining is influenced by both material properties and cutting conditions. For example, in the diamond machining of OFHC copper, a small depth of cut could lead to a good surface quality of the machined parts, but the machining efficiency would be low. However, a large depth of cut will lead to a poor surface quality of the machined parts and also a high cutting force. It is meaningful to investigate the factors that are responsible for the deterioration of the surface quality of OFHC copper at large depths of cut in order to improve both the surface quality and machining efficiency in manufacturing practice. In this research, a taper cutting experiment was conducted to find the relationship between surface roughness and depth of cut. It was found that the formation of surface defects at large depths of cut was the reason that caused the surface roughness of the machined groove to increase. Because the hardness and strength of copper decreases with increase of temperature, it might be helpful to suppress the formation of surface defects of OFHC copper by using a laser to heat up the material in the cutting region during the machining process. This research thus

investigated the influence of laser heating on the surface quality of OFHC copper in the diamond cutting process.

5.2 Surface defects of OFHC copper in diamond cutting

5.2.1 Experimentation

A four-axis ultra-precision lathe from Moore Nanotechnology System Incorporation (Nanotech 350FG from) was employed to perform the experiment. A taper cutting experiment with a continuously increased depth of cut from 0 to 20 μm was conducted. The inclination angle of the grooves to the flat surface was approximately 0.057° , and the cutting speed was 30 mm/min. Figure 5.1 (a) and (c) show the experimental setup and schematic of the taper cutting experiment, respectively. A cylindrical shaped commercial available OFHC copper workpiece and a leaded brass (UNS C37700) workpiece with a size of 31.7 mm in diameter and 15 mm in thickness were used in this experiment, as shown in Figure 5.1 (b). The average grain size of the copper workpiece was around 30 μm . The brass workpiece was composed of the α and β phases. The chemical composition of brass was: Cu 61.70%; Zn 37.65%; Pb 2.08% in weight percent. The metallographic structure of copper and brass are shown as Figure 5.1 (d) and (e), respectively. The micro-hardness of the workpiece was measured at 5 randomly chosen points with a Vickers hardness tester (Type: FM-7e, Future Tech). The average

micro-hardnesses were measured to be 99.3 MPa for the copper workpiece and 115.4 MPa for the brass workpiece at the applied load of 0.1 kg.

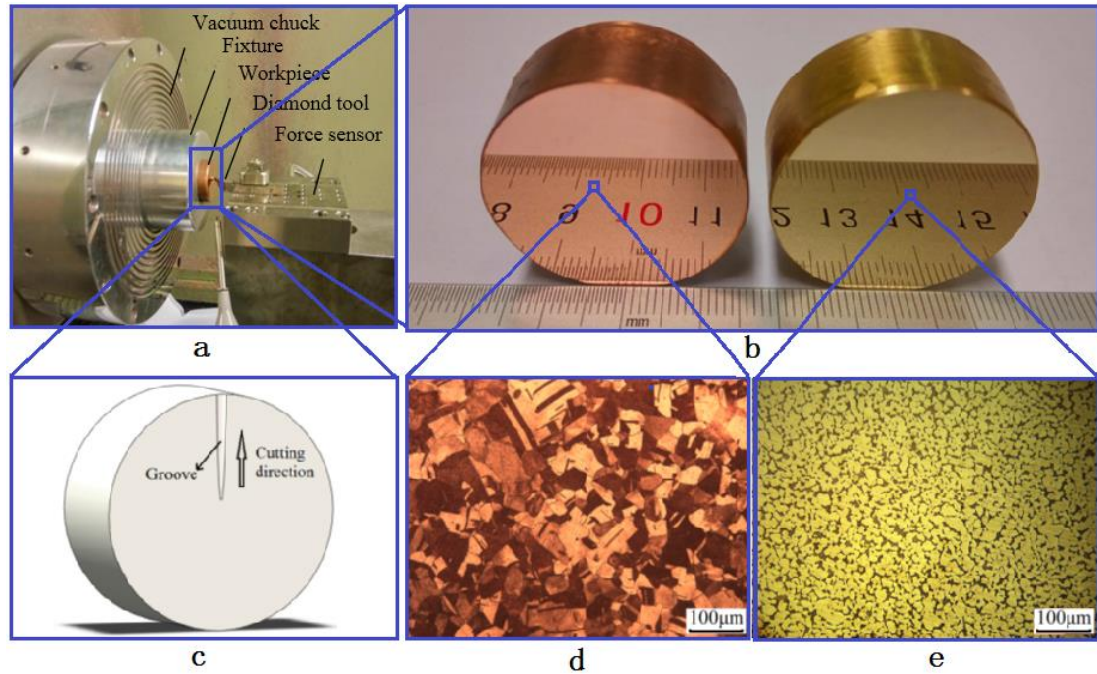


Figure 5.1 (a) Experimental setup; (b) Copper and brass workpiece; (c) Schematic of taper cutting; (d) and (e) Metallographic microstructure of copper and brass

The work surface of the specimen was finished to a roughness of less than 10 nm by diamond turning using the same ultra-precision lathe before the taper cutting experiment was conducted on the same surface. A fresh single crystal diamond tool was used throughout the experiment. The tool nose radius was 0.567 mm, tool clearance angle and rake angles were 10° and 0° , respectively. No lubricant was used in this experiment. Three grooves were generated with identical cutting parameters on each workpiece.

The surface morphology and surface damage of the machined micro-grooves were examined by an optical microscope (Olympus BX60) and a scanning electron microscope (Hitachi, TM3000). The groove cross-section profile and surface roughness were measured by a 3D optical surface profiler (Zygo, Nexview). The sampling area and optical resolution of the surface roughness measurement were $100\ \mu\text{m}\times 100\ \mu\text{m}$ and $0.4\ \mu\text{m}$, respectively.

5.2.2 Results and discussion

The surface roughness (Ra) at the bottom of the grooves at different depths of cut was measured and plotted in Figure 5.3. Figure 5.2 shows the procedure of calculating the surface roughness from a curved surface. Firstly, a square area with fixed dimension of $100\ \mu\text{m}\times 100\ \mu\text{m}$ was extracted as a sampling area from the bottom of the groove at a selected depth of cut. Secondly, the surface waviness profile of the sampling area was removed with only the surface roughness profile left, and then the Ra value was measured. When the depth of cut is smaller than around $2.5\ \mu\text{m}$, the width of the groove will be smaller than $100\ \mu\text{m}$. Hence, the size of the sampling area was chosen as the width of the groove rather than the fixed dimension $100\ \mu\text{m}\times 100\ \mu\text{m}$. Theoretically, the size of the sampling area does not influence the value of surface roughness.

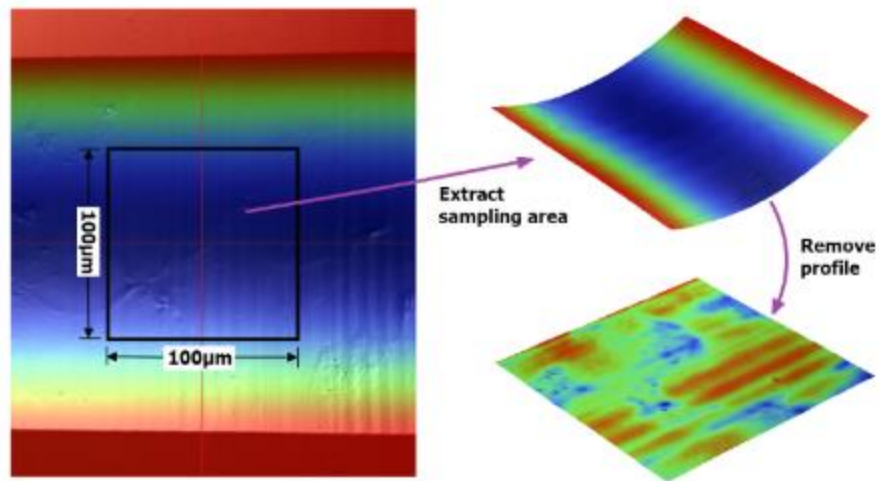


Figure 5.2 The procedure of calculating surface roughness from a curved surface

For the copper workpiece, the average surface roughness of the three grooves at the same depth of cut and its exponential fitted curve were also plotted in Figure 5.3. It clearly shows that the surface roughness increases with increasing of depth of cut. The relationship between surface roughness and depth of cut can be described by the following exponential function:

$$y = 7.2858e^{0.179x}$$

where x denotes the depth of cut, and y denotes the surface roughness. In contrast, the surface roughness of the machined groove surface on the brass workpiece changed only slightly with increasing depth of cut, and could be well fitted with the following linear function:

$$y = 0.465x + 12.941$$

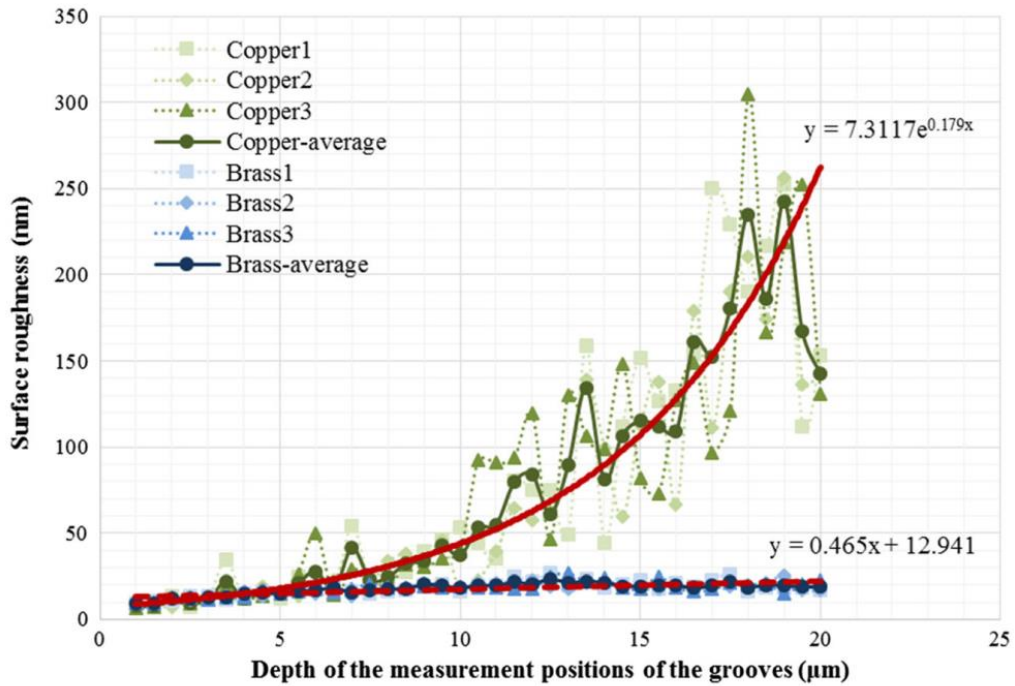


Figure 5.3 Surface roughness at the bottom of the grooves at different depth of cut of copper and brass

A representative (groove 2 of Figure 5.3) surface profile of the groove on the copper workpiece, measured by a 3D optical surface profiler, is shown in Figure 5.4. It was found that, with increasing depth of cut, the surface quality of the groove deteriorated rapidly due to the frequently occurred surface defects. As a comparison, Figure 5.5 shows the result of the groove machined on the brass workpiece (groove 1 of Figure 5.3). There was no observable change of surface quality at different depths of cut.

Further examination through SEM revealed that the surface defects found on the copper workpiece could be mainly classified as two different types, namely ripple-like defects and delamination. The ripple-like defects were found to occur occasionally in depths of

cut around 3 to 13 μm , the density of the defects increasing with increasing depths of cut. While, the delamination appeared from depths of cut around 11 to 20 μm .

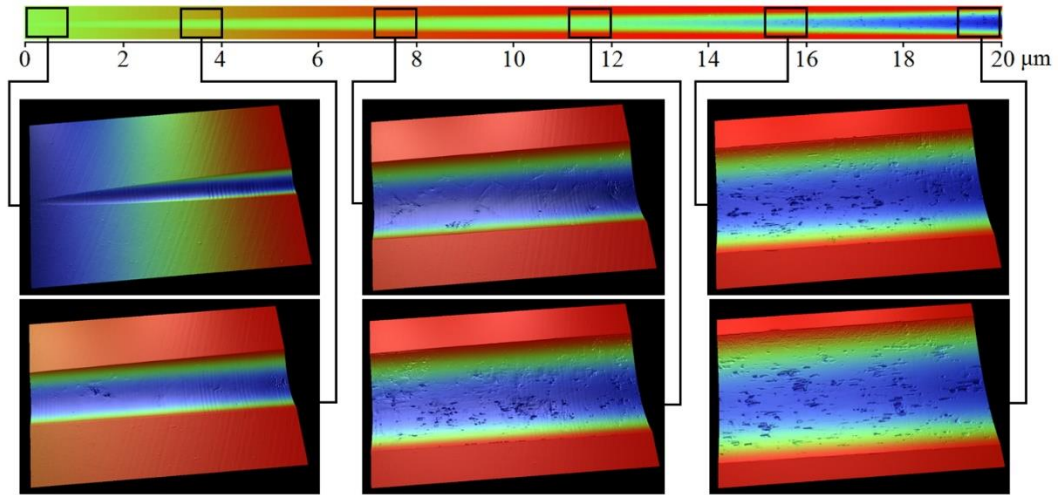


Figure 5.4 Surface profile of micro-groove at different depth of cut measured by 3D optical surface profiler (OFHC copper)

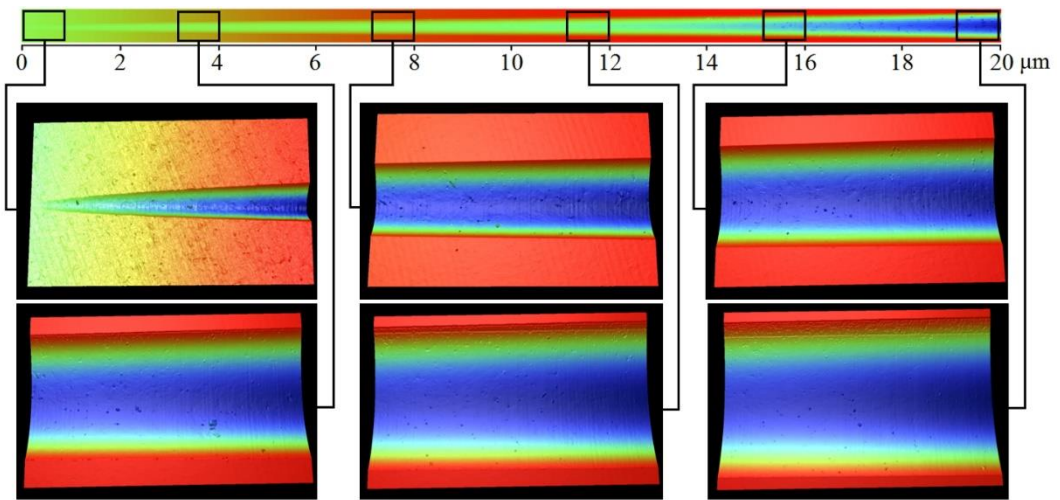


Figure 5.5 Surface profile of micro-groove at different depth of cut measured by 3D optical surface profiler (C37700 brass)

Figure 5.6 (a) shows a typical ripple-like defect which occurred at a depth of cut around 5 μm , and (b) is the detail of the ripple-like defect with an enlarged scale. The generation

of this type of defect was suspected to be influenced by the microstructures of the material, more specifically, the crystal orientations of the grains being cut. Because for an individual copper crystal grain, there exists certain slip planes and the corresponding slip directions along which dislocation motion could occur more easily than in other planes or directions. Those grains with no preferred slip directions are prone to generating ripple-like defects during cutting. This explanation is well supported by the work of many other researchers (Ding et al., 2012), since the ripple-like defects were generally observed to occur within certain individual grains in their study.

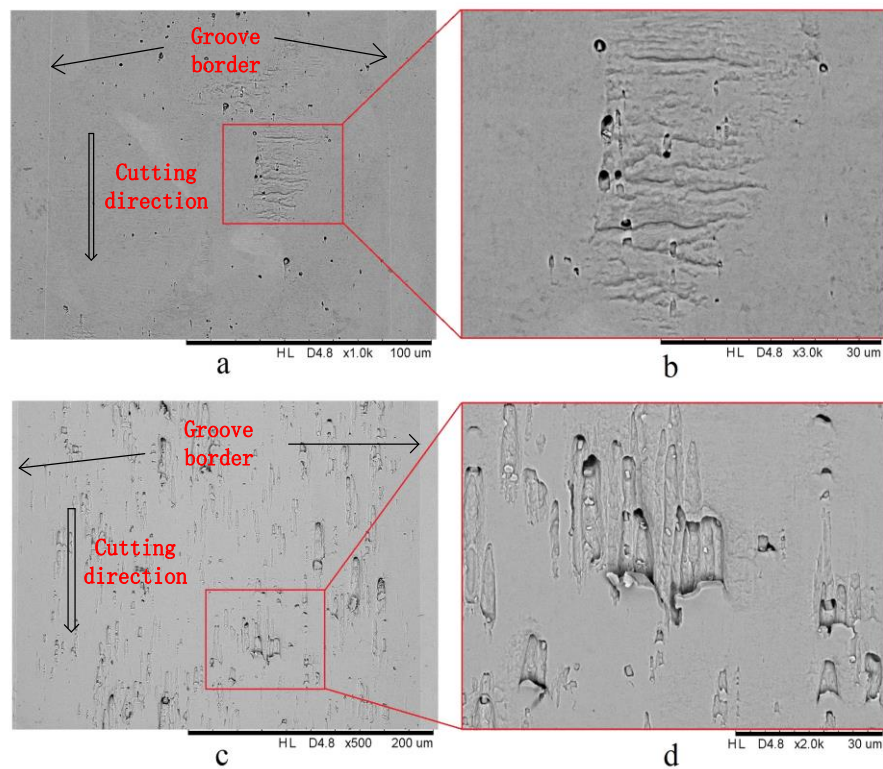


Figure 5.6 SEM image of surface defects: (a) and (b) ripple-like defects at depth of cut around 5 μm; (c) and (d) delamination at depth of cut around 20 μm

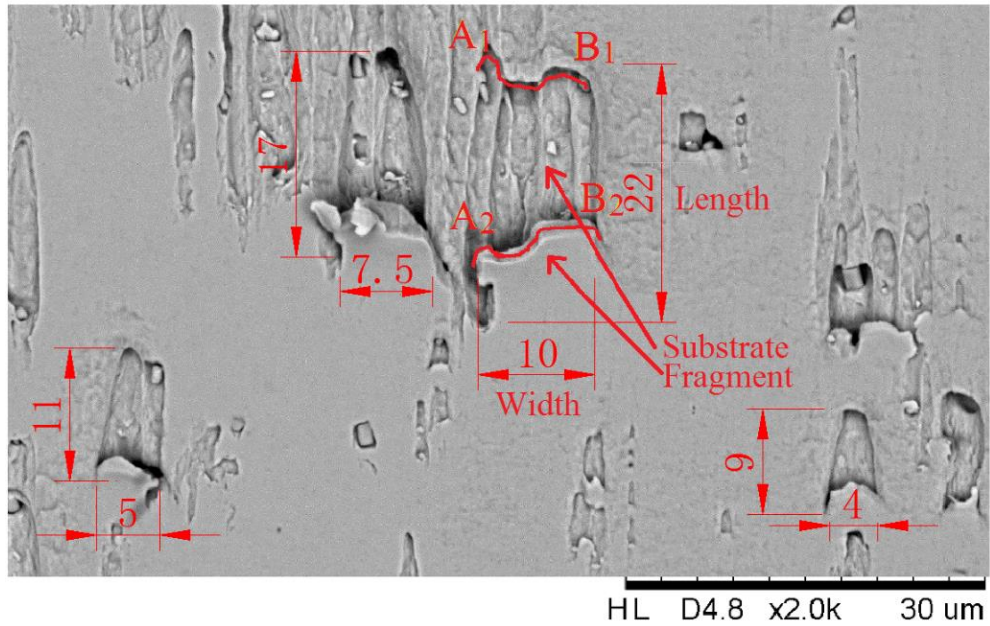


Figure 5.7 Detail of the delamination in Figure 5.6(d) with enlarged scale

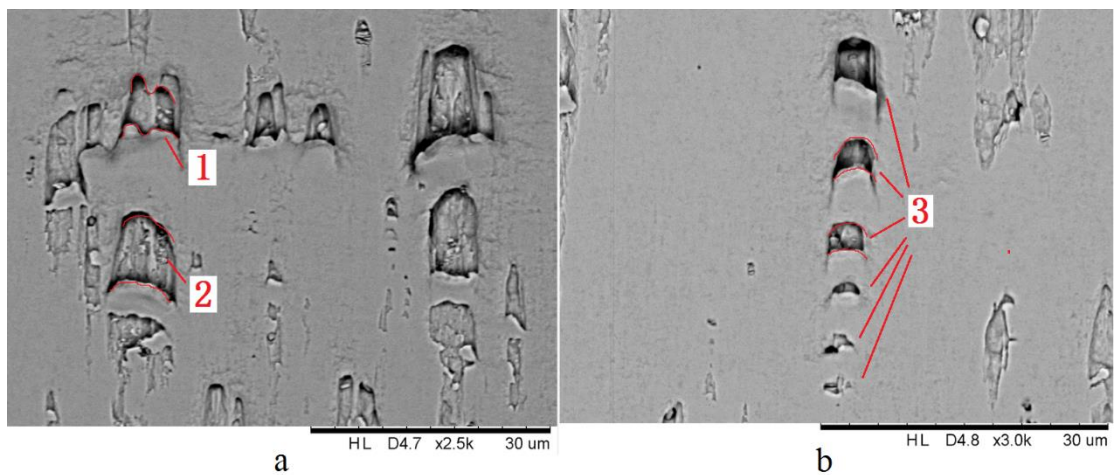


Figure 5.8 Other delamination defects found in this experiment

Figure 5.6 (c) and (d) illustrate the delamination defects, which were found to occur at the depth of cut around 20 μm . The delamination defects were composed of two different features, which we named as the delamination fragment and the delamination substrate, as shown in Figure 5.7, which is the enlarged picture of Figure 5.6 (d). The

typical thickness of the delamination fragments is around 1 μm . There are no obvious variations of the fragments thicknesses that occurred at positions with different depths of cut. The sizes of the delamination features are marked in Figure 5.7, Taking the delamination defect shown at the center of Figure 5.7 as an example, before this defect formed, the yellow curved line A_1B_1 should coincide with line A_2B_2 . A crack was initialized along A_1B_1 due to surface traction caused by friction between the diamond tool and groove surface. After that, line A_2B_2 continued to move to its current position with further movement of the diamond tool. To support this speculation, more delamination defects are shown in Figure 5.8. We can see that there is high similarity between the two edges of the defects. In the defect group, which is marked as “3” in Figure 5.8 (b), a series of defects with different sizes was found arranged in an orderly manner, growing gradually, from small to big. Therefore, the delamination fragment is much smaller than the delamination substrate left behind. The delamination behavior of copper in diamond micro-grooving is the main reason that caused the surface roughness to rise dramatically at a large depth of cut. Figure 5.9 was obtained by plotting the cross-section profiles of the micro-grooves at different depths of cut in one graph. It shows clearly that with increasing depth of cut, the cross-section profiles gradually transformed from smooth to rather rough, due to the progressively increased ripple-like defects and delamination, some of which are highlighted with red ellipse in Figure 5.9.

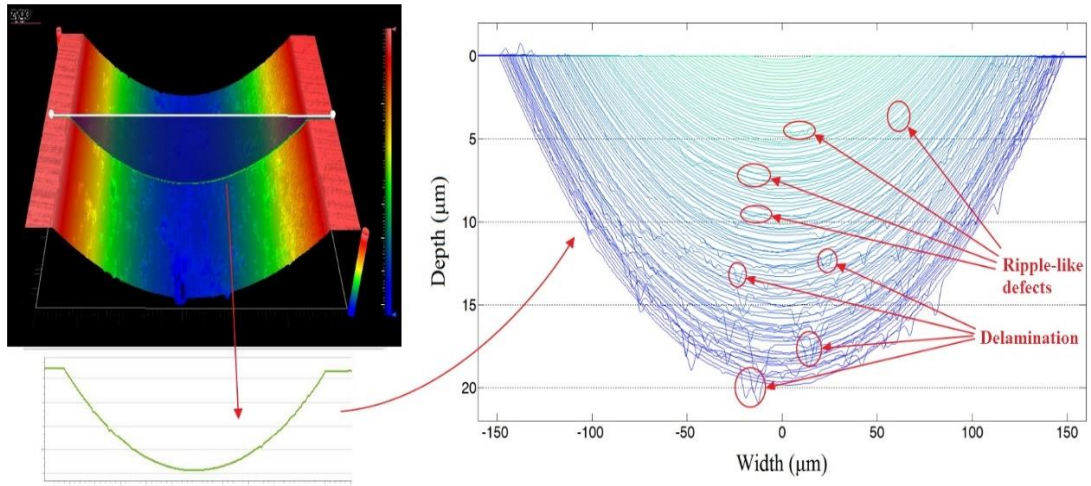


Figure 5.9 Superposition of the cross-section profiles of micro-groove at the depth of cut from 0 to 20 μm

Cutting chips were collected and examined by SEM. As shown in Figure 5.10, the thickness of the cutting chip of OFHC copper at 20 μm depth of cut is much larger than that of C37700 brass. A larger chip thickness corresponds to a bigger chip compression ratio, which indicates that the plastic deformation of material in the cutting area of copper was much more severe than that in brass.

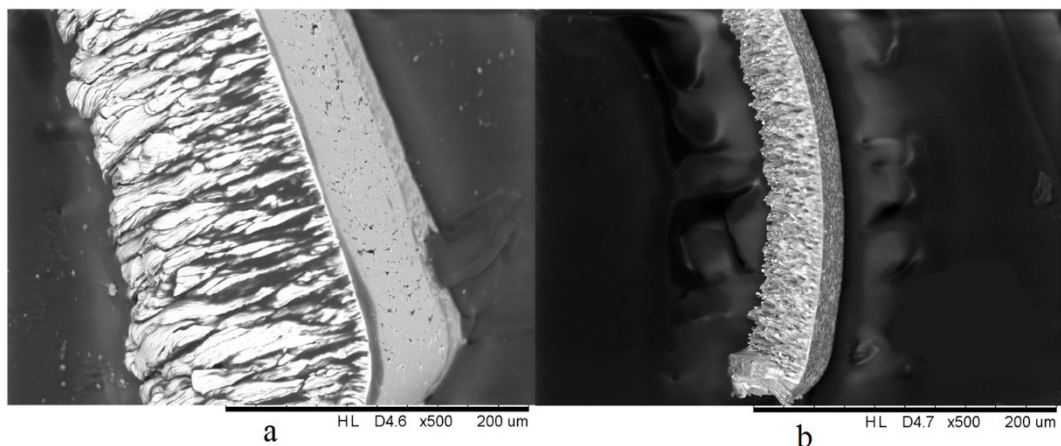


Figure 5.10 Cutting chips at 20 μm depth of cut (a) OFHC copper; (b) C37700 brass

To examine the plastic deformation of the machined groove surface, the workpiece surfaces were chemical etched to reveal the microstructural details of the groove under an optical microscope and SEM. Figure 5.11 and Figure 5.12 are the optical microscopic images of the machined groove surfaces of copper and brass at different depths of cut after chemical etching.

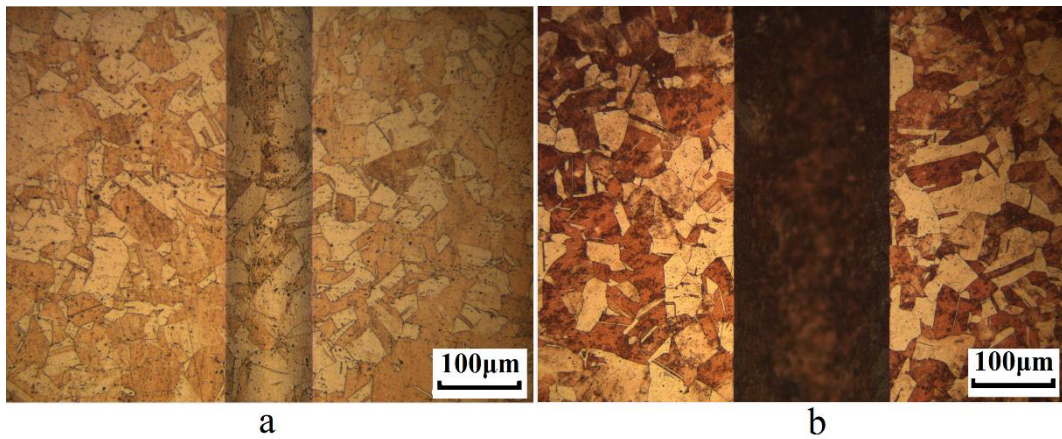


Figure 5.11 Optical microscopic image of machined groove surface of copper after chemical etching (a) depth of cut 3.7 μm ; (b) depth of cut 12.2 μm

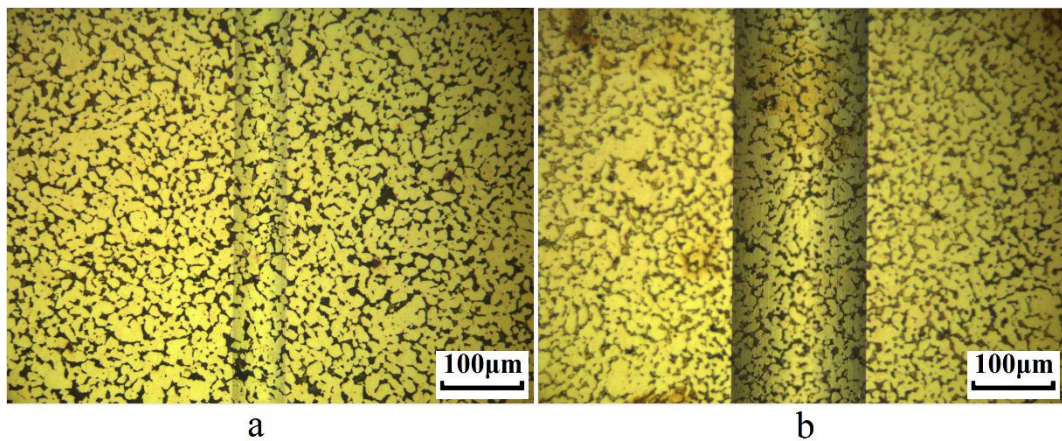


Figure 5.12 Optical microscopic image of machined groove surface of brass after chemical etching (a) depth of cut 1.4 μm ; (b) depth of cut 16.2 μm

For the copper workpiece, when the depth of cut is small, as shown in Figure 5.11 (a), the crystal boundary of the machined groove surface could be observed clearly after chemical etching. When the depth of cut is large, the crystal boundary is totally blurred and cannot be identified (Figure 5.11 (b)). This indicates that the plastic deformation of the machined groove surface of copper at large depth of cut is much more severe than that at small depth of cut.

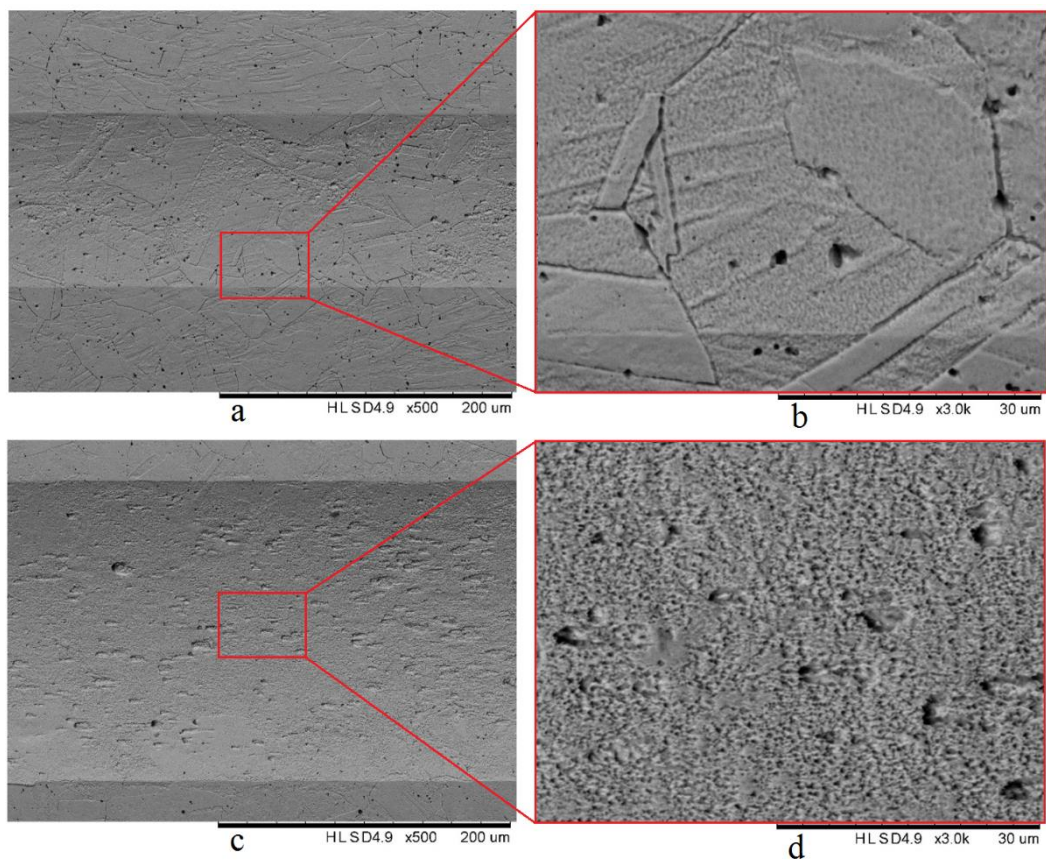


Figure 5.13 SEM image of machined groove surface of copper after chemical etching
(a) and (b) depth of cut 3.7 μm ; (c) and (d) depth of cut 12.2 μm

Figure 5.13 shows the SEM image corresponding to Figure 5.11. It is only at the areas where plastic deformation is severe enough that the surface delamination could be

found in diamond micro-grooving process. For the brass workpiece, a crystal boundary could be observed clearly despite the depth of cut being as large as 16.2 μm , as shown in Figure 5.12 (b). No delamination was found to occur on machined groove surface of brass in any depth of cut.

To understand the differences in the surface plastic deformation and subsurface stress state between copper and brass in diamond cutting process, FEM simulation was performed using Deform 2D software. The material data being used in the simulation process was from the build-in material data library of Deform software which based on real material tests. The tool was considered as a rigid body, and the depth of cut was set to 20 μm . The pure deformation method with continuous adaptive re-meshing technique was adopted in this simulation process to avoid the use of any chip separation criterion. The number of elements was around 40,000. The simulation result is presented in Figure 5.14 and Figure 5.15. The simulated chip morphologies of copper and brass agreed well with the experimental result qualitatively. According to the simulation result, the effective strain of the machined surface of copper is much bigger than that of brass, which is also in agreement with the results of the cutting experiment.

The simulated stress contour of OFHC copper and C37700 brass along the X direction are shown in Figure 5.15. For copper, there existed a large area, marked as S_T in Figure 5.15 (a), within which the materials subjected to high tensile stress. This area is much

larger than that of brass, which means the copper even far behind the cutting tool will still be subjected to tensile stress. This tensile stress could be high enough to induce subsurface cracks to propagate and form the visible delamination defects at large depth of cut. While for brass, this tensile stress region was confined to a much shallower area (Figure 5.15 (b)). These cracks mainly occurred at the tool tip region and no subsurface crack was able to form in the cutting process.

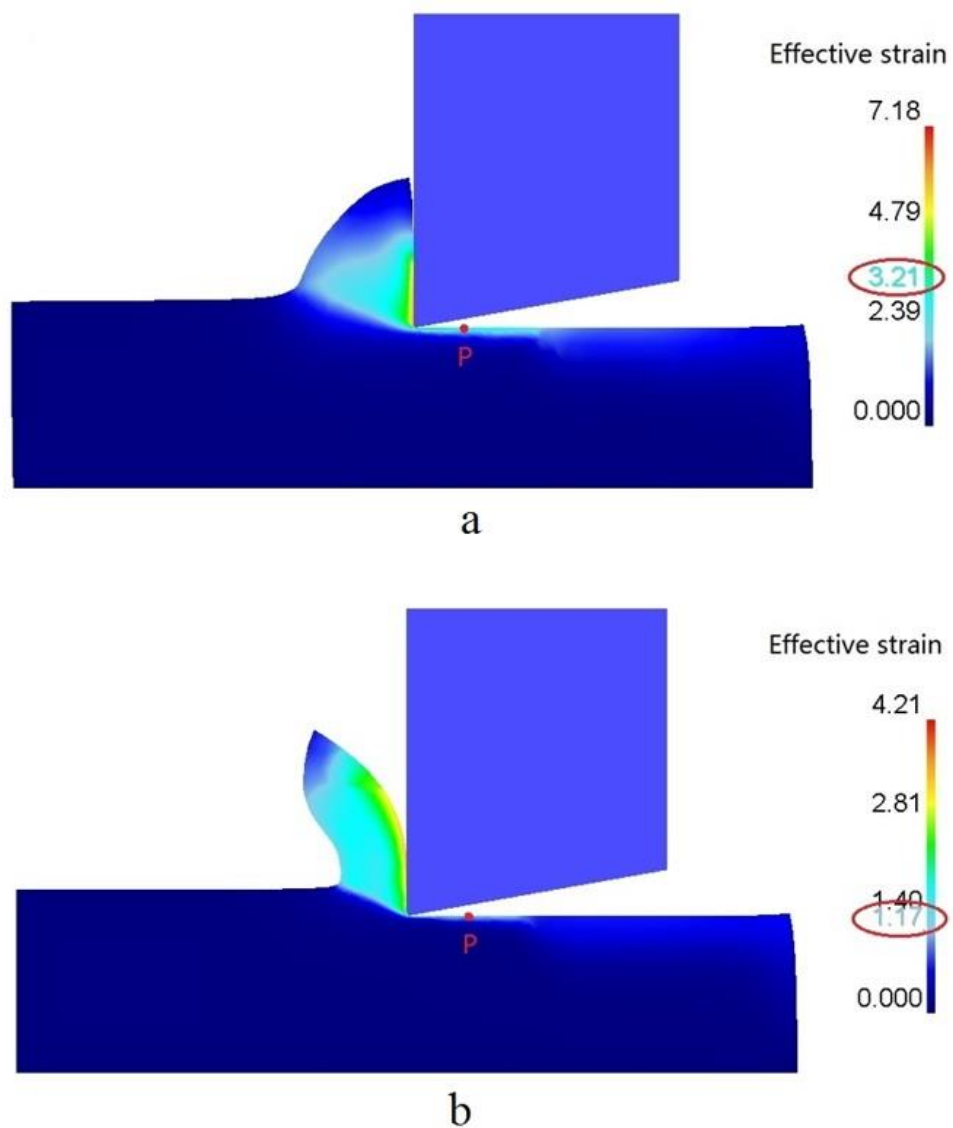


Figure 5.14 Simulated effective strain of (a) OFHC copper and (b) C37700 brass

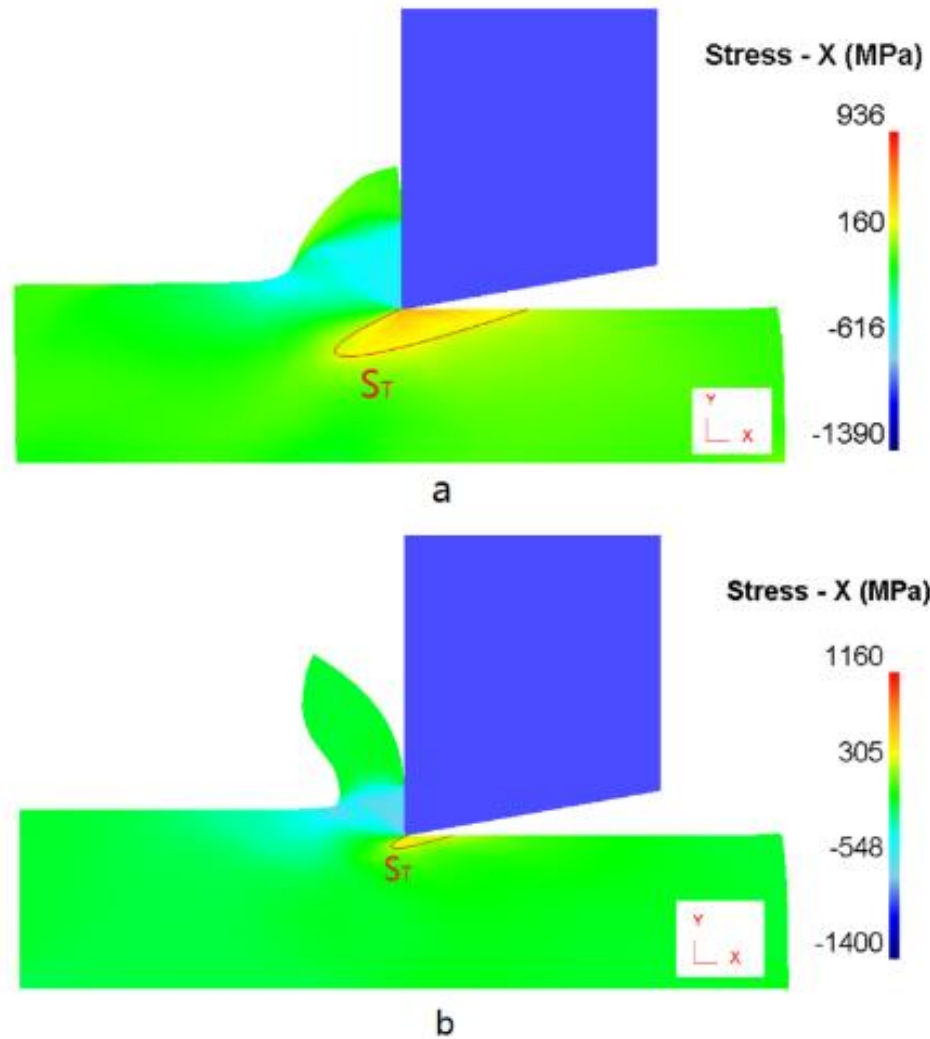


Figure 5.15 Stress contour along X direction (a) OFHC copper; (b) C37700 brass

The formation of delamination in diamond cutting is affected by a number of factors, such as the depth of cut and material brittleness. As in the experimental results, the delamination behavior only occurred at a depth of cut larger than $11 \mu\text{m}$. This is because when the depth of cut is small, the tensile stress in the subsurface area is not high enough to induce subsurface cracks to be initiated and propagate. Also, adequate ductility of the workpiece material is a prerequisite for the formation of delamination in the diamond cutting process.

Even though the surface stress conditions in the diamond cutting process is similar with that in the sliding wear process, the surface delamination phenomenon found in the diamond cutting of copper cannot be explained by the delamination theory of wear. In the sliding wear condition, the delamination wear is a consequence of repeated loads. While in the diamond cutting process, the machined surface is subjected to the load exerted by the cutting tool only one time. Also, in the sliding wear process, a higher hardness or brittleness of the workpiece material is beneficial for the wear debris formation (Jahanmir, 1976). In the diamond cutting process, compared with a harder material such as C37700 brass, soft workpiece materials such as OFHC copper, a higher depth of cut is inductive to form the delamination defects.

5.3 Diamond cutting of OFHC copper assisted with laser heating

5.3.1 Experimentation

Diamond cutting of OFHC copper with laser heating was performed to investigate its cutting performance at elevated temperature. The cutting depth increased continuously from 0 to 20 μm with an inclination angle of approximately 0.057° , and the cutting speed was set as 10 mm/min. A cylindrical shaped commercially available OFHC copper workpiece with a size of 15 mm in diameter and 15 mm in thickness was used

in this experiment. The average grain size of the copper workpiece was around 20 μm . The metallographic structure and hardness of copper is shown as Figure 5.16. The hardness of the bulk material with an indentation load of 1 kg was 105 MPa.

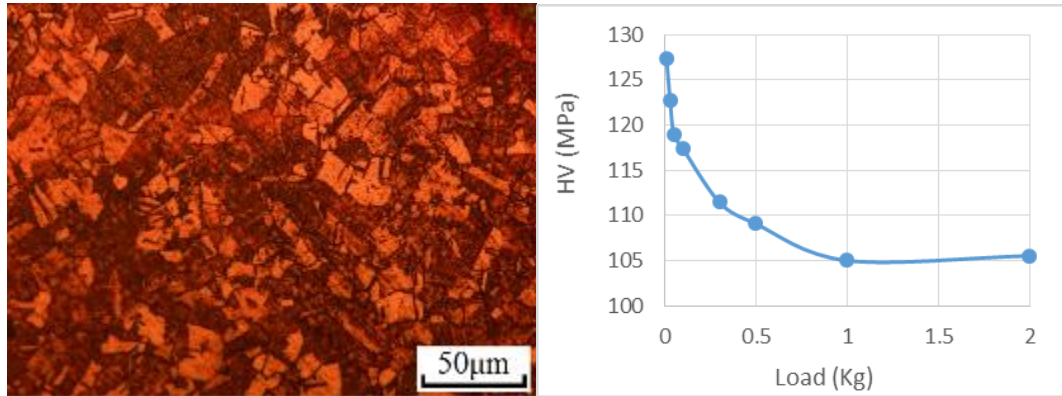


Figure 5.16 The metallographic structure and hardness of copper

Before the experiment, the workpiece surface was diamond turned to a roughness of less than 10 nm. A fresh single crystal diamond tool was used throughout the experiment. The tool nose radius was 0.567 mm, and the tool clearance angle and rake angle were 10° and 0° , respectively. No lubricant was used in this experiment.

The experimental setup is shown as Figure 5.17. The laser used in this experiment was an Nd:YAG laser with a wavelength of 1064 nm and a worked in the continuous mode. The maximum output power of the laser was 20 W. In order to maximize the laser absorbance of OFHC copper, the workpiece surface was painted black using greasy pen. Three grooves were generated in this experiment. One groove was diamond machined without laser heating, while the other two grooves were machined with the assistance

of laser online heating, with the laser output powers were set as 20%, 60% of the maximum power, which were 4 W and 12 W, respectively. To avoid the blocking of cutting chips to the laser light, instead of heating directly in front of the tool tip, the laser spot was focused slightly upper than the tool path. As shown in Figure 5.18, both the distances of OA and AB were around $100\ \mu\text{m}$. The diameter of the laser spot was adjusted to be around $100\ \mu\text{m}$.

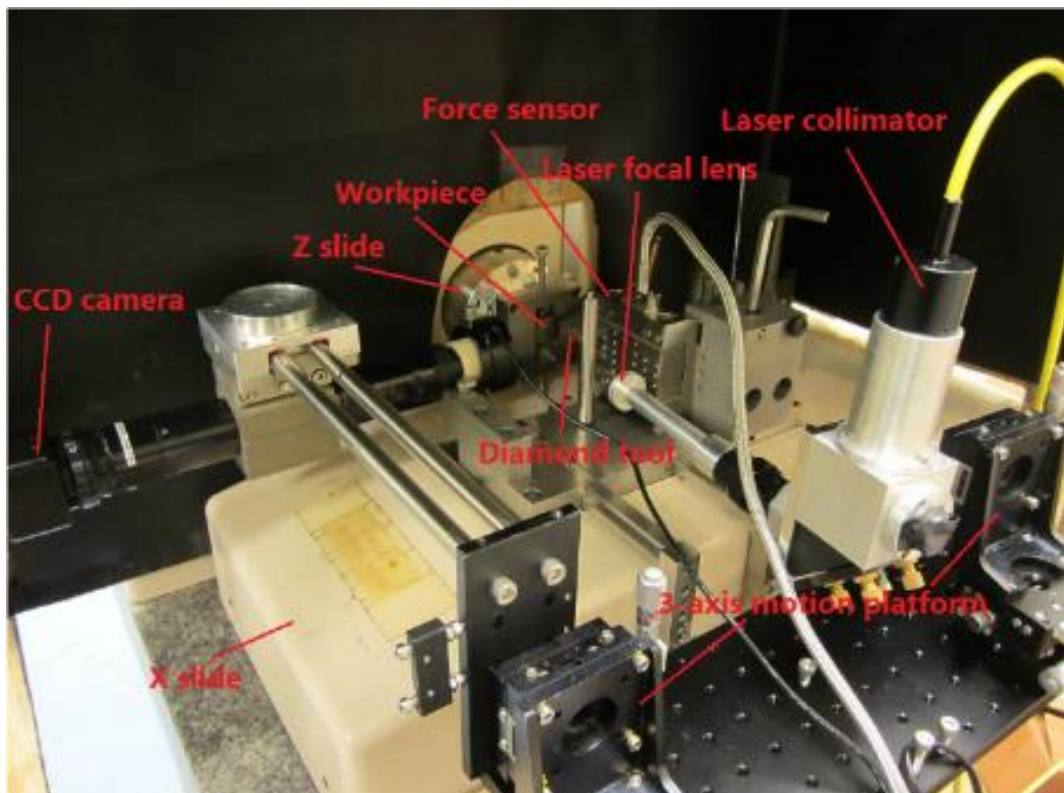


Figure 5.17 Laser assisted diamond cutting experimental setup

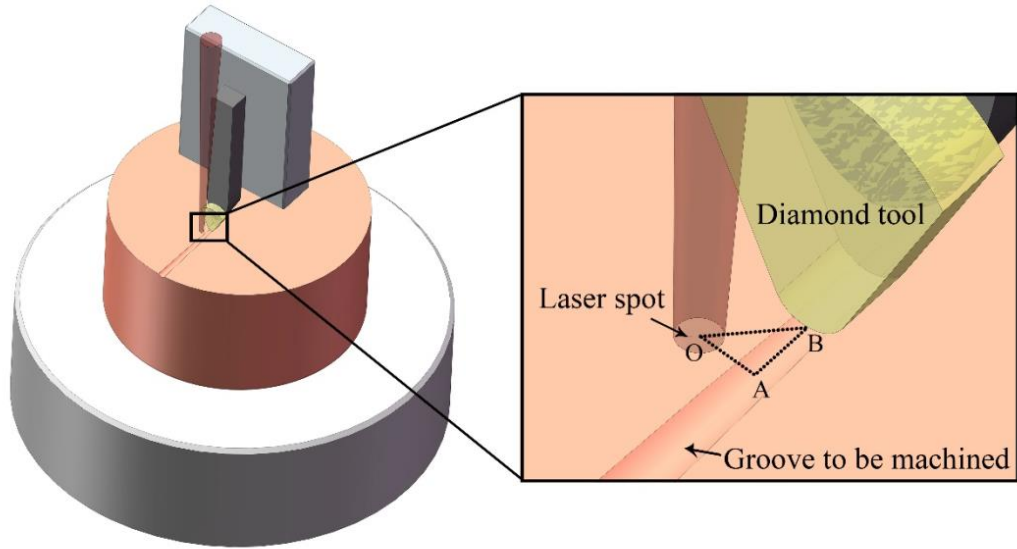


Figure 5.18 Schematic diagram of laser assisted diamond cutting experiment

5.3.2 Simulation of temperature distribution

In order to understand the influence of laser heating on the cutting performance of OFHC copper in diamond cutting process, an estimation of the temperature distribution induced by laser heating is therefore necessary. As the limited size of the laser heated area made it difficult to measure the temperature distribution directly, FEM was adopted to estimate the temperature range of the cutting region in laser heating assisted diamond cutting process.

According to the Fourier law of heat conduction and the law of energy conservation, the heat transfer problem is governed by the following equation:

$$\rho c_p \frac{\partial T}{\partial t} = \frac{\partial}{\partial x} \left(k(T) \frac{\partial T}{\partial x} \right) + \frac{\partial}{\partial y} \left(k(T) \frac{\partial T}{\partial y} \right) + \frac{\partial}{\partial z} \left(k(T) \frac{\partial T}{\partial z} \right)$$

where ρ, c_p, k are the density, specific heat and thermal conductivity, respectively.

The term on the left-hand side represents the laser energy absorption by workpiece material, and the terms on the right-hand side represent the energy diffusion along three dimensions.

The initial condition at time $t = 0$ is given by the initial workpiece temperature T_0 .

$$T(x, y, z, t = 0) = T_0$$

The boundary condition of the surface under laser irradiation takes into account the heat flux, convection and radiation and can be defined by

$$-k \frac{\partial T}{\partial z} = q(x, y) - h(T - T_0) - \sigma \varepsilon (T^4 - T_0^4)$$

where $q, h, \sigma, \varepsilon$ are the heat flux, air convection coefficient, Stefan-Boltzmann constant for radiation and emissivity, respectively.

The laser beam was regarded as a Gaussian beam, and the heat flux q is defined as (Dahotre and Harimkar, 2008)

$$q(x, y) = \frac{2P}{\pi r^2} \exp\left(-\frac{2(x^2 + y^2)}{r^2}\right)$$

where P is the laser power and r is the laser spot radius.

The values of the parameters adopted in this simulation are listed in Table 5.1.

Table 5.1 The values of the simulation parameters

Parameter	Symbol	Value	Unit
<i>Density</i>	ρ	8960	kg/m^3
<i>Specific heat</i>	c_p	385	$J/(kg \cdot K)$
<i>Thermal conductivity</i>	k	401	$W/(m \cdot K)$
<i>Ambient temperature</i>	T_0	20	$^{\circ}C$
<i>Air convection coefficient</i>	h	30	$W / (m^2 \cdot K)$
<i>Stefan-Boltzmann constant</i>	σ	5.67e-8	$W/(m^2 \cdot K^4)$
<i>Emissivity</i>	ε	0.78	-
<i>Laser power</i>	P	4, 12	W
<i>Laser spot radius</i>	r	5e-5	m
<i>Laser scan speed</i>	v	1.667e-4	m/s

The simulated temperature field distribution of the laser heated region with laser powers of 4 W and 12 W are shown in Figure 5.19 and Figure 5.20 respectively. Since the thermal conductivity of OFHC copper is very large while the laser scan speed was very small, the isothermal surface was roughly a hemisphere as shown in the simulation result. Therefore, the temperature of the material in the diamond tool tip region, marked as point B in Figure 5.18, can be considered as close to the temperature of the material in the region marked as point C in Figure 5.19 and Figure 5.20, as long as the distance of OC equals OB, which was around 140 μm . The transient temperature distribution along line MN at a given time is plotted in Figure 5.21. According to the simulation result, when the laser power is 4 W, the temperature at point C is 32.4 $^{\circ}C$, and when the laser power is 12W, the temperature is 57 $^{\circ}C$. Further, it was assumed that the laser

energy was absorbed fully by the workpiece material in this simulation, while in the actual situation, there should be energy loss due to the reflectance of the workpiece material. Therefore, the actual temperature should be lower than the simulated result.

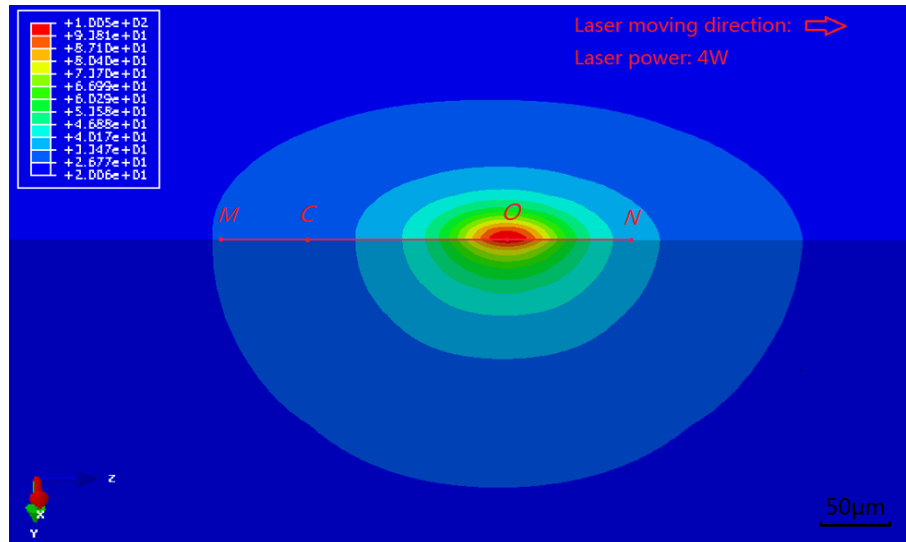


Figure 5.19 Cross-section view of simulated temperature field distribution to a laser power of 4W

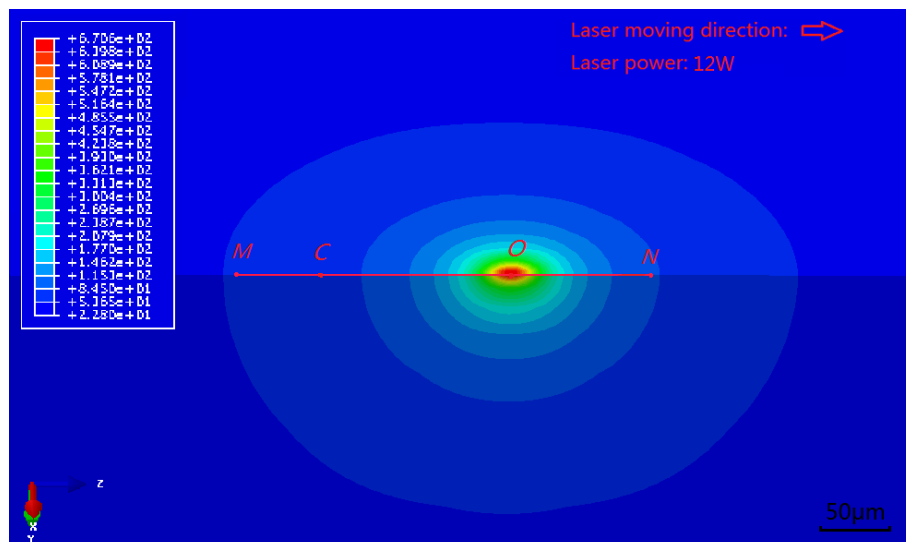


Figure 5.20 Cross-section view of simulated temperature field distribution to a laser power of 12W

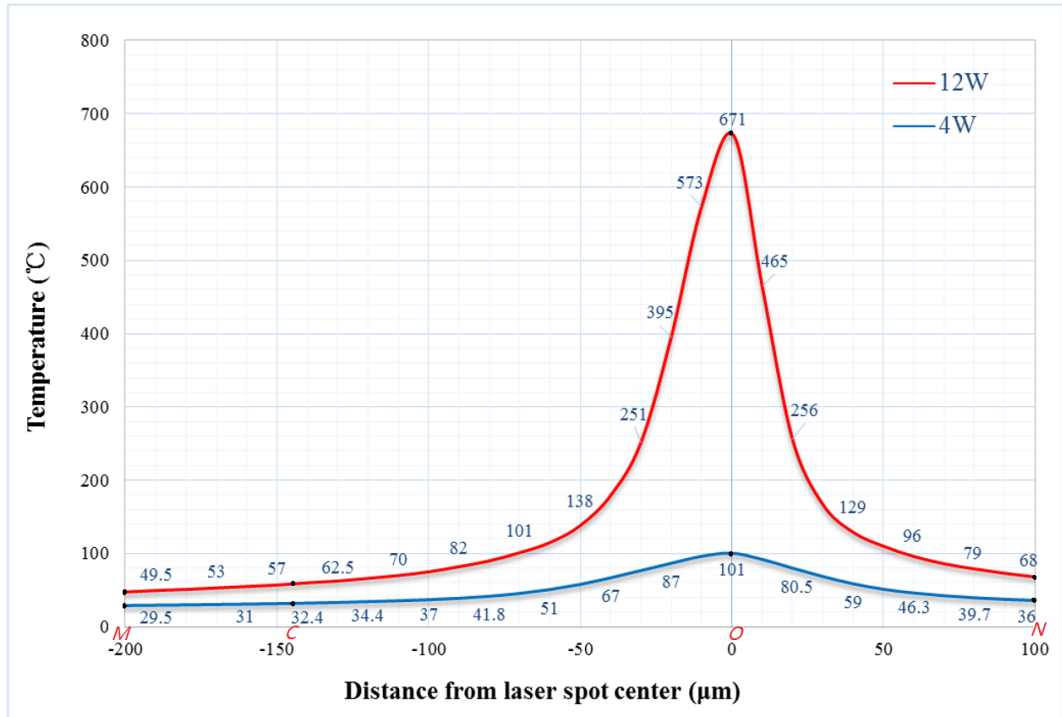


Figure 5.21 Transient temperature distribution along line MN

5.3.3 Results and discussion

The surface roughness at the bottom of the grooves at different depth of cut was measured and plotted in Figure 5.22. When there was no laser heating, the surface roughness of the machined groove increased dramatically with increasing of depth of cut, especially when the depth of cut was larger than 10 µm. This was because of the formation of surface delamination defects, as discussed in the previous section. When there was laser heating during the diamond cutting process, the surface roughness of the machined grooves was improved compared with that of not using laser heating. Furthermore, higher laser power led to a greater improvement of the surface quality of the machined groove.

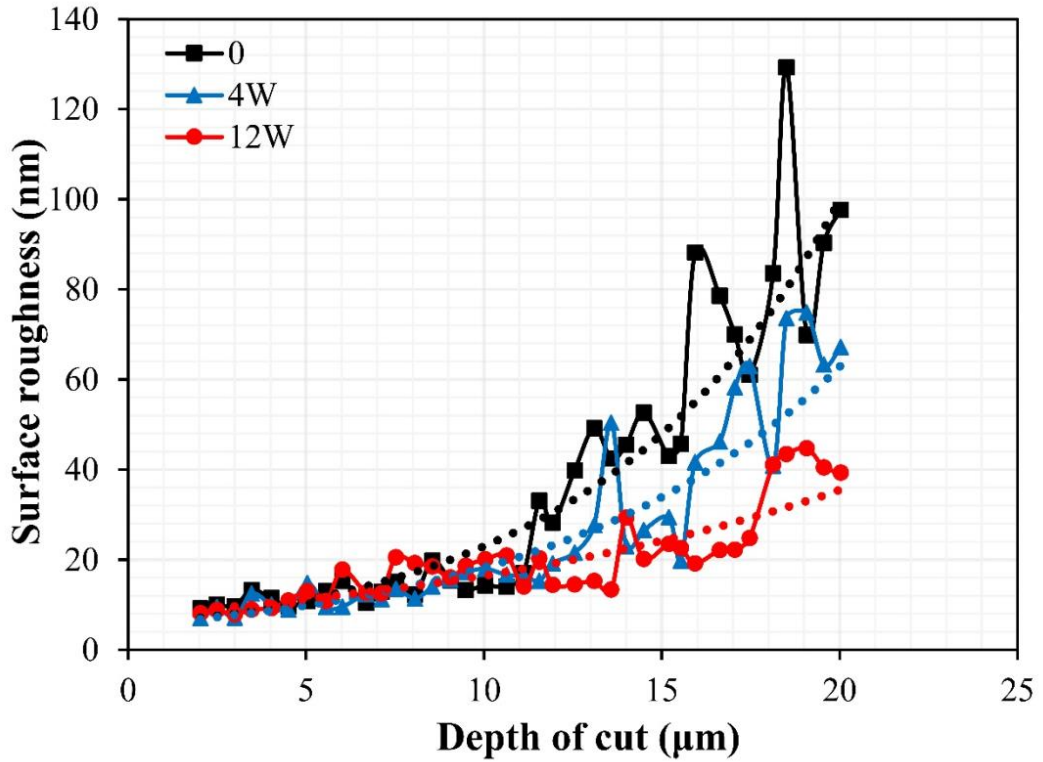


Figure 5.22 Surface roughness of machined grooves with and without laser assistance

Figure 5.23 shows the surface quality of the grooves measured by Zygo at depth of cut of around 19-20 μm. Figure 5.24 shows the SEM image of the groove surfaces at a depth of cut around 19-20 μm.

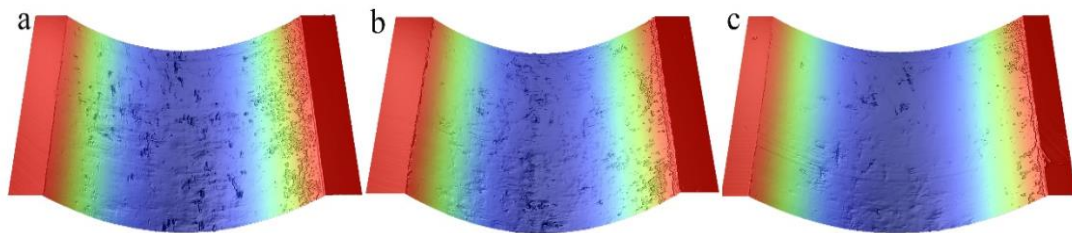


Figure 5.23 Surface quality of the grooves measured by Zygo at depth of cut around 19-20 μm: (a) no laser; (b) laser power: 4 W; (c) laser power: 12 W

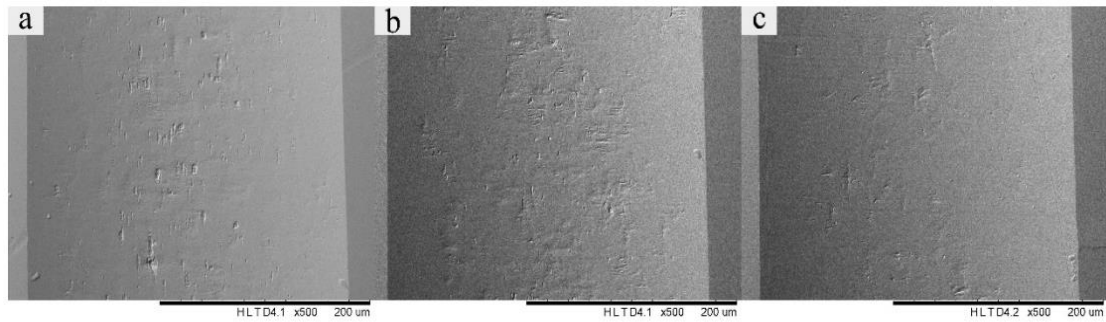


Figure 5.24 Surface quality of the grooves measured by SEM at depth of cut around 19-20 μm : (a) no laser; (b) laser power: 4 W; (c) laser power: 12 W

From these images, one can see that the surface quality of the machined grooves was improved by using laser heating prior to cutting. Higher laser power led to a better surface quality. The defects that occurred at large depths of cut were suppressed when using the laser to assist machining.

Figure 5.25 was obtained by plotting the cross-section profiles of the micro-grooves at different depths of cut in one graph. It shows clearly that with the increasing laser power, the cross section profile of the grooves at large depth of cut became smoother. Thus, laser heating can improve the surface quality of OFHC copper when the depth of cut is relatively large, as found in the diamond cutting of OFHC copper experiments. Figure 5.26 shows the main cutting force in the laser assisted diamond cutting process. With the increasing laser power, the cutting force was reduced dramatically at a depth of cut larger than 14 μm . When the depth of cut was smaller than 13 μm , the influence of laser heating on the cutting force was not pronounced.

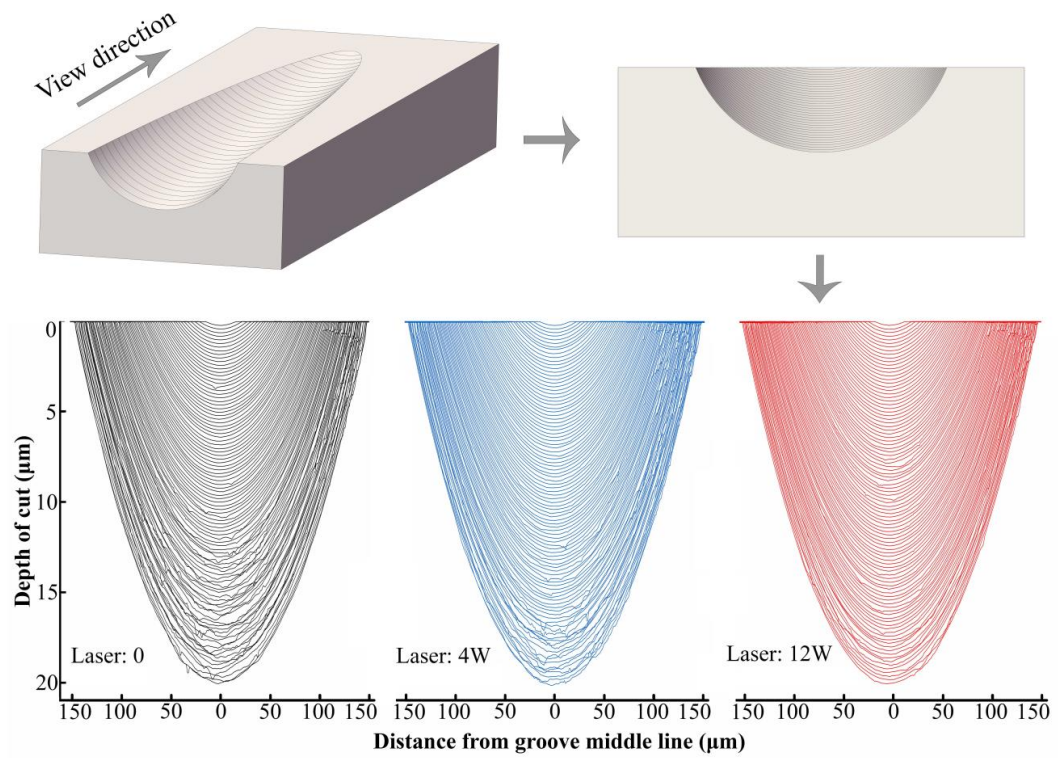


Figure 5.25 Superposition of the cross-section profiles of micro-grooves at the depth of cut from 0 to 20 μm

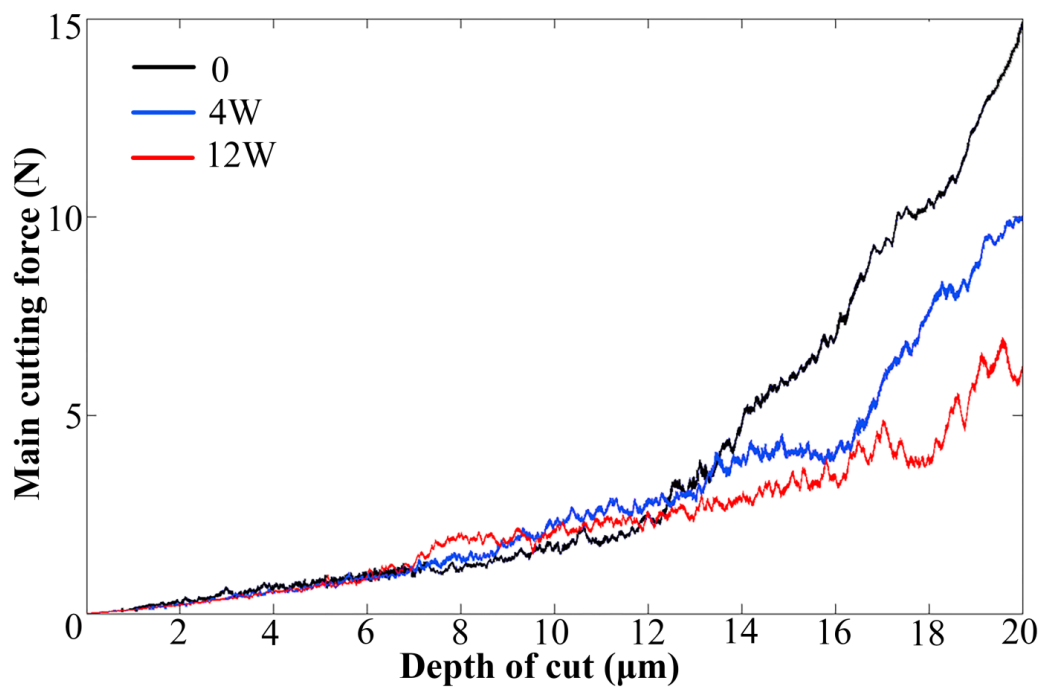


Figure 5.26 Main force in cutting grooves with varying depth of cut

As discussed in previous chapter, that the ductility of the workpiece material exerts a big influence on the formation of surface delamination defects, which was the main reason responsible for the increase of surface roughness at large depth of cut in diamond cutting process. Ductility is the ability of a solid material to undergo large plastic deformation. It can be influenced by elevating working temperature. For OFHC copper, the ductility decreases with the increasing of temperature. This can be explained as following.

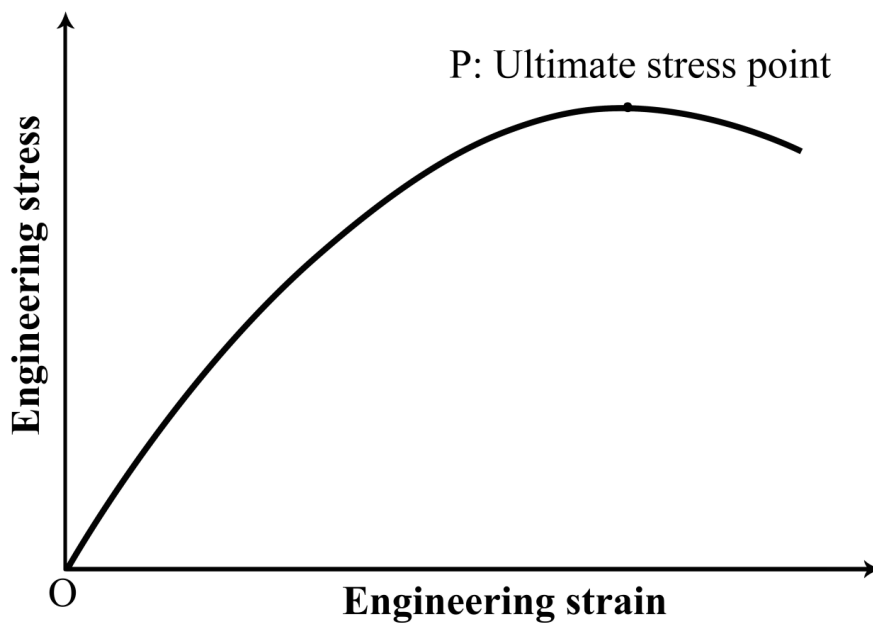


Figure 5.27 Schematic diagram of engineering stress strain curve of OFHC copper

Figure 5.27 shows the schematic diagram of engineering stress strain curve of OFHC copper. The ultimate stress point which marked as P in the figure indicates the initiation of necking of the specimen in the tensile test. At this point, the applied load F reaches its maximum value. Thus

$$dF = 0 \quad (1)$$

Let σ denotes the true stress, and A denotes the cross sectional area of the necking region of the specimen. Then, we can get

$$F = \sigma * A \quad (2)$$

From equations (1) and (2), equation (3) can be derived

$$\sigma dA + Ad\sigma = 0 \quad (3)$$

This also can be written as

$$\frac{d\sigma}{\sigma} = - \frac{dA}{A} \quad (4)$$

Consider a small volume of the testing material in the necking region, l denotes the length of this region. In the stretching process, the volume of this portion of material keeps invariant, thus we have

$$d(A * l) = 0 \quad (5)$$

This equals to

$$Adl + ldA = 0 \quad (6)$$

Thus

$$- \frac{dA}{A} = \frac{dl}{l} = d\varepsilon \quad (7)$$

Where, ε denotes true strain. Combine equation (4) and (7), we can get

$$\frac{d\sigma}{\sigma} = d\varepsilon \quad (8)$$

Or written as

$$\frac{d\sigma}{d\varepsilon} = \sigma \quad (9)$$

In this equation, $d\sigma/d\varepsilon$ is the strain hardening rate. This means necking begins when the strain hardening rate equals to the true stress during the tensile test. For OFHC

copper, the critical resolved shear stress keeps almost invariant when the temperature increases, while the strain hardening rate decreases with the increasing of temperature, which resulted to the decrease of ductility of OFHC copper at elevated temperature. An illustrative diagram is shown in Figure 5.28 (Shi and Zhu, 2006). As can be seen from this diagram, since the flow stress always decrease with the increasing of temperature, at a lower temperature, the slope of the true stress strain curve, which is exactly the definition of strain hardening rate, will be smaller than that at a higher temperature. Thus the projection of the intersection point between the true stress strain curve and the strain hardening rate curve along true strain axis is smaller at a higher temperature, which indicated that necking will initiate under a smaller strain at a higher temperature during the tensile test. Thus the ductility of OFHC copper reduces at an elevated temperature. This theoretical derivation is well supported by an experimental result in the literature which is shown in Figure 5.29. From the real material test of OFHC copper, the elongation at break was reduced at elevated temperatures. This indicated the deterioration of ductility of OFHC copper at elevated temperatures.

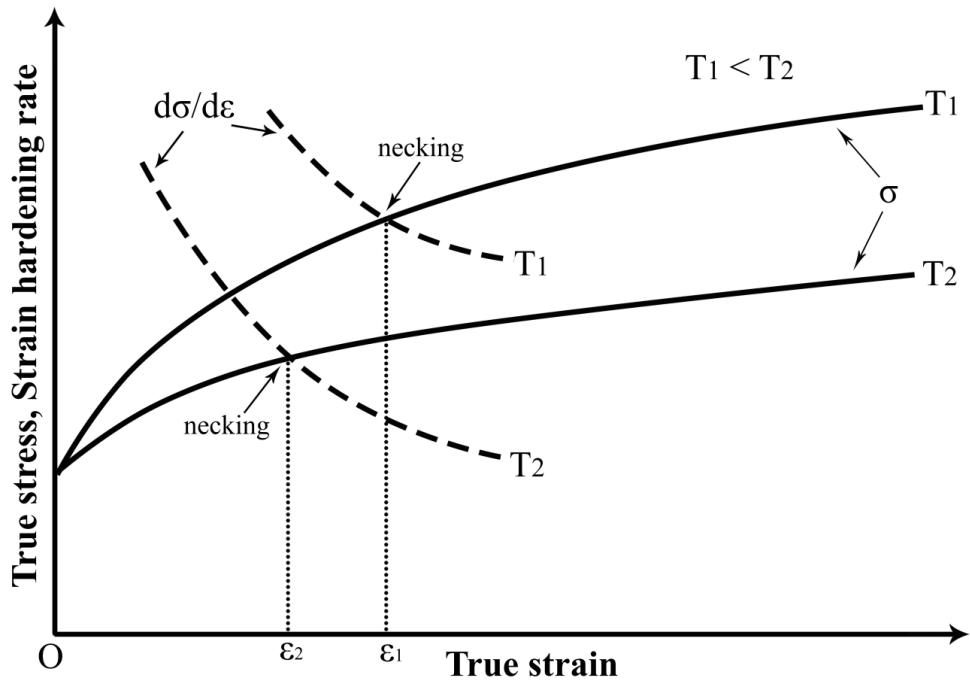


Figure 5.28 Influence of temperature on true stress strain curve and strain hardening rate of OFHC copper (Shi and Zhu, 2006)

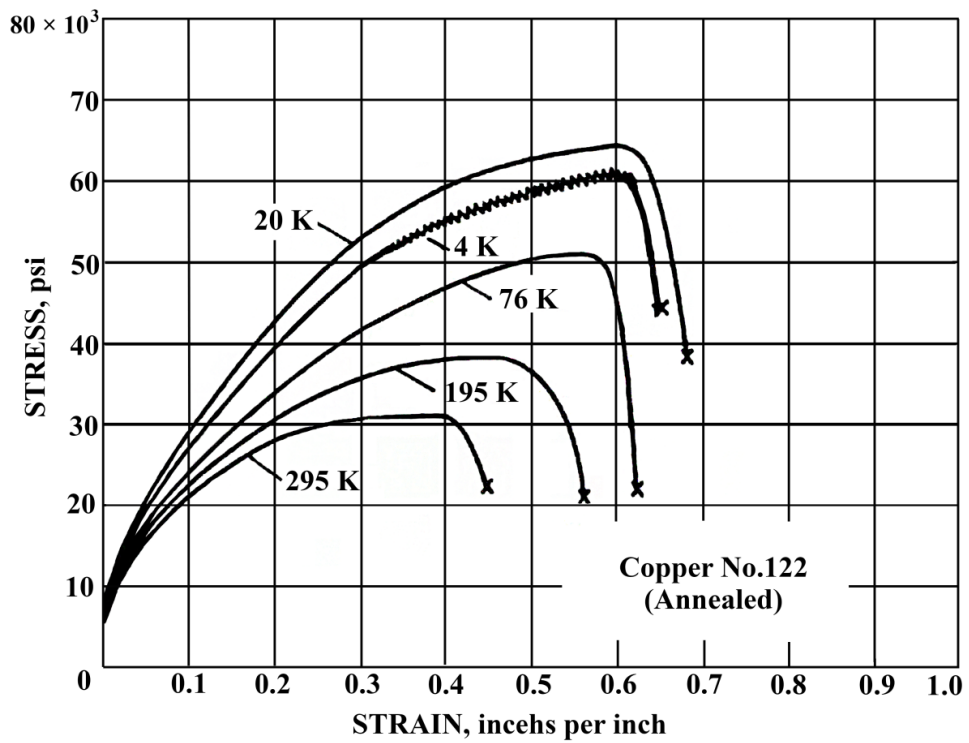


Figure 5.29 Engineering stress strain curve of OFHC copper at different temperatures

(https://www.copper.org/resources/properties/144_8/)

The ductility of OFHC copper could affect the formation of surface defects in diamond cutting process in two aspects. Firstly, a higher ductility usually leads to a larger chip compression ratio which corresponds to a larger cutting force. Secondly, a higher ductility tends to yield a higher degree of plastic deformation of the machined surface. With the assistance of laser heating in diamond cutting process, the ductility of the OFHC copper workpiece was reduced, and thus led to a reduction of cutting force and plastic deformation of the machined surface. It is the combination of smaller cutting force and lower degree of plastic deformation of machined surface that contributed to the alleviation of the formation of surface delamination defects. As a result, the surface quality was improved while using laser to assist diamond cutting of OFHC copper.

This part of work may enhance our understanding of the influence of thermal effects on the machinability change of OFHC copper, and is also helpful in designing suitable experiment parameters in diamond machining OFHC copper so as to improve the surface finish.

5.4 Summary

The surface finish of OFHC copper deteriorates in ultra-precision machining, as surface defects, such as delamination, form when the depth of cut is relatively large. In this research, we investigated the factors responsible for the formation of surface defects. It was found that the formation of surface delamination of OFHC copper in the diamond

cutting process was a result of large cutting force and large plastic deformation at the machined surface. Laser heating of the workpiece was conducted to investigate its effect on the cutting performance of OFHC copper. The main conclusions are as follows:

1. The surface roughness of OFHC copper at the bottom of the groove increased with increasing depth of cut. The relationship between surface roughness and depth of cut can be described by an exponential function, while the surface roughness of the machined C37700 brass groove surface is almost invariant with increasing depth of cut, and the relationship is almost linear.
2. The formation of surface defects, mainly the delamination-like defects, were responsible for the deterioration of the surface quality at large depths of cut of OFHC copper. Finite element modelling was used to help understand the formation of delamination of OFHC copper during the cutting process. The formation of these defects was suspected to be influenced by plastic deformation and the stress state of the workpiece material at the machined surface.
3. Laser heating was found to be beneficial for the suppression of surface delamination of OFHC copper at large depths of cut, and thus led to the improvement of surface quality. It could be explained by the influence of temperature on ductility of OFHC copper, that when temperature increases, its ductility will reduce.

Chapter 6 Overall conclusions and suggestions for future studies

6.1 Overall conclusions

The use of diamond tool to generate structured surfaces with high precision to achieve designed functions is becoming a popular and important technique in recent years. Components with very small surface roughness around several nanometers and high form accuracy within 0.1 μm can be fabricated with the diamond machining method which found wide applications in many opto-electronic products. Normally, these high precision components are made of materials that are not only diamond machinable but also have excellent machinability. However, there are technical or economical restrictions on the use of ultra-precision machining such as for machining brittle materials or when a large depth of cut is required. In this study, the laser approach was adopted to assist in the diamond cutting process. Two aspects of using lasers to assist machining were investigated. This research therefore can be divided into two parts. Part 1 is an exploratory study on the use of diamond tool to perform the final shaping of a silicon groove roughly cut by laser. In part 2, the focus was on the investigation of the reasons for the formation of surface defects of OFHC copper in the diamond cutting process, and is concerned with the performance of laser heating on the reduction of surface defects of OFHC copper in the diamond cutting process. The overall conclusions are as follows:

1. A hybrid machining process combining laser grooving and diamond shaping.

In order to increase the machining efficiency as well as reduce tool wear in fabricating silicon lenticular lens mold inserts used in precision glass molding, a hybrid machining process combining laser grooving with diamond shaping was proposed. A feasibility study was performed to investigate the influence of various laser and diamond cutting parameters on the machining performance. Firstly, a laser micro-machining device was designed and set up to perform laser grooving experiment. This experimental setup was composed of three parts: a three-dimensional motion platform, a laser controller and transmission module and a visualization module. The influence of the laser parameters on the grooving depth was investigated systematically. It was found that there was a linear relationship between the laser power and laser grooving depth, and also the relationship between laser scan speed and laser grooving depth. While the effect of the defocus depth on the laser grooving depth was non-linear. Grooves of various depth were generated on the silicon workpiece surface with the designed profile shape. Secondly, diamond shaping of laser generated grooves was conducted to investigate the influence of the finish cutting depth on the surface quality of the machined grooves. The experimental results show that the surface roughness of machined grooves can be improved by reducing the finish cutting depth. When the finish cutting depth was 4 μm , the surface roughness was 644 nm, and was reduced to 126 nm when the finish cutting depth was 0.2 μm .

2. Diamond cutting of OFHC copper assisted with laser heating

Because of the high thermal conductivity and high purity of OFHC copper, it is the most suitable material to make high power laser mirrors which require high quality defect-free surfaces to ensure a high laser damage threshold can be achieved. While the cutting performance of OFHC copper in ultra-precision machining is sensitive to machining parameters, the machined surface quality of OFHC copper deteriorates quickly with the increasing cutting depth. In this research, a taper cutting experiment was conducted to study the relationship between surface roughness and depth of cut. It was found that the surface roughness of OFHC copper at the bottom of machined grooves increased dramatically with increasing of depth of cut. The relationship between the surface roughness and depth of cut could be described by an exponential function. As a comparison, the surface roughness of machined C37700 brass grooves remained almost invariant with increasing depth of cut. The experimental result showed that the formation of surface defects at large depths of cut, which were mainly exhibited as delamination, was the reason that causes the surface roughness of machined grooves in the OFHC copper workpiece to increase. The factors that are responsible for the formation of surface defects were investigated. By comparing with the experimental result of brass, the formation of surface defects of OFHC copper was suspected to be influenced by plastic deformation and the stress distribution of the material at the machined surface in the diamond cutting process. FEM was conducted to help understanding the formation of the delamination of the OFHC copper during the

diamond cutting process. It was suspected that the formation of surface delamination on the OFHC copper workpiece was influenced by plastic deformation and the stress state of the material in the subsurface area in the diamond cutting process. Laser online heating of the material at the cutting region was introduced to the diamond cutting process to investigate its effect on the cutting performance of OFHC copper. It was found that the formation of the surface delamination defects in the diamond cutting process can be alleviated by using laser heating to assist the machining, and thus led to a better surface quality of the machined grooves of OFHC copper at a relatively large depth of cut.

6.2 Suggestions for further studies

In this research, two aspects of using laser to assist machining were investigated which demonstrated the benefits of the use of a laser in the diamond cutting process. So far only pilot feasibility studies have been conducted and further optimization of the equipment and process is needed.

- 1) For the laser diamond hybrid machining process which was aimed at machining silicon lenticular lens mold inserts, the surface quality of machined parts is far from satisfactory, and further research is needed to investigate how to improve the surface quality of the machined grooves, such as further reducing the finish cutting depth using a negative diamond tool in the finish cutting process or in seeking other appropriate post-polishing methods.

- 2) For investigation of the surface defects of OFHC copper in the diamond cutting process, there are many factors that could influence the formation of surface delamination, such as the grain size of the workpiece, tool wear and the tool rake angle that were not addressed in this research. These could be possible future research directions in order to get a better understanding on the formation of surface delamination
- 3) LAM of brittle materials in conventional machining process has been well researched already. Laser assisted ultra-precision machining of brittle materials could also be a future research direction, since little work has been done in using a laser to assist machining brittle materials in ultra-precision machining process.

References

- Abdelmoneim M. E., Scrutton R. F., "Tool edge roundness and stable build-up formation in finish machining", *Journal of Engineering for Industry*, 96.4, (1974): 1258-1267.
- Abdulghani O., et al., "Modeling and simulation of laser assisted turning of hard Steels", *Modeling and Numerical Simulation of Material Science*, (2013).
- Albrecht P., "New development in the theory of the metal-cutting process: part II—the theory of chip formation", *Journal of Engineering for Industry*, 83.4, (1961): 557-568.
- Amin A. K. M., Turnad L. G., "Heat-assisted machining", Elsevier Ltd., (2014): 297-331.
- Armarego E. J. A., Robert H. B., "The machining of metals", Rrentice-Hall Inc., (1969): 437.
- Bailey J. A., "Friction in metal machining—mechanical aspects", *Wear*, 31.2, (1975): 243-275.
- Basuray P. K., Misra B. K., Lal G. K., "Transition from ploughing to cutting during machining with blunt tools", *Wear*, 43.3, (1977): 341-349.
- Bäuerle D. W., "Laser processing and chemistry", Springer Science & Business Media, (2013).
- Bitans K., Brown R. H., "An investigation of the deformation in orthogonal cutting", *International Journal of Machine Tool Design and Research*, 5.3, (1965): 155-165.

- Blackley W. S., Scattergood R. O., "Ductile-regime machining model for diamond turning of brittle materials", *Precision Engineering*, 13.2, (1991): 95-103.
- Boothroyd G., "Fundamentals of metal machining and machine tools", Crc Press, 28, (1988).
- Bourell D. L., et al., "Selective laser sintering of metals and ceramics", *International Journal of Powder Metallurgy*, 28.4, (1992): 369-381.
- Brinksmeier E., et al., "Residual stresses—measurement and causes in machining processes", *CIRP Annals-Manufacturing Technology*, 31.2, (1982): 491-510.
- Brinksmeier E., Schönemann L., "Review on diamond-machining processes for the generation of functional surface structures", *CIRP Journal of Manufacturing Science and Technology*, 5.1, (2012): 1-7.
- Brinksmeier E., Schmütz J., "Generation and texture of surfaces in ultraprecision cutting of copper", *Machining Science and Technology*, 1.2, (1997): 185-193.
- Brown M. S., Craig B. A., "Fundamentals of laser-material interaction and application to multiscale surface modification", *Laser Precision Microfabrication*, Springer Berlin Heidelberg, (2010): 91-120.
- Cahill D. G., Grigoropoulos C. P., "Melting and surface deformation in pulsed laser surface micromodification of Ni-P disks", *Urbana*, 51, (2000): 61801.
- Chryssolouris E., "Laser machining: theory and practice", Springer Science & Business Media, (2013).
- Dahotre N. B., "Lasers in surface engineering", ASM International, 1, (1998).

- Dahotre N. B., and Sandip Harimkar. "Laser fabrication and machining of materials", Springer Science & Business Media, (2008).
- Davies M. A., et al., "Application of precision diamond machining to the manufacture of microphotonic components", Optical Science and Technology, SPIE's 48th Annual Meeting, International Society for Optics and Photonics, (2003).
- Ding X., et al., "A study of the cutting performance of poly-crystalline oxygen free copper with single crystalline diamond micro-tools", Precision Engineering, 36.1, (2012): 141-152.
- Dobrzański L. A., et al., "Laser surface treatment of multicrystalline silicon for enhancing optical properties", Journal of Materials Processing Technology, 201.1, (2008): 291-296.
- Donachie M. J., "Titanium: a technical guide", ASM International, (2000).
- Dornfeld D., Sangkee M., "A review of burr formation in machining", Burrs-Analysis, Control and Removal, Springer Berlin Heidelberg, (2010): 3-11.
- Ernst, Hans, and Merchant M. E., "Chip formation, friction and finish", Cincinnati: Cincinnati milling machine Company, (1941).
- Evans C., Bryan J. B., "Cryogenic diamond turning of stainless steel", CIRP Annals-Manufacturing Technology, 40.1, (1991): 571-575.
- Fang F. Z., et al., "Nanometric cutting of single crystal silicon surfaces modified by ion implantation", CIRP Annals-Manufacturing Technology, 60.1, (2011): 527-530.
- Franssila, S., "Introduction to microfabrication", John Wiley & Sons, (2010).

- Gaspar B., "Microstructural characterization of Ti-6Al-4V and its relationship to sample geometry", California Polytechnic State University, (2012).
- Geusic J. E., Marcos H. M., Legrand V. U., "Laser oscillations in Nd-doped yttrium aluminum, yttrium gallium and gadolinium garnets", Applied Physics Letters, 4.10, (1964): 182-184.
- Glass A. J., Arthur H. G., "Laser induced damage in optical materials: 7th ASTM symposium", Applied Optics, 15.6, (1976): 1510-1529.
- Groover M. P., "A survey on the machinability of metals", SME Technology Paper, (1976).
- Goel S., et al., "Diamond machining of silicon: a review of advances in molecular dynamics simulation", International Journal of Machine Tools and Manufacture, 88, (2015): 131-164.
- Govila V. M. G., Smita G., "Diode laser applications in periodontics", Indian Journal of Dental Sciences, 3.5, (2011).
- Harris D. C., Michael D. B., "Symmetry and spectroscopy: an introduction to vibrational and electronic spectroscopy", Courier Corporation, (1978).
- Hick A. J., "Rapid surface heat treatments-a review of laser and electron beam hardening", Heat Treatment of Metals, 10.1, (1983): 3-11.
- Hiroshi O., Jin M., et al., "Novel lenticular lens fabrication method on glass by using ink-jet printer", SID Symposium Digest of Technical Papers, 42.1, (2011): 1364–1367.

- Hong S. Y., Irel M., Woo C. J., "New cooling approach and tool life improvement in cryogenic machining of titanium alloy Ti-6Al-4V", *International Journal of Machine Tools and Manufacture*, 41.15, (2001): 2245-2260.
- Horváth R., Palásti K. B., Sipos S., "Environmental-friendly cutting of automotive parts made of aluminium castings", *Hungarian Journal of Industry and Chemistry*, 38.2, (2010): 99-105.
- Ikawa N., et al., "An atomistic analysis of nanometric chip removal as affected by tool-work interaction in diamond turning", *CIRP Annals-Manufacturing Technology*, 40.1, (1991): 551-554.
- Ikuhiro I., et al., "Nippon steel & sumitomo metal technical report" No. 106 July 2014.
<http://www.nssmc.com/en/tech/report/nssmc/pdf/106-05.pdf>
- Jahanmir S., "A fundamental study on the delamination theory of wear", Diss. Massachusetts Institute of Technology, (1977).
- Johnson G. R., William H. C., "A constitutive model and data for metals subjected to large strains, high strain rates and high temperatures", *Proceedings of the 7th International Symposium on Ballistics*, 21, (1983).
- Kawasegi N., et al., "Single-crystal diamond tools formed using a focused ion beam: Tool life enhancement via heat treatment", *Diamond and Related Materials*, 49, (2014): 14-18.
- Kiliçaslan C., "Modelling and simulation of metal cutting by finite element method", Diss. İzmir Institute of Technology, (2009).

- Kim K. W., Woo Y. L., Hyo C. S., "A finite element analysis for the characteristics of temperature and stress in micro-machining considering the size effect", *International Journal of Machine Tools and Manufacture*, 39.9, (1999): 1507-1524.
- King R. F., Tabor D., "The strength properties and frictional behaviour of brittle solids", *Proceedings of the Royal Society of London A: Mathematical, Physical and Engineering Sciences*, 223.1153, (1954).
- Knight Optical Website: <http://www.knighthoptical.com/stock/optical-components/uvvisnir-optics/lenses/aspheric-lenses/diamond-turned-aspheric-lenses/>
- Komanduri R., Chandrasekaran N., Raff L. M., "Effect of tool geometry in nanometric cutting: a molecular dynamics simulation approach", *Wear*, 219.1, (1998): 84-97.
- Komanduri R., Lucca D. A., Tani Y., "Technological advances in fine abrasive processes", *CIRP Annals-Manufacturing Technology*, 46.2, (1997): 545-596.
- Kumar M., Melkote S., and Lahoti G., "Laser-assisted microgrinding of ceramics", *CIRP Annals-Manufacturing Technology*, 60.1, (2011): 367-370.
- Lane B. M., et al., "Diamond tool wear when machining Al6061 and 1215 steel", *Wear*, 268.11, (2010): 1434-1441.
- Lawn B. R., Jensen T., Arora A., "Brittleness as an indentation size effect", *Journal of Materials Science*, 11.3, (1976): 573-575.
- Li X. P., et al., "Characteristics of ductile mode chip formation in nanoscale cutting of brittle materials", *International Journal of Abrasive Technology*, 1.1, (2007): 37-58.

- Liu K., Shreyes N. M., "Finite element analysis of the influence of tool edge radius on size effect in orthogonal micro-cutting process", *International Journal of Mechanical Sciences*, 49.5, (2007): 650-660.
- Liu K., Shreyes N. M., "Material strengthening mechanisms and their contribution to size effect in micro-cutting", *Journal of Manufacturing Science and Engineering*, 128.3, (2006): 730-738.
- Liu X. Y., Paul K. C., Ding C. X., "Surface modification of titanium, titanium alloys, and related materials for biomedical applications", *Materials Science and Engineering: R: Reports*, 47.3, (2004): 49-121.
- Liu X. Y., Richard E. D., Shiv G. K., "Model-based analysis of the surface generation in microendmilling—part I: model development", *Journal of Manufacturing Science and Engineering*, 129.3, (2007): 453-460.
- Lucca D. A., Rhorer R. L., Komanduri R., "Energy dissipation in the ultraprecision machining of copper", *CIRP Annals-Manufacturing Technology*, 40.1, (1991): 69-72.
- Lucca D. A., Seo Y. W., Komanduri R., "Effect of tool edge geometry on energy dissipation in ultraprecision machining", *CIRP Annals-Manufacturing Technology*, 42.1, (1993): 83-86.
- Lucca D. A., Seo Y. W., Rhorer R. L., "Energy dissipation and tool-workpiece contact in ultra-precision machining", *Tribology Transactions*, 37.3, (1994): 651-655.
- Malkin S., Joseph N., "Minimum energy in abrasive processes", *Wear*, 32.1, (1975): 15-23.

- Markopoulos A. P., Dimitrios E. M., "Modeling of micromachining", *Modern Mechanical Engineering*, Springer Berlin Heidelberg, (2014): 285-323.
- Masood S. H., Kelly A., Milan B., "An experimental study of laser-assisted machining of hard-to-wear white cast iron", *International Journal of Machine Tools and Manufacture*, 51.6, (2011): 450-456.
- Masuko M., "Fundamental Research on the Metal Cutting—Second Report", *Bull, JSME*, 22, (1956): 371-377.
- Matsumoto Y., Hashimoto F., Lahoti G., "Surface integrity generated by precision hard turning", *CIRP Annals-Manufacturing Technology*, 48.1, (1999): 59-62.
- Maurotto A., et al., "Enhanced ultrasonically assisted turning of a β -titanium alloy", *Ultrasonics*, 53.7, (2013): 1242-1250.
- Micheletti G. F., "Work on machinability in the cooperative group C of CIRP and outside this group". Collège Internationale pour la Recherche sur la Production Mécanique, General Assembly, (1969).
- Mechanical Properties of Copper and Copper Alloys at Low Temperatures:
https://www.copper.org/resources/properties/144_8/
- Moriwaki T. N. S., Sheng L., "Combined stress, material flow and heat analysis of orthogonal micromachining of copper", *CIRP Annals-Manufacturing Technology*, 42.1, (1993): 75-78.
- Moriwaki T., "Machinability of copper in ultra-precision micro diamond cutting", *CIRP Annals-Manufacturing Technology*, 38.1, (1989): 115-118.

Nakayama K., Kiyoshi T., "Size effect in metal-cutting force", *Journal of Engineering for Industry*, 90.1, (1968): 119-126.

Orloff J., Lynwood S., Mark U., "High resolution focused ion beams: FIB and its applications: the physics of liquid metal ion sources and ion optics and their application to focused ion beam technology". Springer Science & Business Media, (2003).

Patel C. K. N., "Continuous-wave laser action on vibrational-rotational transitions of CO₂", *Physical Review*, 136.5A, (1964): A1187.

Photonics website : <http://www.photonics.com/EDU/Handbook.aspx?AID=25164>

Pramanik A., et al., "Ultraprecision turning of electroless nickel: effects of crystal orientation and origin of diamond tools", *The International Journal of Advanced Manufacturing Technology*, 43.7-8, (2009): 681-689.

Prohászka J., et al., "Effect of cutting tools and cut materials on integrity of mirror surfaces", *Surface Engineering*, 22.4, (2006): 294-298.

Puttick K. E., et al., "Single-point diamond machining of glasses", *Proceedings of the Royal Society of London A: Mathematical, Physical and Engineering Sciences*, 426.1870, (1989).

Rahman M., Yoke S. W., Rahmath Z. A., "Machinability of titanium alloys", *JSME International Journal Series C Mechanical Systems, Machine Elements and Manufacturing*, 46.1, (2003): 107-115.

- Ravindra, et al., "Ductile mode material removal and high-pressure phase transformation in silicon during micro-laser assisted machining", *Precision engineering*, 36.2, (2012): 364-367.
- Shaw M. C., "A new mechanism of plastic flow", *International Journal of Mechanical Sciences*, 22.11, (1980): 673-686.
- Shaw M. C., "Energy conversion in cutting and grinding", *CIRP Annals-Manufacturing Technology*, 45.1, (1996): 101-104.
- Shaw M. C., "Metal cutting principles". New York: Oxford University Press, 2, (2005).
- Shimada S., et al., "Brittle-ductile transition phenomena in microindentation and micromachining", *CIRP Annals-Manufacturing Technology*, 44.1, (1995): 523-526.
- Sima M., Tuğrul Ö., "Modified material constitutive models for serrated chip formation simulations and experimental validation in machining of titanium alloy Ti-6Al-4V", *International Journal of Machine Tools and Manufacture*, 50.11, (2010): 943-960.
- Singh R., Shreyes N. M., "Characterization of a hybrid laser-assisted mechanical micromachining (LAMM) process for a difficult-to-machine material", *International Journal of Machine Tools and Manufacture*, 47.7, (2007): 1139-1150.
- Shi D., Zhu W., "Material physics", Beijing: Mechanical Industry Press, (2006). (In Chinese)
- Stephenson D. A., John S. A., "Metal cutting theory and practice", CRC Press, (2016).

- Sun S. J., James H., Milan B., "Parametric investigation of laser-assisted machining of commercially pure titanium", *Advanced Engineering Materials*, 10.6, (2008): 565-572.
- Taminiau D. A., Dautzenberg J. H., "Bluntness of the tool and process forces in high-precision cutting", *CIRP Annals-Manufacturing Technology*, 40.1, (1991): 65-68.
- Tani G., et al., "Laser surface hardening of martensitic stainless steel hollow parts", *CIRP Annals-Manufacturing Technology*, 59.1, (2010): 207-210.
- Thomas T., Joel O. V., "Laser-assisted milling process", U.S. Patent No. 5,906,459. 25 May 1999.
- Tjong S. C., Tsang H. C., "Laser surface melting of an austenitic Fe-26Mn-7Al-0.9 C alloy", *Surface and Coatings Technology*, 57.2-3, (1993): 139-144.
- Trent E. M., Paul K. W., "Metal cutting", Butterworth-Heinemann, (2000).
- To S., Wang H., and Jelenković E. V., "Enhancement of the machinability of silicon by hydrogen ion implantation for ultra-precision micro-cutting", *International Journal of Machine Tools and Manufacture*, 74, (2013): 50-55.
- Veiga C., Davim J. P., and Loureiro A. J. R., "Properties and applications of titanium alloys: a brief review", *Reviews on Advanced Materials Science*, 32.2, (2012): 133-148.
- Vyas A., Shaw M. C., "Mechanics of saw-tooth chip formation in metal cutting", *Journal of Manufacturing Science and Engineering, Transactions of the ASME*, 121.2, (1999): 163-172.

Washio K., "Laser devices and optical systems for laser precision microfabrication", Springer Berlin Heidelberg, 2010. 63-89.

Weast R. C., Melvin J. A., William H. B., "CRC handbook of chemistry and physics". Boca Raton, FL: CRC press, 69, (1988).

Wikipedia, https://en.wikipedia.org/wiki/Monocrystalline_silicon

Yang X. P., Liu C. R., "Machining titanium and its alloys", Machining Science and Technology, 3.1, (1999): 107-139.

Yeh C. H., et al., "Microlenticular lens replication by the combination of gas-assisted imprint technology and LIGA-like process", Journal of Micromechanics and Microengineering, 22.9, (2012): 095021.

Yellup J. M., "Laser cladding using the powder blowing technique", Surface and Coatings Technology, 71.2, (1995): 121-128.

Zareena A. R., Veldhuis S. C., "Tool wear mechanisms and tool life enhancement in ultra-precision machining of titanium", Journal of Materials Processing Technology, 212.3, (2012): 560-570.

Zhang S. J., et al., "A review of surface roughness generation in ultra-precision machining", International Journal of Machine Tools and Manufacture, 91, (2015): 76-95.

Zhang X. Q., Woon K. S., and Rahman M., "11.09-Diamond Turning", Comprehensive Materials Processing, SHFBJVT Yilbas, Editor (2014): 201-220.

Zhang X. J., Zhang Y. K., "Study on the surface quality of a diamond-turned oxygen-free high-conductance copper reflector used in a high-power CO₂ laser", *Optical Engineering*, 36.3, (1997): 825-830.

Zong W. J., et al., "Analysis for the wear resistance anisotropy of diamond cutting tools in theory and experiment", *Journal of Materials Processing Technology*, 210.6, (2010): 858-867.

Zorev, Nikolaevich N., "Metal cutting mechanics", Pergamon, Headington Hill Hall, Oxford, England, (1966): 526P.